T 1256

A MECHANICAL EQUATION OF STATE FOR BRITTLE ROCK

by

B. T. Brady

ProQuest LLC.
789 East Eisenhower Parkway
P.O. Box 1346
Ann Arbor, MI 48106 – 1346

A thesis submitted to the Faculty and the Board of Trustees of the Colorado School of Mines in partial fulfillment of the requirements for the degree of Doctor of Philosophy in the departments of Mathematics and Mining Engineering.

Signed: B. T. Brady

B. T. Brady

Golden, Colorado

Date: April 28, 1969

APPROVED

Walter Whitman
Thesis Advisor

Niles Grosvenor
Thesis Advisor

Joseph R. Lee
Head
Mathematics Department

Golden, Colorado

Date: April 28, 1969

John J. Reed
Head
Mining Engineering Department

Golden, Colorado

Date: April 28, 1969

ACKNOWLEDGMENTS

The author wishes to express his appreciation to Professors W. Whitman, J. D. Lubahn, D. Foreman, and N. Grosvenor of the Colorado School of Mines for their pertinent suggestions and guidance during the course of the investigation. Special thanks are extended to Mr. F. Leighton of the United States Bureau of Mines who generously provided his time to perform the numerical calculations for the illustrative problem discussed in the test. The author is deeply indebted to Lorene E. Giddings for her expert typing of this manuscript.

CONTENTS

ILLUSTRATIONS

Page

TABLES

ABSTRACT

The results of a theoretical study of the mechanical behavior of brittle rock up to and including total failure are presented. It is shown that the constant temperature deformational behavior of brittle rock can be described by means of three equations which relate the three principal stresses and the three principal inelastic strains resulting from microcracking occurring within the rock structure. These equations are shown to form the brittle-material counterparts of the three "laws" governing the plastic behavior of ductile materials. The three equations are used to solve a hypothetical engineering design problem which is concerned with predicting the collapse of a circular tunnel in a brittle rock which is subject to a uniform hydrostatic stress at large radial distances from the opening.

INTRODUCTION

Rock mechanics like all engineering disciplines must have a theoretical foundation. However, this foundation should be of such a form that it can be used with some ease by the engineer in the design of engineering structures in rock. The development of analytical methods which may aid in the rational design and in determining the stability of engineering structures in competent brittle rock materials forms the subject matter of this thesis. By the design of an engineering structure in rock, we refer to the design of any excavated subsurface opening, the design of any open surface structure, or the design of any system of openings in rock that is virtually self-supporting. A self-supporting system of openings is defined as a system where the structural stresses are carried by the rock without requiring the use of artificial support systems.

There are two essential prerequisites necessary in the rational design of engineering structures in rock. (1) The stress distribution in the vicinity of the proposed structure must be known beforehand. (2) The design engineer must determine the ability of the proposed structure to withstand these stresses without undergoing structural instability — a process commonly referred to as total failure. It is recognized that the design of engineering structures in rock is in a number of ways a more difficult problem than, say, the design of structures made with steel or concrete. There are at least three reasons for this state of affairs. (1) The stress and displacement field in the vicinity of the structure are at

best understood only qualitatively. (2) The geology is generally poorly defined and its influence on the stress and displacement distributions near the structure is little understood. (3) There is a general absence of suitable analytical procedures to aid in the initial design of the proposed structure.

Because of these problems, the engineer cannot apply either the same analytical procedures or achieve the precision in designing structures in rock as is commonly used in the design of conventional structures using steel or concrete. In fact, it should be accepted from the beginning that a different approach to the problem in designing structures in rock should be developed. This approach should be one in which it is recognized that only an approximate design can be made before the structure is built and that such a design must be modified as more information becomes available during the course of the construction.

One factor necessary for designing or evaluating the stability of any kind of structure is a knowledge of the mechanical properties of its material, i.e., stress-strain behavior, fracturing characteristics, et cetera. The composition of most structural materials such as metals and concrete is uniform and reproducible to the degree that their mechanical properties in service are somewhat the same as those measured in the laboratory. Consequently, a rational design can be made on the basis of published mechanical property values. On the other hand, the same equivalence does not exist for rock materials for two reasons. (1) The composition of even the most common rock types is highly variable. (2) The

problem of the size effect is present because unless the mechanical property tests are conducted at a scale such that the test specimen includes these effects in a normal proportion, the test results will not be representive of the in situ rock mass. Of course, the alternative is to perform the test in situ. Comparatively few tests of this nature have been performed in this manner because of both the physical limitations of the test equipment and the prohibitive cost of such experiments. The current procedure is to design the structure on the basis of the results of the small scale laboratory measurements with a safety factor usually determined by the experience of the design engineer. While this procedure is somewhat unsatisfactory, laboratory measurements can and do provide a useful basis for the initial design.

To fully understand the ground control problems involved in the design of large-scale engineering structures in rock, it is essential that the design engineer have at his disposal a quantitative knowledge of the actual mechanical behavior of the rock. To this end, the mechanical properties of rock under controlled conditions of pressure, temperature, environment, and strain rate have been extensively studied in recent years (Brace, 1964; Mogi, 1966; Brace, et al., 1966; Scholz, 1968a). The objective of these investigations was to develop a mechanical equation of state[1/] for rock. However, in spite of the large number of controlled laboratory experiments on small test

---

[1/] A mechanical equation of state is defined as a general relationship between intensive variables (stress, strain, temperature, strain rate, etc.) and/or extensive variables (volume, heat capacity, etc.). A knowledge of such an equation for a given material enables an estimate of the behavior of the material under general conditions once certain material properties are evaluated.

specimens of rock materials, this problem has yet to be completely resolved. One possible reason for this involves the procedure in testing specimens. The objective of the laboratory test is to give a response characteristic (stress-strain relation, fracture strength, etc.) of the rock which is a property of the rock system alone and not the combined response of both the rock and the loading system. A knowledge of the true rock response characteristics is one of the first steps in the development of an equation of state for the rock. It is known that the existence of end effects can adversely affect the response characteristics of the test specimen because of the elastic mismatch between the specimen and the loading end plates (Mogi, 1966; Brady and Blake, 1968). While recent improvements in sample design (Brace, 1964; Mogi, 1966) have largely eliminated this phase of the problem, the problem of determining a mechanical equation of state for rock materials persists. There is evidence suggesting that this problem is a result of a general absence of analytical techniques which can be used to describe the mechanical behavior of rock.

THESIS OBJECTIVES

This thesis is concerned with developing analytical procedures which can be used to describe the constant temperature mechanical behavior of rock under multiaxial stress conditions. We shall restrict the study to brittle rock materials which are characterized by a tight pore structure[2/].

[2/] A tight pore structure is a structure wherein the porosity is due primarily to the presence of inter-and transgranular cracks.

There are four primary objectives of this thesis. These objectives roughly follow the general outline of the thesis. They include: (1) the background of the problem and the development of a physically realistic mathematical model of brittle rock; (2) the formulation of a theory of the mechanical behavior for brittle rock materials under multiaxial stress; (3) the systematic compilation of a set of equations which can easily be used to determine the deformational behavior of brittle rock materials under multiaxial stress conditions; (4) the application of these equations to solve a hypothetical engineering design problem in brittle rock.

BACKGROUND OF THE PROBLEM

Experimental Background

During the past decade, a number of experiments have been performed in which the mechanical behavior of rock under varying conditions of temperature, strain rate, and confining pressure was examined in detail. Some of these investigations of rock behavior were concerned with determining the stress-strain relations and the variation of the elastic properties of rock within the brittle domain (Brace, 1964; Mogi, 1959). Other investigations have been concerned with the brittle-ductile transition (Heard, 1960) and the ductile behavior of rock both at high temperatures and confining pressures (Griggs, et al., 1960; Handin and Hager, 1957; Matsushima, 1960). In this thesis the former phase is examined in detail; namely, the stress-strain relationships, the variation of the elastic properties with stress, and the fracturing characteristics of brittle granular materials displaying a tight pore structure.

For most rock materials exhibiting brittle behavior, the axial stress-strain curve is concave upward for stresses on the order of a kilobar (1 kilobar = 15,000 psi) or greater. The lateral stress-strain relation is often concave downward over the same stress interval (Jaeger, 1962; Walsh, 1965a, b, c). Some investigators (Birch, 1960, 1961; Brace, 1964) have suggested that these effects are due to the presence of pores and/or minute cracks present within the rock structure. Figure 1 illustrates diagrammatically the typical axial and lateral stress-strain behavior of brittle rock in conventional uniaxial compression tests performed at room temperature[3]. The axial and lateral strains are denoted by ϵ_{11}^* and ϵ_{33}^*, respectively. The axial stress is denoted by σ_{11}. Following a convention established by Brace (1964), both the axial and lateral stress-strain curves will be categorized into four regions of behavior.

In region I the axial stress-strain curve is characterized by a concave upward slope. The radius of curvature increases as the applied axial stress increases. The lateral stress-strain relationship is concave downward over the same stress interval. As the applied axial stress increases, both the Young's modulus and Poisson's ratio increase. The amount and rate of increase of these properties are a function of both the rock material and the amount of closable pore space (Brace, 1964).

During region II the elastic moduli have values. Brace (1964) showed that the ratio of axial and lateral strain is approximately constant. Region II deformation ends when the maximum principal stress attains a critical value after which any increase in the applied

[3] In a conventional compression test, an increasing force is applied to the ends of the specimen throughout the test.

stress results in localized failure, i.e., microcracking (Brace, et al., 1966). If unloading occurs in either regions I or II, a slight hysteresis loop is observed, attributed by Walsh (1965b) to the frictional sliding of closed cracks.

Region III deformation is characterized by permanent changes occurring in the microscopic fabric of the rock. Microcracking is taking place and the lateral strain is increasing at a faster rate than the axial strain. This region is characterized by a volume increase due to the microcracking process. This change is attributed by Brace (1964) to result from a cracking of the individual grains and/or a loosening of the grain structure. There is a slight tendency for the slope of the axial stress-strain curve to increase during this region. Brace, et al. (1966), defined this increase as "crack hardening" because the stress required to make the microcracks grow increased after some microcrack growth had occurred. Region III deformation ends when the slope of the axial stress vs. volumetric strain ($\epsilon_1^* = \epsilon_{11}^* + 2\epsilon_{33}^*$) curve becomes infinite. Figure 2 illustrates diagramatically a typical axial stress vs. volumetric strain curve for brittle rock.

In region IV the lateral strain is increasing rapidly and the apparent Poisson's ratio approaches large values (> 0.50) near incipient failure. The total lateral strain becomes quite large during the latter portions of region IV. This is because a large number of voids (microcracks) have been generated throughout the specimen (Brace, 1964). If the specimen is stressed to total failure (i.e., collapse of the test specimen), large through-going fractures form out of both the microcrack systems and the grain boundaries. This eventually leads to the formation of a macroscopic fracture surface (Brace, 1964; Brace, et al., 1966).

There is substantial experimental evidence suggesting that time-dependent deformation at constant stress (creep) occurs in brittle rock during regions III and IV. For example, Matsushima (1960) found in room temperature creep tests on a granite in uniaxial compression that the creep strain (time dependent deformation) normal to the axis of compression was larger than the creep strain in the axial direction and that the lateral creep rate increased much more rapidly with stress than did the axial creep rate. Scholz (1968b) also found evidence of creep in a granite during regions III and IV. Both authors concluded that the volume of the rock increased during creep and that the creep strain was due to the generation of microcracks within the rock structure.

The above observations suggest that the mechanical behavior of brittle rock materials is influenced by the presence of cracks. The curvature of the stress-strain curves as well as the attenuation and wave propagation characteristics of low amplitude stress waves in brittle rock (Walsh, 1966; Brady, 1968) suggest that the closing and/or frictional sliding of these cracks have a significant effect on the overall static and dynamic mechanical behavior of brittle rock. The experimental results indicate a need for theoretical work and, apparently, little success will be obtained unless effects are directed along the lines of statistical analysis. In short, theoretical studies on the mechanical behavior of rock materials must be statistical in their very nature. The physical and chemical makeup of rock suggests such an approach.

Theoretical Background

The problem of determining the elastic mechanical behavior of a polycrystalline aggregate (polycrystal) in terms of the elastic properties of the constituting crystals has received repeated attention (Hashin, 1959; Bishop and Hill, 1951; Hill, 1952). The first contribution was made by Voight (1928) who calculated the elastic moduli of the polycrystal by averaging over all possible orientations of the individual crystals and then making the simplifying assumption that all the crystals would be subjected to the same uniform strain as that applied to the polycrystal. Reuss (1929), using a similar approach, averaged the elastic compliances. This approach would be equivalent to assuming that all the crystals are in the same state of uniform stress as that applied to the polycrystal. Both theories assume that there are no cavities or cracks within the aggregate. Bishop and Hill (1951) have shown theoretically that the Voight and Reuss models actually form upper and lower bounds, respectively, for the elastic moduli of a polycrystalline aggregate.

When one considers aggregates containing cavities, there is no longer a well-developed theory to serve as a guideline since both the Voight and Reuss theory only apply for aggregates composed of a single crystal phase without any cavities. The theoretical treatment of such materials as quasi-isotropic bodies relies on the assumption that the cavities are uniformly distributed both in space and orientation. Thus, there will be no outstanding directional properties for samples containing a large number of cavities.

Walsh (1965a,b,c) evaluated theoretically the effect of cracks on the mechanical deformation of brittle rock materials. He advanced a mathematical model wherein a brittle rock structure was represented by an elastic isotropic continuum containing a large number of randomly oriented cracks. He confirmed analytically the experimental result that the compressibility (compressibility is defined to be the ratio of the volumetric strain to the hydrostatic pressure which produces the volumetric strain) of porous materials is greater than that of the solid material of identical composition. Walsh showed that the difference between the two cases, irregardless of the pore shape or concentration, was equal to the rate of change of porosity with pressure, i.e.,

$$\beta^* = \beta - \frac{d\eta}{dP} , \qquad (1)$$

where P is the pressure β^* and β are the effective and intrinsic (crack-free) compressibilities, and η is the porosity of the aggregate. This expression was evaluated by Walsh (1965a) for both spherical and ellipsoidal pore shapes and it was shown that the latter shape can increase the compressibility nearly as much as a spherical pore of the same diameter as the maximum length of ellipsoidal pore, even though the porosity in the two cases is considerably different.

Walsh (1965b,c) also evaluated the effect of narrow ellipsoidal-like cracks on the uniaxial elastic moduli of brittle rocks. He demonstrated analytically that an increase in the magnitude of the Young's

modulus and Poisson's ratio occurs as these cracks close under an increasing compressive stress. For example, Walsh (1965c) found that the initial (region I) and final (region II) Poisson's ratios could be expressed as

$$\nu_i = \nu \left(E_i/E\right)$$
$$\nu_f = \nu + \tfrac{1}{2}\left(1-2\nu\right)\left(1-E_f/E\right) , \qquad (2)$$

where ν_i, ν_f, and ν are the initial, final, and intrinsic (crack-free) Poisson's ratios and E_i, E_f, E are the initial, final, and intrinsic Young's moduli, respectively. Walsh showed that when the applied compressive stress is large enough to close most of the cracks, Young's modulus (E_f) and Poisson's ratio (ν_f) do not equal their intrinsic values because frictional sliding along some crack interfaces occurs. Because frictional sliding can occur in the Walsh model, the theory predicts a hysteresis effect during an unloading cycle, i.e., cracks, although suitably oriented for sliding, do not slide immediately in the reverse sense when unloading occurs (refer to appendix F). This prediction is in accord with experimental observations on the stress-strain behavior of brittle rock during regions I and II (Brace, 1964).

THE MECHANICAL BEHAVIOR OF BRITTLE ROCK UNDER MULTIAXIAL STRESS STATES

Synopsis

In this section, we are concerned with extending the model of brittle rock presented by Walsh to multiaxial stress states. In particular, we are concerned with developing a physically realistic empirical model of

brittle rock behavior and in laying the theoretical foundation necessary to develop the ground rules required to describe the behavior of brittle rock when microcracking is occurring within the rock structure.

Behavior During Regions I And II

To analytically describe the behavior of brittle rock under multiaxial stress, we make the following assumptions. (1) Like Walsh, we assume that a tight brittle rock structure can be mathematically modeled by an elastically isotropic continuum containing a large number of ellipsoidal-like cracks of which some may close under applied compression loads and when the closed cracks are suitably oriented with respect to the applied stresses, they may undergo frictional sliding. (2) These cracks can be collectively characterized by the distribution function $P(c,\beta,\varphi)$, where c is the crack half-length, β is the inclination of the crack major axis to the direction of the maximum principal stress (σ_{11}), and φ is the angle between the crack normal projected onto the intermediate and least principal stress[4] plane and the x_2 axis. Figure 3 illustrates the nomenclature used to specify orientation of the crack to both the stress axes ($\sigma_{11},\sigma_{22},\sigma_{33}$) and the coordinate axes (x_1,x_2,x_3). (3) The crack interaction effects can be neglected as a first order approximation.

The third assumption enables us to express the differential strain energy density of a material containing N_e voids as (Hashin, 1959)

---

[4] The maximum, intermediate, and least principal stresses are denoted by $\sigma_{11},\sigma_{22},\sigma_{33}$, respectively. In this thesis compressive stress is taken to be positive.

$$\sigma_{ij}\,d\epsilon^{*}_{ij} = \sigma_{ij}\,d\epsilon^{o}_{ij} + \frac{1}{V}\sum_{n=1}^{N_e}\left[\sigma_{ij}\,d\left(\oint\!\!\oint u_i\,\bar{\nu}_j\,dA_c\right)_n\right] , \qquad (3)$$

where the superscripts "*" and "o" refer to the effective strain and purely elastic (intrinsic or crack-free) strains in the specimen, respectively, $\bar{\nu}_j$ is a unit vector in the j (j=1, 2, 3) direction, u_i (i=1, 2, 3) is the displacement of the void surface in the $\bar{\nu}_j$ (j=1, 2, 3) direction, and $\bar{\nu}_j dA_c$ is the differential cross sectional area of the void normal in the $\bar{\nu}_j$ direction. The latter terms in equation 3 are the additional differential strain energy density components resulting from the presence of the N_e voids in a specimen of volume V .

The effective strains are derived from equation 3 using the identity $d\epsilon^{*}_{ij} = \frac{\partial}{\partial\sigma_{ij}}(\sigma_{ij}\,d\epsilon^{*}_{ij})$ (Jaeger, 1962). The effective strains in the principal directions are

$$\begin{aligned}
d\epsilon^{*}_{11} &= d\epsilon^{o}_{11} + \frac{1}{V}\sum_{n=1}^{N_e} d\left[\oint\!\!\oint u_1\,\bar{\nu}_1\,dA_c\right]_n \\
d\epsilon^{*}_{22} &= d\epsilon^{o}_{22} + \frac{1}{V}\sum_{n=1}^{N_e} d\left[\oint\!\!\oint u_2\,\bar{\nu}_2\,dA_c\right]_n \qquad (4) \\
d\epsilon^{*}_{33} &= d\epsilon^{o}_{33} + \frac{1}{V}\sum_{n=1}^{N_e} d\left[\oint\!\!\oint u_3\,\bar{\nu}_3\,dA_c\right]_n .
\end{aligned}$$

When the voids are modeled by narrow ellipsoidal slots, the strain components can be evaluated for the cases where some of the N_e cracks are open and where others are both closed and undergoing frictional sliding. As the applied stresses (assumed to be compressive) increase, some of the N_e voids close and if the closed cracks are suitably oriented, frictional sliding can

occur along the crack surfaces. Both the closure of cracks and the frictional sliding of suitably oriented cracks give rise to the strain increments in equation 4. These strain components can be easily evaluated for an arbitrary primary crack distribution[5].

When the primary cracks are randomly distributed throughout the rock structure, certain approximations for these additional strain components are possible if both the open crack density (ρ_{op}) and the density of closed cracks suitably oriented for frictional sliding (ρ_{cls}) are known. For the open crack ("op") components, the differential strain increments can be written as (see appendices B and E for justification)

$$\begin{aligned} d\epsilon_{11}^{op} &\cong A_{11}\rho_{op}d\sigma_{11} \\ d\epsilon_{22}^{op} &\cong A_{11}\rho_{op}d\sigma_{22} \\ d\epsilon_{33}^{op} &\cong A_{11}\rho_{op}d\sigma_{33} \quad , \end{aligned} \tag{5}$$

where A_{11} is a constant (see appendix B). When the applied stress system is axisymmetric ($\sigma_{22}=\sigma_{33}$), the differential strain increments for the closed sliding crack ("cls") components are (see appendices B and E for justification)

$$\begin{aligned} d\epsilon_{11}^{cls} &\cong B_{11}\rho_{cls}d\sigma_{11} \\ d\epsilon_{22}^{cls} &\cong B_{22}\rho_{cls}d\sigma_{11} = -\frac{1}{2}B_{11}\rho_{cls}d\sigma_{11} \\ d\epsilon_{33}^{cls} &\cong B_{33}\rho_{cls}d\sigma_{11} = -\frac{1}{2}B_{11}\rho_{cls}d\sigma_{11} \quad , \end{aligned} \tag{6}$$

where $B_{22} = B_{33}$. Since the sum of the principal strain components ($d\epsilon_{ii}^{cls}$) must be zero for this mode of deformation, $B_{33} = -\frac{1}{2}B_{11}$. In equation 5 and 6,

---

[5] The reader may refer to appendices A through E for a discussion of these details.

the constants A_{11} and B_{11} are unknowns to be evaluated from experimental data for each rock type (see equations 13 and 14).

General relationships for the crack densities (ρ_{op}, ρ_{cLs}) are derived in appendix D. When the primary cracks are uniformly distributed throughout the material structure the distribution function can be written $P(c,\beta,\varphi) = \frac{\cos\beta d\beta d\varphi dc}{4\pi(c_{max}-c_{min})}$. If $\rho_{op}^{I}\left(\rho_{op}^{I}=\frac{N_{op}^{I}}{N_o}\right)$ and $\rho_{cL}^{I}\left(\rho_{cL}^{I}=1-\rho_{op}^{I}\right)$ are the "densities" of cracks open and closed before loading, then when the primary cracks are uniformly distributed through the structure the crack densities during a loading cycle can be written

$$\rho_{op} = \frac{N_{op}}{V} = \rho_{op}^{I}\sin\beta_o$$

$$\rho_{cLs} = \rho_{cL}^{I}\left(\sin\beta_{max}-\sin\beta_{min}\right) , \tag{7}$$

where

c_{max} = length of the largest primary crack

c_{min} = length of the smallest primary crack

N_{op} = total number of open cracks

N_{cLs} = total number of sliding cracks

V = specimen volume .

When $d\sigma_{22}=d\sigma_{33}$, the angular limits β_o, β_{max}, and β_{min} are (see appendices C and E)

$$\beta_o = \sin^{-1}\left[\frac{\frac{B}{c\sigma_{11}} - k}{1-k}\right]^{\frac{1}{2}}$$

$$\beta_{min}^{max} = \frac{1}{2}\left[\tan^{-1}\frac{1}{\mu} \pm \cos^{-1}\frac{(1+k)\mu}{(1-k)\sqrt{1+\mu^2}}\right] \qquad (8)$$

$$k = d\sigma_{33}/d\sigma_{11} \quad , \quad B = \text{constant} \quad .$$

The angular coordinates β_o, β_{max}, and β_{min} refer to the angular limits of open cracks and closed sliding cracks, respectively. Figure 4 illustrates these angular orientations for a specimen subjected to an axisymmetric state of stress ($\sigma_{22}=\sigma_{33}$). Notice that the long axes of cracks contained within the angular range $-\beta_o \leqslant \beta \leqslant \beta_o$ are open and those contained within the angular range $\beta_{min} \leqslant \beta \leqslant \beta_{max}$ are closed and suitably oriented for frictional sliding.

When $\sigma_{22} \neq \sigma_{33}$, equation 6 will be approximated by the expression

$$\begin{aligned} d\epsilon_{11}^{cls} &\cong B_{11}\, \rho_{cls}\, d\sigma_{11} \\ d\epsilon_{22}^{cls} &\cong B_{33}\left(\frac{1-k_2}{1-k_3}\right)^R \rho_{cls}\, d\sigma_{11} \\ d\epsilon_{33}^{cls} &\cong B_{33}\, \rho_{cls}\, d\sigma_{11} \quad , \end{aligned} \qquad (9)$$

where

$B_{33} \cong -\dfrac{B_{11}}{1+\left(\frac{1-k_2}{1-k_3}\right)^R}$, $k_2 = \dfrac{d\sigma_{22}}{d\sigma_{11}}$, and $k_3 = \dfrac{d\sigma_{33}}{d\sigma_{11}}$. There are two reasons for choosing the functional relationship in equation 9. (1) When $k_2=k_3$, this equation reduces to equation 6. (2) When $k_2 \neq k_3$, the amount of strain in the direction of the intermediate principal stress must decrease as k_2 increases because there are fewer primary cracks suitably oriented for sliding. This equation satisfies both requirements.

To calculate the uniaxial "elastic" moduli during the initial stages of regions I and II, the total principal strains can be expressed as

$$
\begin{aligned}
d\epsilon_{11}^{*} &\cong d\epsilon_{11} + d\epsilon_{11}^{op} + d\epsilon_{11}^{cl\,s} \\
d\epsilon_{33}^{*} &\cong d\epsilon_{33} + d\epsilon_{33}^{op} + d\epsilon_{33}^{cl\,s} \\
d\epsilon_{22}^{*} &\cong d\epsilon_{33}^{*} \quad ,
\end{aligned}
\tag{10}
$$

where ϵ_{11} and ϵ_{33} represent the elastic strains. The relationship between the elastic strains and the principal stresses is given by Hooke's law. The uniaxial Young's modulus and Poisson's ratio during the initial stages of region I ($\rho_{op} = \rho_{op}^{I}$, $\rho_{cl} = \rho_{cl}^{I}$) and region II ($\rho_{op} = 0$, $\rho_{cl} = 1.0$) are easily found from equations 5, 6, and 10 to be

$$
\begin{aligned}
\frac{1}{E_i} &\cong \frac{1}{E} + (A_{11}\rho_{op}^{I} + B_{11}\rho_{cl}^{I}) \\
\frac{1}{E_f} &\cong \frac{1}{E} + B_{11} \\
\frac{\nu_i}{E_i} &\cong \frac{\nu}{E} + \tfrac{1}{2}B_{11}\rho_{cl}^{I} \\
\frac{\nu_i}{E_f} &\cong \frac{\nu}{E} + \tfrac{1}{2}B_{11}
\end{aligned}
\tag{11}
$$

where the subscripts "i", "f" refer to the initial region I and initial region II values, respectively. The intrinsic (i.e., crack-free) values of Young's Modulus and Poisson's ratio and denoted by E and ν, respectively. Equation 11 leads to the identities

$$\nu_1 = \nu \left(\frac{E_1}{E}\right) + \rho_{cL}^{I} E_1 \left(\frac{\nu_f}{E_f} - \frac{\nu}{E}\right)$$

$$\nu_f = \nu + \tfrac{1}{2}(1-2\nu)\quad(1 - E_f/E) \quad . \tag{12}$$

When $\rho_{op}^{I} = 1.0$, these relations reduce to Walsh's (1965c) results (see equation 2).

The relationships between the constants A_{11}, B_{11}, and ρ_{cL}^{I} are found from equation 11 to be

$$A_{11} = \frac{\left(\frac{1-2\nu_1}{E_1} - \frac{1-2\nu}{E}\right)}{1 - \frac{2\left(\frac{\nu_1}{E_1} - \frac{\nu}{E}\right)}{\frac{1}{E_f} - \frac{1}{E}}} \tag{13}$$

$$B_{11} = \frac{1}{E_f} - \frac{1}{E} \tag{14}$$

$$\rho_{cL}^{I} = 2\left(\frac{\nu_1}{E_1} - \frac{\nu}{E}\right)\left(\frac{1}{E_f} - \frac{1}{E}\right) \quad . \tag{15}$$

These constants can be calculated by measuring the slopes of the axial and lateral stress-strain curves during the initial stages of regions I and II, respectively. The intrinsic values of Young's modulus (E) and Poisson's ratio (ν) can be determined by measuring the velocities of longitudinal and shear waves in the rock when it is subjected to a hydrostatic pressure large enough to close the open cracks within the rock[6]. As an example of the

[6]The reader may refer to Simmons and Brace (1965) for a description of the experimental procedure to measure these properties.

procedure to calculate the above constants, we refer to figure 9a. This figure shows a typical axial and lateral stress-strain curve for a cylindrical specimen of the Westerly granite deformed under uniaxial compression (after Brace, et al., 1966). This rock is a low porosity, hard brittle rock known to display elastic behavior (i.e., the strain is completely recoverable) in uniaxial compression for values of the applied stress up to approximately 15,000 psi. The values of the Young's moduli and Poisson's ratios during the initial stages of regions I and II are found from figure 9a to be 6×10^6 psi and 0.20 and 8.5×10^6 psi and 0.31, respectively. The intrinsic (crack-free) values of Young's modulus and Poisson's ratio have been found by Simmons and Brace (1965) to be approximately 12×10^6 psi and 0.24, respectively. If these values are substituted into equations 13, 14, and 15, we find the values of the constants A_{11}, B_{11}, and ρ_{cL}^{I} to be 0.233×10^{-6}/psi, 0.0417×10^{-6}/psi, and 0.64, respectively. Therefore the strain components due to open cracks and closed cracks undergoing frictional sliding can now be calculated under any combination of the applied stresses.

Behavior During Regions III and IV

Experiment has shown (Paulding, 1965; Brace, et al., 1966; Bieniawski, 1967) that during regions III and IV the strains (when the applied stresses are compressive) due to microcracking can be accounted for by the opening of voids (i.e., microcracks), the long axes of which make a small angle to the direction of the maximum principal compressive stress. These experiments have shown also that there is little or no permanent strain parallel

to the maximum principal stress direction and that the volume change could be accounted for by a permanent increase in the cross-sectional area of the specimen.

We shall consider in this thesis two possible classes of failure initiation in brittle rock. The term failure initiation refers to the beginning of microcrack growth. (1) Failure initiation when the applied stresses are compressive occurs from closed cracks which can undergo frictional sliding (i.e., there is no grain boundary cement present to inhibit movement on the crack surface). This class of failure initiation is denoted as the "cls" class and is operative when the orientation of the cracks satisfies the modified Griffith criterion, i.e., failure initiation from closed cracks occurs when the difference between the shear stress acting along the crack surface exceeds a critical value. If $\tau^{(n)}$ and $\tau_f^{(n)}$ ($\tau_f^{(n)} \simeq \mu\sigma_N^{(n)}$, where $\sigma_N^{(n)}$ is the normal stress acting on the n^{th} crack surface and μ is the coefficient of friction along the crack surface) are the shear and frictional shear stress, respectively, on the n^{th} crack surface, then failure initiation occurs for cracks which satisfy the condition

$$\tau^{(n)} - \tau_f^{(n)} \geq \tau_c \quad , \tag{16}$$

where τ_c is a constant. This quantity is a measure of the stress required to initiate frictional sliding along the crack surface. Figure 5 (a,b) illustrates diagrammatically two possible modes of failure initiation in this class, namely intergranular (opening of the grain boundary) (figure 5a) and intragranular (microcrack growth initiating at a grain boundary and

propagating within a host grain) (figure 5b). Notice that the constants τ_c would be different for each mode. (2) Failure initiation in brittle rock when the applied stresses are tensile is assumed to occur from open cracks once the tensile stress acting normal to the crack surface exceeds a critical value, i.e., microcrack growth in applied tension occurs when

$$\sigma_N^{(n)} \leq \sigma_c \tag{17}$$

where (-) σ_c is the tensile stress required to initiate microcracking from an open crack whose long axis is normal to the least principal stress (σ_{33}). Figure 6 shows a typical microcrack occurring along a grain boundary for an open crack whose orientation is such that equation 17 is satisfied. This class of failure initiation is denoted as the "opt" class.

Once the crack distribution (i.e., grain boundaries and other microfractures) in the rock has been determined by standard petrofabric measurements, the number of cracks suitably oriented for failure initiation for either the "cls" or "opt" class can be calculated. The actual microcrack density (number of microcracks per unit volume) within rock is approximated by advancing the hypothesis that the total number of microcracks for a fixed stress level is proportional to the number of

cracks suitably oriented for failure initiation. The reader can refer to appendix G for the procedure involved in determining the microcrack density.

Once the microcrack densities in the rock for the "cls" and "opt" failure initiation classes are known, it is possible to estimate the strains occurring within the rock by making the equations to satisfy the following three conditions. (1) The strains due to microcracking are proportional to the density of microcracks within the rock. (2) The volumetric microcrack strain (i.e., the sum of the three principal microcrack strains) vs. the maximum principal compressive stress relation should be of a form such that the volume of the specimen tends to increase as the applied stress is increased above the critical stress required to initiate microcracking. This condition arises because the microcrack growth process is not an instantaneous process (Brace, et al., 1966). The microcracks tend to grow larger as the applied stress(es) increase. (3) Near total failure (or structural instability) of the rock, the microcrack stress-strain relations must express the experimental observation that the microcracks are in the process of joining, i.e., at total failure where the specimen ruptures into two or more parts, the strains normal to the direction of maximum compression tend to become quite large (Brace, et al., 1966). Appendix H illustrates an

empirical approach which was used to determine the microcrack strains. However, the reader will notice that there are two major criticisms against these expressions. (1) The equations are difficult to evaluate. Accordingly, their use in solving practical problems involving the design of engineering structures in brittle rock is limited because of this complexity. (2) These equations do not take into account the known rate sensitive properties of brittle rock. The next section of the thesis is concerned with developing the stress-strain relations of brittle rock during regions III and IV which eliminate both of the above criticisms.

A MECHANICAL EQUATION OF STATE FOR BRITTLE ROCK

Synopsis

We are concerned in this section with developing the groundrules governing the behavior of brittle materials once microcracking is initiated within the material structure. It is shown that the groundrules are somewhat analagous to the "laws" of classical plasticity when plastic strain hardening is occurring. Because of this similarity, a brief discussion of the plasticity "laws" is presented in the following section.

The Laws of Classical Plasticity

Introduction

Plasticity can be defined as that property of a material where it can be deformed continuously and permanently without rupture during the application of stresses which exceed those necessary to cause gross yielding of the material. This permanent deformation occurs under stress and this deformation can build up to large amounts once the yield stress is exceeded. The final configuration of the material depends on the history of loading.

For the most part, materials are used under conditions where they remain elastic and so the theory of elasticity is of prime importance. However, there are areas of manufacture and applications where the plastic behavior must be considered. For example, the study of plasticity is important in the mechanics of metal forming where the materials are prepared and converted into the desired geometrical form. In general, both the design engineer and the metallurgist are interested in the more practical aspects of plastic deformation and their relation to industrial materials, either in forming processes or in the mechanical properties that these processes develop. The "laws" of classical plasticity provide the metals engineer with the necessary analytical tools to solve such practical engineering problems.

Most elasticity problems involve six variables, namely, the three principal stresses and the three principal strains. Therefore, we need

only six equations to solve such problems. Three of these equations are provided by Hooke's law. The physical conditions inherent in the particular problem provide the remaining equations, namely, the compatibility and equilibrium of force conditions and the associated boundary conditions imposed by the problem.

There are three additional variables, over and above the six variables needed to express the elastic behavior once plastic deformation occurs in the material. The additional three variables are the plastic components of the three principal total (elastic and plastic) strains. There are now three additional equations needed to solve problems when plastic deformation is occurring within the material. These three additional equations are provided by the three "laws" of classical plasticity.

The First Plasticity "Law" - The Mechanical Equation of State

The most important of the plasticity "laws" required to analyze the plastic deformation in materials is the condition governing yielding (or equivalently, the initiation of plastic flow) and the relationship of the stresses to the plastic strains resulting from these stresses. To this end, a number of yield conditions have been proposed. However not one of them is completely satisfactory both from the viewpoints of accuracy and simplicity. All of these yield conditions are empirical because they cannot be derived from fundamental considerations. These yield conditions are also restricted to their use because they can apply only to isotropic materials.

The simplest yielding condition is the shear stress (Tresca) criterion. This is expressed by the equation

$$S_o = \sigma_{11} - \sigma_{33} \quad , \tag{18}$$

where S_o is the stress in a uniaxial test when yielding first occurs and σ_{11} and σ_{33} are the values of the greatest and least principal stresses at the beginning of yielding. The maximum observed error when this criterion is used is on the order of 10 percent. A more complex yield condition is the distortional energy condition. This is expressed as

$$S_o = \frac{1}{\sqrt{2}} \sqrt{(\sigma_{11}-\sigma_{22})^2+(\sigma_{22}-\sigma_{33})^2+(\sigma_{11}-\sigma_{33})^2} \quad , \tag{19}$$

where σ_{22} is the intermediate principal stress. It is known that this yield condition gives rise to a maximum error of approximately 5 percent (Lubahn and Felgar, 1961). There have been proposed other yielding conditions such as the equivalent shearing stress condition but they are in general very complex and consequently their use in performing engineering calculations is severely restricted. Interestingly, the simple shear stress yield criterion has been found to be quite adequate for engineering purposes.

For most materials, a larger and larger stress is required to cause plastic flow to continue as the plastic strain increases. This phenomenon is defined as strain hardening and it is manifested by a rising stress-strain curve in the plastic region. It has been found that for many materials the strain hardening characteristics for a fixed plastic strain rate can be often represented by the simple equation

$$S_o = A \left(\varepsilon_o^{(p)}\right)^m \quad , \tag{20}$$

where S_o and $\epsilon_o^{(p)}$ are the stress and the plastic strain in a uniaxial test, m is a constant defined to be the strain hardening exponent, and A is a constant termed the "strength coefficient". If logarithms are taken of both sides of equation 20, we see that if the mechanical behavior is correctly represented by this equation, then the log S_o vs. log $\epsilon_o^{(p)}$ relationship for the uniaxial test will be a straight line, where m is the slope and log A is the intercept of the straight line on the log S_o coordinate axis.

It is essential to make a definition of strain hardening that will apply to multiaxial stress states, not just to the case of uniaxial loading specified by equation 20. There have been proposed several definitions of strain hardening. However, they all give values of the strain hardening characteristics of materials which are within 15 percent of each other (Lubahn and Felgar, 1961). For example, some authors make use of the definition that the strain hardening is measured by the numerically largest principal plastic strain while other prefer to use the definition that the strain hardening is best measured by the difference between the maximum and least principal plastic strains.

The first law of classical plasticity is that the yielding conditions give the relationship between the stresses in the uniaxial test and the principal stresses in the general multiaxial stress case if there is the same amount of strain hardening in the uniaxial case and the multiaxial case. This law can be stated mathematically as

$$F(\sigma_{11}, \sigma_{22}, \sigma_{33}) = G(\epsilon_{11}^{(p)}, \epsilon_{22}^{(p)}, \epsilon_{33}^{(p)}) \quad , \tag{21}$$

where F and G represent suitable functions of the principal stresses and principal plastic strains, respectively, which result in the above equality. Equation 21 is referred to as the universal stress-strain relation or simply, the mechanical equation of state for a material at constant temperature and a fixed plastic strain rate exists.

For many engineering materials, it has been found that the universal stress-strain relationship can be written as

$$S_o = \sigma_{11} - \sigma_{33} = A \left| \epsilon^{(p)} \right|^n \quad , \tag{22}$$

where $\epsilon^{(p)}$ is the numerically largest principal plastic strain and the brackets $|\ |$ refer to the absolute value (Lubahn and Felgar, 1961). When plastic strain rate effects are included, the equation

$$S_o = A_1 \left(\epsilon_o^{(p)}\right)^m \left(\dot{\epsilon}_o^{(p)}\right)^n \quad , \tag{23}$$

where A_1 is a constant, and $\dot{\epsilon}_o^{(p)}$ denotes the equivalent plastic strain rate, and n is the strain hardening rate exponent, often is observed to fit the experimental data quite accurately provided no metallurgical changes occur and the test data is obtained at a fixed uniform temperature. Equation 23 provides the design engineer with one of the three equations needed to solve problems where plastic deformation is occurring.

The Second Plasticity "Law" - The Constant Volume Condition

The second plasticity law is considerably simpler than the first law. This law states that the volumetric plastic strain is zero, i.e.,

$$\epsilon_{11}^{(p)} + \epsilon_{22}^{(p)} + \epsilon_{33}^{(p)} = 0 \quad . \tag{24}$$

This law states that the volume of the material is not affected by plastic deformation.

The Third Plasticity "Law" - The Lévy-Mises Condition

The third plasticity law, the Lévy-Mises condition states that the principal plastic strains and the principal stresses satisfy the following condition:

$$\frac{\sigma_{11} - \sigma_{33}}{\epsilon_{11}^{(p)} - \epsilon_{33}^{(p)}} = \frac{\sigma_{11} - \sigma_{22}}{\epsilon_{11}^{(p)} - \epsilon_{22}^{(p)}} = \frac{\sigma_{22} - \sigma_{33}}{\epsilon_{22}^{(p)} - \epsilon_{33}^{(p)}} \quad . \tag{25}$$

If λ is defined to equal $[\sigma_{22} - \frac{1}{2}(\sigma_{11}+\sigma_{33})] / \frac{1}{2}(\sigma_{11}-\sigma_{33})$, this law has been found experimentally to be accurate only for values of λ equal to -1.0, 0, or +1.0. The maximum error (approximately 20 percent) is found to occur when $\lambda = \pm 0.50$ (Lubahn and Felgar, 1961).

Summary

It must be understood that the above "laws" of classical plasticity apply only to homogeneous, isotropic materials subjected to continuously increasing loads in a manner so as to cause the principal stress ratios to remain constant, i.e., a state of proportional loading must exist. Situations wherein the principal stress ratios vary during plastic flow can be

handled by a modification in which the "laws" are applied only to small increments of deformation, i.e., an incremental theory of flow should be employed. Actually, the "laws" of plasticity should always be written in terms of strain increments rather than those shown by equation 21 through 31 which represent a total strain theory. However, when a state of proportional loading prevails, the two theories (incremental and total strain theories) are identical.

The Equations Governing the Behavior of Brittle Materials

Introduction

Brittleness is defined in this thesis to be a property of a material where it can be deformed continuously and permanently with no noticeable plastic deformation during the application of stresses which exceed those necessary to initiate microcracking within the material. Like ductile materials, the final configuration of brittle materials depends on the history of loading.

If equations governing the mechanical behavior of brittle materials can be found, the problems confronting the design engineer would be somewhat lessened. Of course like the "laws" of classical plasticity, the equations governing the behavior of brittle materials will be only approximate and they will be somewhat empirical in their mathematical makeup. This is a result of the complexity of the microcracking process in brittle materials.

Once microcracking has been initiated within a brittle material, there are three additional variables (over and above the six variables needed to express the elastic behavior) necessary to describe the mechanical behavior of the material. These additional variables are the microcrack components of the three printipal total (elastic and nonelastic) strains. We now need three additional equations to solve problems involving microcracking in brittle materials.

Throughout the remainder of this section we shall assume for simplicity that the cracks are uniformly distributed in the material and that the primary cracks are all of equal length (i.e., the material is isotropic).

The First Equation Governing Brittle Behavior - The Constant Microcrack Strain Criterion

We recall that there are two major failure initiation classes in brittle materials, namely, the "cls" failure class and the "opt" failure class. The "cls" failure class is operative whenever the maximum principal compressive stress, σ_{11}, exceeds the critical value σ_{11}^{cr}, where σ_{11}^{cr} is the value of the maximum principal compressive stress required to initiate a microcrack of the "cls" class[7]. The "opt" failure mode is operative whenever one or more of the principal stress are tensile and are greater than or equal to the critical stress σ_c, where σ_c is the value of the tensile stress required to initiate a microcrack of the "opt" class.

[7] The critical stress σ_{11}^{cr} is known to vary linearily with the least principal stress σ_{33}, i.e., $\sigma_{11}^{cr} = a + b\,\sigma_{33}$, where a and b are constants (McClintock and Walsh, 1962; the reader may refer to appendix G for a derivation of this stress). The constants a and b can be measured by a procedure discussed later in the thesis

The first equation we shall hypothesize to govern the behavior of brittle materials is that the incremental principal strain due to microcracking in the direction of the maximum principal stress (σ_{11}) axis is approximately zero for either the "cls" failure mode or the "opt" failure mode. Mathematically, this equation is written

$$\begin{aligned} d(\epsilon_{11}^{m\,c})_{cls} &\cong 0 \qquad (\sigma_{11} \geq \sigma_{11}^{cr}) \\ d(\epsilon_{11}^{m\,c})_{opt} &\cong 0 \quad . \qquad (\sigma_{33} \leq -\sigma_c) \quad . \end{aligned} \tag{26}$$

This equation has been verified experimentally (Brace, 1964; Brace, et al., 1966; Bieniawski, 1967).

The Second Equation Governing Brittle Behavior - The Constant Stress Difference - Microcrack Strain Difference Ratio Criterion

The second rule we hypothesize to govern the behavior of brittle materials is that the principal microcrack strains and the principal stresses satisfy the condition

$$d(\epsilon_{22}^{m\,c})_{cls} \cong d(\epsilon_{33}^{m\,c})_{cls} \left(\frac{1-k_2}{1-k_3}\right)^N \tag{27}$$

for the "cls" failure mode and

$$d(\epsilon_{22}^{m\,c})_{opt} \cong d(\epsilon_{33}^{m\,c})_{opt} \left(\frac{1-k_2}{1-k_3}\right)^M \tag{28}$$

for the "opt" failure mode. The exponents N and M are constants which are to be evaluated from the experimental data. To calculate the exponents N and M in equations 27 and 28, the values of the microcrack strains must be determined in the general multiaxial ($\sigma_{11} \neq \sigma_{22} \neq \sigma_{33}$) stress state. The quantities k_2 and k_3 are σ_{22}/σ_{11} and σ_{33}/σ_{11}, respectively. The similarity between

equations 27 and 28, and equation 25 is quite noticeable when the exponents N and M are unity.

There are three reasons for choosing the functional relationships of equations 27 and 28. (1) When the intermediate and least principal stresses are equal, the microcrack strains (ϵ_{22}^{mc} and ϵ_{33}^{mc}) must be equal. (2) When these stresses are not equal, the microcrack strain, ϵ_{22}^{mc}, must be smaller than ϵ_{33}^{mc} because there are fewer cracks suitably oriented for failure initiation in the direction of the x_2 axis. (3) When the maximum and intermediate principal stresses are equal (k_2=1), equations 27 and 28 must reduce to equation 26.

It is unfortunate that there is an absence of accurate experimental data to check the above equations. However, it is reasonable to expect that equations 27 and 28 can provide a first approximation to the value of the intermediate principal microcrack strain when a true state of triaxial stress ($\sigma_{11} \neq \sigma_{22} \neq \sigma_{33}$) exists.

The Third Equation Governing Brittle Behavior - The Mechanical Equation of State

Preface

The relationship between the principal stresses, the principal microcrack strains, and the principal microcrack strain rates constitutes the mechanical equation of state for brittle materials deformed at constant temperature. To determine the mechanical equation of state, we shall postulate that there is a relationship between the stresses in the uniaxial test and the principal stresses in the general multiaxial case. Therefore, there is a function for each failure mode of the principal stresses $F(\sigma_{11}, \sigma_{22}, \sigma_{33})$, and the volumetric microcrack strain rate such that

$$F(\sigma_{11}, \sigma_{22}, \sigma_{33}) \equiv G\ (\epsilon_{11}^{mc}) \tag{29}$$

Two models of brittle materials are examined in detail to determine the form of the mechanical equation of state for each failure mode. In the first model, we shall discuss the format of equation 29 governing failure of the "cls" class. In the second model, the format of equation 29 governing failure of the "opt" class is discussed. For simplicity, we shall assume that the principal stresses vary in a fixed ratio to each other, i.e., a state of proportional loading exists.

The Mechanical Equation of State for the "cls" Failure Mode:

Failure initiation of primary cracks in the "cls" mode occurs whenever the quantity $(\tau-\mu\sigma_N)$ equals τ_c, where τ and σ_n are the shear and normal stresses acting on the primary crack just undergoing failure initiation. This criterion is known as the modified Griffith failure condition (McClintock and Walsh, 1962). Figure 7 illustrates the angular range, $(\beta_1^{cLs})_{(n-1)}$ to $(\beta_2^{cLs})_{(n-1)}$, of primary cracks which have undergone failure initiation or are suitably oriented for failure initiation under the applied maximum principal compressive stress $(\sigma_{11})_{(n-1)}$ $(\geq\sigma_{11}^{cr})$. The subscript "(n-1)" refers to the increment levels (n=1,2,$\cdots$) of the applied stresses. For illustrative purposes and for ease of calculation, we shall let $k_2=k_3$ in this derivation.

As the stress $(\sigma_{11})_{(n-1)}$ is incremented by an amount $\Delta\sigma_{11}$ to the new value of $(\sigma_{11})_{(n)}$, two effects occur within the material structure. (1) The plans of primary cracks oriented within the incremental angular range, $[(\beta_2^{cLs})_{(n)}-(\beta_1^{cLs})_{(n)}]-[(\beta_2^{cLs})_{(n-1)}-(\beta_1^{cLs})_{(n-1)}]$, become suitably oriented for failure initiation (figure 7). (2) Further microcrack growth occurs from the

primary cracks oriented within the angular range $[(\beta_2^{cLs})_{(n-1)} - (\beta_1)_{(n-1)}]$. Both effects (1) and (2) result in an addition of volumetric microcrack strain due to void growth. However, the bulk of this additional volumetric microcrack strain should come from the latter effect. We shall postulate this to be the case. We shall further postulate that as the applied maximum principal stress is increased from $(\sigma_{11})_{(n-1)}$ to $(\sigma_{11})_{(n)}$, the change in the effective shear stress $[(\tau-\mu\sigma_n)]$ results in an increment in volumetric microcrack strain. If we neglect the volumetric microcrack strain rate, this condition will be mathematically formulated as

$$[(\tau)_{(n)} - \mu(\sigma_N)_{(n)}]_{\beta=(\beta_2^{cLs})_{(n-1)}} \cong B_1^{cLs}(\Delta\epsilon_{ii}^{mc})^p \quad , \tag{30}$$

where

$$(\tau)_{(n)} = \tfrac{1}{2}[(\sigma_{11})_{(n)} - (\sigma_{33})_{(n)}]\sin 2\beta$$

$$\mu(\sigma_N)_{(n)} = \tfrac{1}{2}\mu\left\{[\sigma_{11})_{(n)} + (\sigma_{33})_{(n)}] - [(\sigma_{11})_{(n)} - (\sigma_{33})_{(n)}]\cos 2\beta\right\} \tag{31}$$

$$\Delta\epsilon_{ii}^{mc} = (\epsilon_{ii}^{mc})_{(n)} - (\epsilon_{ii}^{mc})_{(n-1)} \quad .$$

The angle β in equation 30 is to be evaluated at the maximum value (β_2^{cLs}) when the applied stresses are $(\sigma_{11})_{(n-1)}$ and $(\sigma_{33})_{(n-1)}$. This angle delineates the boundary between the primary cracks suitably oriented for microcracking and those not suitably oriented for microcracking. This angle is derived in appendix G. The result is

$$(\beta_2^{cLs})_{(n-1)} = \frac{1}{2}\left[\tan^{-1}\frac{1}{\mu} + \cos^{-1}\frac{2\tau_c + \mu[(\sigma_{11})_{(n-1)} + (\sigma_{33})_{(n-1)}]}{\sqrt{1+\mu^2}\,[(\sigma_{11})_{(n-1)} - (\sigma_{33})_{(n-1)}]}\right] . \quad (32)$$

In equation 30, B_1^{cLs} and p are constants. If we assume proportional loading, $(\sigma_{33})_{(n-1)} = k(\sigma_{11})_{(n-1)}$, $(\sigma_{33})_{(n)} = k(\sigma_{11})_{(n)}$, and substitute equations 31 and 32 into equation 30, we find

$$\tau_c \frac{(\sigma_{11})_{(n)}}{(\sigma_{11})_{(n-1)}} \cong B_1^{cLs}(\Delta\epsilon_{11}^{mc})^p . \quad (33)$$

If we now sum over all the strain increments, $\epsilon_{11}^{mc} = \sum_{n=1}^{N}(\Delta\epsilon_{11}^{mc})$ (N is the number of stress increments), then

$$\epsilon_{11}^{mc} = \sum_{n=1}^{N}\left(\frac{\tau_c}{B_1^{cLs}}\right)^{\frac{1}{p}}\left[\frac{(\sigma_{11})_{(n)}}{(\sigma_{11})_{(n-1)}}\right]^{\frac{1}{p}} . \quad (34)$$

We shall define $(\sigma_{11})_{(o)} \equiv \sigma_{11}^{cr}$. If the stress increment $\Delta\sigma_{11}[\Delta\sigma_{11} = (\sigma_{11})_{(n)} - (\sigma_{11})_{(n-1)}]$ is constant, we can write $(\sigma_{11})_{(n)}$ and $(\sigma_{11})_{(n-1)}$ as

$$(\sigma_{11})_{(n-1)} = \sigma_{11}^{cr} + (n-1)\,\Delta\sigma_{11}$$

$$(\sigma_{11})_{(n)} = \sigma_{11}^{cr} + n\,\Delta\sigma_{11} ,$$

and equation 34 becomes

$$\epsilon_{11}^{mc} = \sum_{n=1}^{N}\left(\frac{\tau_c}{B_1^{cLs}}\right)^{\frac{1}{p}}\left[\frac{1 + n\,\frac{\Delta\sigma_{11}}{\sigma_{11}^{cr}}}{1+(n-1)\,\frac{\Delta\sigma_{11}}{\sigma_{11}^{cr}}}\right]^{\frac{1}{p}} . \quad (35)$$

Since ϵ_{11}^{mc} is the total volumetric microcrack strain, then if the total volumetric microcrack strain in the uniaxial test is to equal the same value in the general multiaxial case, then the ratio $\frac{\Delta\sigma_{11}}{\sigma_{11}^{cr}}$ in equation 35 must be an invariant, i.e.,

$$\frac{\Delta\sigma_{11}}{\sigma_{11}^{cr}} = \frac{\Delta c}{C_o} \tag{36}$$

where Δc is the stress increment in the uniaxial compression test and C_o is the stress required to initiate microcracking in the uniaxial compression test.

Equation 35 represents the mechanical equation of state for the "cls" failure mode when a condition of proportional loading exists and when both the temperature and volumetric microcrack strain rate are constant. The unknown constants B_1^{cLs} and p are to be evaluated from the simple uniaxial compression test.

When the functional relationship between the stress and volumetric microcrack strain can be approximated by a simple power function, equation 35 can be approximated by the equation

$$\epsilon_{11}^{mc} \simeq \left(\frac{1}{A_1^{cLs}}\right)^{\frac{1}{n}} \left[\frac{\sigma_{11}-\sigma_{11}^{cr}}{\sigma_{11}^{cr}}\right]^{\frac{1}{n}}$$

or (37)

$$\frac{\sigma_{11}-\sigma_{11}^{cr}}{\sigma_{11}^{cr}} \simeq A_1^{cLs} \left(\epsilon_{11}^{mc}\right)^n \quad .$$

This exponent $\underline{n}$ in equation 37 is a measure of the stress, over and above the stress required to initiate microcracking, required to cause total failure of the material. Accordingly, we shall define $\underline{n}$ to be the volumetric microcrack strain "hardening" exponent. The constant A_1^{cLs} will be defined the brittle strength coefficient.

The criterion of total failure (see appendix J and K) i.e., strength instability, is that total failure occurs once the volumetric microcrack strain attains a critical value, i.e., total failure occurs when

$$\epsilon_{11}^{m\,c} = \epsilon_f = \left[\frac{\sigma_{11}^f - \sigma_{11}^{cr}}{A_1^{cls}\,\sigma_{11}^{cr}} \right]^{\frac{1}{n}} , \tag{38}$$

where σ_{11}^f is the value of the maximum principal compressive stress at failure[8].

When the effects of volumetric microcrack strain rate are considered, an analysis similar to that above can be undertaken. This leads to the postulate that the mechanical equation of state governing failure of the "cls" class can be written as

$$\frac{\sigma_{11} - \sigma_{11}^{cr}}{\sigma_{11}^{cr}} \simeq H_1^{cls} (\epsilon_{11}^{m\,c})^n \; (\dot{\epsilon}_{11}^{m\,c})^m , \tag{39}$$

where H_1^{cls} is a constant, $\dot{\epsilon}_{11}^{m\,c} \left(\dot{\epsilon}_{11}^{m\,c} \equiv \frac{d\epsilon_{11}^{m\,c}}{dt} \right)$ is the volumetric microcrack strain rate, and the exponent $\underline{m}$ is a constant we shall define to represent the volumetric microcrack strain hardening rate.

The extension of the above analysis to the situation where a condition of true triaxial stress exists, while straightforward, is quite complex and such a derivation serves no practical use at this time. The effect of the intermediate principal stress (σ_{22}) for this class of failure initiation is shown in appendix J to be insignificant. If this conclusion can be verified experimentally, then equation 39 is suitable for engineering purposes.

---

[8] This failure criterion is shown in appendix J to be equivalent to the condition that total failure occurs when the total microcrack density attains a critical value, i.e., total failure occurs when a sufficient number of microcracks develop so that the probability is large of their joining up to form a macroscopic fracture surface.

The Mechanical Equation of State for the "opt" Failure Mode:

We recall that failure initiation of primary cracks in the "opt" mode occurs whenever the stress normal to the primary crack equals or exceeds $-\sigma_c$, i.e., $\sigma_N \leq -\sigma_c$ for failure initiation of the "opt" class. Figure 8 illustrates the angular range, $-(\beta_3^{opt})_{(n-1)}$ to $+(\beta_3^{opt})_{(n-1)}$, of primary cracks which are suitably oriented for failure initiation in this class. As the tensile stress $(\sigma_{33})_{(n-1)}$ is incremented by an amount $\Delta\sigma_{33}$ to the new value of $(\sigma_{33})_{(n)}$, the corresponding change in the normal stress results in an increment of volumetric microcrack strain due to continued void growth from primary cracks oriented within the above angular range. The procedure leads to the relationship

$$2\sigma_c \frac{(\sigma_{33})_{(n)}}{(\sigma_{33})_{(n-1)}} \simeq B_1^{opt} \ (\Delta\epsilon_{ii}^{mc})^s \quad , \tag{40}$$

where B_1^{opt} and $\underline{s}$ are constants and $\Delta\epsilon_{ii}^{mc}$ is the increment of volumetric microcrack strain occurring because of the increase of $(\sigma_{33})_{(n-1)}$ to the new value $(\sigma_{33})_{(n)}$. If we follow the approach used in deriving the equation of state for the "cls" failure mode, the mechanical equation of state at constant temperature for the "opt" failure mode can be written (proportional loading)

$$\frac{\sigma_{33}-\sigma_{33}^{cr}}{\sigma_{33}^{cr}} \simeq A_1^{opt} \ (\epsilon_{ii}^{mc})^r$$

$$(\sigma_{33}^{cr} = -\sigma_c) \tag{41}$$

for a fixed volumetric microcrack strain rate. We shall postulate that the general mechanical equation of state can be written

$$\frac{\sigma_{33}-\sigma_{33}^{cr}}{\sigma_{33}^{cr}} \cong H_1^{opt} (\epsilon_{ii}^{m\,c})^r \ (\dot{\epsilon}_{ii}^{m\,c})^q \quad . \tag{42}$$

In equation 42, the exponents r and q have identical meanings as their counterparts n and m in the "cls" failure mode.

Summary:

The three equations we have proposed to specify the behavior of brittle materials for the "cls" failure mode are

$$\begin{aligned} \epsilon_{11}^{m\,c} &\cong 0 \\ \epsilon_{22}^{m\,c} &\cong \left(\frac{1-k_2}{1-k_3}\right)^N \epsilon_{33}^{m\,c} \\ \frac{\sigma_{11}-\sigma_{11}^{cr}}{\sigma_{11}^{cr}} &\cong H_1^{cls} \ (\epsilon_{ii}^{m\,c})^n \ (\dot{\epsilon}_{ii}^{m\,c})^m \quad , \end{aligned} \tag{43}$$

and for the "opt" failure mode

$$\begin{aligned} \epsilon_{11}^{m\,c} &\cong 0 \\ \epsilon_{22}^{m\,c} &\cong \left(\frac{1-k_2}{1-k_3}\right)^M \epsilon_{33}^{m\,c} \\ \frac{\sigma_{33}-\sigma_{33}^{cr}}{\sigma_{33}^{cr}} &\cong H_1^{opt} \ (\epsilon_{ii}^{m\,c})^r \ (\dot{\epsilon}_{ii}^{m\,c})^s \quad . \end{aligned} \tag{44}$$

In equation 43 and 44, the constants H_1^{cls}, H_1^{opt}, n, m, r, and s are evaluated from the simple uniaxial compression and uniaxial tension test. The following section will illustrate the procedure required to measure these quantities.

THE MECHANICAL EQUATION OF STATE FOR WESTERLY GRANITE

Synopsis

The Westerly granite is a low porosity, hard brittle rock known to display brittle behavior over a wide range of conditions which include confining pressures of at least 75,000 psi and a variety of strain rates ranging from 10^{-5}/sec to 10^{-8}/sec (Brace, 1964; Brace, et al., 1966; Byerlee, 1968; Scholz, 1968a,b). Because of the extensive amount of experimental data available on the Westerly granite under confining compression, it is appropriate to compare the predictions of mechanical equation of state governing the "cls" failure mode to the experimental data of this material.

The Equation of State for the "cls" Failure Mode

Figure 9a illustrates the variation of the volumetric microcrack strain, ϵ_{ii}^{mc}, of the Westerly granite deformed at atmospheric pressure with a quantity defined as the percent of fracture stress (after Scholz, 1968a). The axial strain rate of this experiment was 1×10^{-5} /sec. Figure 9b shows the functional relationship of ϵ_{ii}^{mc} and the quantity $\left(\frac{\sigma_{11}-\sigma_{11}^{cr}}{\sigma_{11}^{cr}}\right)$ on a logarithmic ordinate-abscissa scale. The graph of log ϵ_{ii}^{mc} and log $\left(\frac{\sigma_{11}-\sigma_{11}^{cr}}{\sigma_{11}^{cr}}\right)$ is linear although there is a slight tendency for nonlinearity near structural instability (i.e., rupture) where the axial stress, σ_{11}, becomes equal to $1.88\,\sigma_{11}^{cr}$.

Recall that the equation of state (for a constant strain rate) for the "cls" failure mode was given by the relation

$$\frac{\sigma_{11}-\sigma_{11}^{cr}}{\sigma_{11}^{cr}} \cong A_1^{cls} \ (\epsilon_{11}^{mc})^n \quad . \tag{45}$$

If we take logarithms of both sides of equation 45 and determine the best fit of this equation to the data in figure 9b, the constants A_1^{cls} and n are found to be approximately 6.28 and 0.29, respectively. The solid curve connecting the data points in figure 9a was obtained from the equation

$$\frac{\sigma_{11}-\sigma_{11}^{cr}}{\sigma_{11}^{cr}} \cong 6.28 \ (\epsilon_{11}^{mc})^{0.29} \quad , \tag{46}$$

where the percent of fracture stress is replaced by the term $(\sigma_{11}-\sigma_{11}^{cr})/\sigma_{11}^{cr}$.

Table 1 shows the results of confined compression ($\sigma_{22}=\sigma_{33}=P$) tests on the Westerly granite (Scholz, 1968a). The critical stress (σ_{11}^{cr}) required to initiate microcracking, the fracture stress (σ_{11}^{f}), the value of the ratio of the difference between the fracture stress and the critical stress to the critical stress ($\frac{\sigma_{f1}-\sigma_{11}^{cr}}{\sigma_{11}^{cr}}$), and the value of the volumetric microcrack strain (F) taken at 95 percent of the fracture stress are shown. The best straight line fit of the critical stress ($<\sigma_{11}^{cr}>$) to initiate microcracking versus confining pressure (P) and the ratio $\frac{\sigma_{11}^{f}-<\sigma_{11}^{cr}>}{<\sigma_{11}^{cr}>}$ are also shown for comparison. Interpretation of this data suggests the following observations. (1) There is little significant variation of the quantity F with confining pressure. (2) The variation with confining pressure of the critical stress required to initiate microcracking is linear to a first order approximation. (3) The variation of fracture stress (σ_{11}^{f}) with confining pressure is clearly nonlinear. How-

ever, the magnitude of the nonlinearity tends to diminish as the confining pressure increases.

This data suggests that the dilatancy at fracture is not appreciably affected by the addition of confining pressure. Supporting this interpretation, Brace, et al., (1966), found evidence that the dilatancy at the fracture was not affected by confining pressure. Consequently, there may be a critical void ratio or equivalently, a critical volumetric microcrack strain, at fracture in the Westerly granite. Equation 38 is the analytical representation of this failure criterion.

TABLE 1

Results of Compression Tests on the Westerly Granite
(after Scholz, 1968a)
(1 kb≡15,000 psi)

Pressure (P) (kb)	σ_{11}^{cr} (kb)	$\langle\sigma_{11}^{cr}\rangle$ (kb)	σ_{11}^{f} (kb)	$\frac{\sigma_{11}^{f}-\sigma_{11}^{c}}{\sigma_{11}^{c}}$	$\frac{\sigma_{11}^{f}-\langle\sigma_{11}^{c}\rangle}{\langle\sigma_{11}^{c}\rangle}$	F (10^{-3})
0	1.44		2.81			0.78
0	1.50	1.50	2.82	0.88	0.88	0.88
0	1.56		2.84			0.89
1.00	5.34	3.90	8.90	0.66	1.28	1.66
2.00	7.00	6.20	13.40	0.91	1.16	1.13
3.00	8.16	8.50	16.60	1.03	0.95	1.96
4.00	9.70	10.80	19.80	1.04	0.91	0.98
5.00	12.40	13.20	21.80	0.76	0.65	1.20

$[\langle\sigma_{11}^{cr}\rangle \cong 22,500 \text{ psi} + 2.40\ P]$

For the Westerly granite, the uniaxial compressive (σ_{11}^{f}) and the failure initiation stress (σ_{11}^{cr}) are found from table 1 to be approximately 42,000 psi and 22,500 psi, respectively. Substituting these values into equation 38 gives a calculated critical volumetric microcrack strain value at fracture equal to 1.15×10^{-3}.

A typical uniaxial stress-strain curve of the Westerly granite is shown in figure 10a (after Brace, et al., 1966). The compressive strength for this rock at atmospheric pressure was found to be approximately 34,500 psi when the rock was deformed at an average axial strain rate of 10^{-6}/sec. In the test reported in figure 10a, the axial stress was increased at a rate of approximately 1500 psi/sec up to about one-half the fracture strength. The load was then held constant for several minutes at increments of a few hundred bars, giving the steps in both the axial (ϵ_{11}^*) and lateral (ϵ_{33}^*) stress-strain curves. Figure 10b shows the experimentally determined variation of the effective Poisson's ratio calculated from figure 10a. The theoretical value of the effective Poisson's ratio (ν^*) is determined from equations 12 and 46. The result is

$$\nu^* \cong \nu_f + \frac{E_f}{2\sigma_{11}} \left[\frac{\sigma_{11} - \sigma_{11}^{cr}}{6.82\ \sigma_{11}^{cr}} \right]^{3.45} , \qquad (47)$$

where

$$\nu_f \cong \nu + \tfrac{1}{2}(1-2\nu)\left(1 - \frac{E_f}{E}\right) . \qquad (48)$$

Here ν_f and E_f are the region II Poisson's ratio and Young's modulus, respectively. The intrinsic (crack-free) values of Young's modulus and Poisson's ratio are denoted by E and ν_1, respectively. The intrinsic values are known to be 0.24 for Poisson's ratio and 12×10^6 psi for Young's modulus (see Simmons and Brace, 1965). The region II values of the moduli are found from the slopes of the axial and lateral stress-strain curves in figure 10a. The results are approximately 0.31 and 8.5×10^6 psi for Poisson's ratio and

Young's modulus, respectively. If we substitute the values for E_f, E, and ν into equation 48, the theoretical value for ν_f is 0.31. This value is in agreement with the measured value.

The agreement between the theoretical and experimental variation of ν^* during regions III and IV is good although there is the tendency for the theoretical value to be somewhat less than the experimental value. This discrepancy may be due in part to the influence of the axial strain rate, i.e., the material constants used in equation 46 were obtained at an axial strain rate of approximately 10^{-5}/sec (Scholz, 1968a) while the experimental data illustrated in figure 10a was obtained with an axial strain rate value considerably less than 10^{-5}/sec (Brace, et al., 1966).

Figure 11a shows the observed stress dependence of creep (time dependent deformation) for the Westerly granite deformed under uniaxial compression (after Scholz, 1968b). There are three values of the volumetric microcrack strain rate reported; 0.5×10^{-6}/sec, 0.25×10^{-6}/sec, and 0.10×10^{-6}/sec. Figure 11b shows the constant stress creep data obtained from figure 11a on a log-log scale. Note that a linear relationship between $\log \epsilon_{11}^{mc}$ and $\log t$ ($t \equiv$ time) is indicated for a fixed value of the applied stress. The functional relationship of the mechanical equation of state ("cls" failure mode) is hypothesized to be

$$\frac{\sigma_{11}-\sigma_{11}^{cr}}{\sigma_{11}^{cr}} \cong H_1^{cLs} (\epsilon_{11}^{mc})^n \ (\dot{\epsilon}_{11}^{mc})^m \quad , \tag{49}$$

where $H_1^{cl\,s}$ is a constant, $\dot{\epsilon}_{ii}^{m\,c}$ is the volumetric microcrack strain rate, and m is a constant defined to be the volumetric microcrack strain hardening rate. If we take logarithms of both sides of equation 49 and determine the best fit of this equation to the experimental data in figure 11b, we find the constants $H_1^{cl\,s}$, n, and m to be approximately 544, 0.29, and 0.26, respectively. Notice that the exponent n determined from figure 11b agrees closely with the value of 0.29 calculated from figure 9b. The constant temperature mechanical equation of state for the Westerly granite can then be expressed as

$$\frac{\sigma_{11}-\sigma_{11}^{cr}}{\sigma_{11}^{cr}} \cong 544\ (\epsilon_{ii}^{m\,c})^{0.29}\ (\dot{\epsilon}_{ii}^{m\,c})^{0.26} \quad . \tag{50}$$

Because the exponent m is large, the mechanical behavior and in particular the fracture stress is sensitive to the volumetric microcrack strain rate. For example, a 100-fold increase or decrease in $\dot{\epsilon}_{ii}^{m\,c}$ results in a corresponding 3-fold increase or decrease in the quantity $\left(\frac{\sigma_{11}-\sigma_{11}^{cr}}{\sigma_{11}^{cr}}\right)$.

ILLUSTRATIVE PROBLEM: STABILITY OF A CIRCULAR TUNNEL IN BRITTLE ROCK

Synopsis

In this section the equations derived earlier in the thesis are used to solve the hypothetical problem of determining the collapse pressure for a circular tunnel driven into a cohesive brittle rock which is subjected to a uniform hydrostatic compressive stress field at a large radial distance from the opening (figure 12). Only the "cls" fracture mode is operative in this problem because all three principal stresses are compressive (Timoshenko and Goodier, 1951). The techniques used to solve this problem will also apply to problems where the "opt" failure mode is operative.

Statement of the Problem

In a certain region the ground stress is equal in all directions and increases linearly with depth at a rate of 1.24 psi/ft. Find the maximum safe depth at which an unsupported circular tunnel can be driven if the rock is the Westerly granite. The maximum safe depth is taken to occur at that depth where the pressure is large enough to result in the formation of a rupture (i.e., total failure accompanying initiation of spalling) zone in the rock mass. The factor of safety in this problem is unity.

In the statement of the problem, the term "safe" means that pieces of rock will not spall off from the tunnel surface. Spalling constitutes an instability that will result in total collapse, because as spalling continues, the conditions for continued spalling, namely a circular tunnel in the presence of a given ground stress, continue to exist. The hypothesis

which is the basis for this thesis is that collapse occurs when the calculated volumetric microcrack strain reaches a critical level which is characteristic of the rock in question. Thus, the critical volumetric microcrack strain is being regarded as a "property" of the rock. In this problem, the critical volumetric microcrack strain is determined from a uniaxial compression test, and is then used to determine the tunnel collapse pressure.

For the Westerly granite, rupture initiation occurs when the volumetric microcrack strain is 1.15×10^{-3}, as shown in figure 9b. To keep the mathematics comparatively simple, the effects of time dependent deformation (creep) and the additional strain components due to the deformation of open cracks and closed cracks undergoing frictional sliding are neglected. The errors due to neglecting the former effects are probably unacceptably large for engineering purposes, while those due to neglecting the latter effects might be acceptable. The hypothesis, however, does take these effects into account, and this hypothetical problem could be solved with these effects properly considered, if the numerical solution were properly modified to do so.

Test Data

The intrinsic (crack-free) values of Young's modulus and Poisson's ratio for the Westerly granite are 12×10^6 psi and 0.24, respectively. These values

have been calculated by Simmons and Brace (1965)[8]. The constants for the time independent mechanical equation of state are $A_1^{cls} = 6.28$ and $n = 0.29$. The critical value of the maximum principal stress required to initiate the first microcrack is $\sigma_{11}^{cr} \cong 22{,}500$ psi + 2.40 σ_{33} (see table 1), where σ_{33} is the value in psi of the least principal stress.

Analysis

We observe from the geometry of this problem that the radial, tangential, and axial directions are the principal directions. If the elastic strains in the tangential, radial, and axial directions are denoted by $\epsilon_{\theta\theta}$, ϵ_{rr}, and ϵ_{zz}, respectively, then the intrinsic (crack-free) elastic stress-strain relations for the Westerly granite can be written

$$\begin{aligned}
\epsilon_{\theta\theta} &= \frac{1}{12\text{x}10^6}\left[\sigma_{\theta\theta} - 0.24(\sigma_{rr}+\sigma_{zz})\right] \\
\epsilon_{rr} &= \frac{1}{12\text{x}10^6}\left[\sigma_{rr} - 0.24(\sigma_{\theta\theta}+\sigma_{zz})\right] \qquad (51) \\
\epsilon_{zz} &= \frac{1}{12\text{x}10^6}\left[\sigma_{zz} - 0.24(\sigma_{rr}+\sigma_{\theta\theta})\right] ,
\end{aligned}$$

where $\sigma_{\theta\theta}$, σ_{rr}, and σ_{zz} are the tangential, radial, and axial stresses, respectively. In this problem the maximum, intermediate, and least

---

[8]The intrinsic values of Young's modulus (E) and Poisson's ratio (ν) are determined by measuring the velocities of longitudinal and shear waves in a specimen subjected to a hydrostatic pressure which is large enough to close most of the open cracks in the specimen. If ρ is the specimen mass density and V_p and V_s denote the longitudinal and shear velocities when most open cracks are closed, then E and ν can be calculated from elasticity theory to be

$$E = \rho(3V_p^2 - 4V_s^2)\left[\left(\frac{V_p}{V_s}\right)^2 - 1\right]$$

$$\nu = \frac{1-2\left(\frac{V_s}{V_p}\right)^2}{2\left[1-\left(\frac{V_s}{V_s}\right)^2\right]}$$

principal compressive stresses are denoted by $\sigma_{\theta\theta}$ ($\sigma_{\theta\theta}\equiv\sigma_{11}$), σ_{zz} ($\sigma_{zz}\equiv\sigma_{22}$), and σ_{rr} ($\sigma_{rr}\equiv\sigma_{33}$). The equations governing the material behavior when microcracking of the "c1s" failure mode is occurring were derived earlier in the thesis (see equation 43). If $\epsilon^{mc}_{\theta\theta}$, ϵ^{mc}_{rr}, and ϵ^{mc}_{zz} denote the principal strains due to microcracking in the rock structure near the tunnel, then the equations relating these strains to the principal stresses for the Westerly granite were shown earlier to be

$$\epsilon^{mc}_{\theta\theta} \cong 0$$

$$\sigma_{\theta\theta} - \sigma^{cr}_{\theta\theta} \cong 6.28\ \sigma^{cr}_{\theta\theta}\ (\epsilon^{mc}_{ii})^{0.29} \qquad (52)$$

$$\epsilon^{mc}_{zz} \cong \left(\frac{\sigma_{\theta\theta}-\sigma_{zz}}{\sigma_{\theta\theta}-\sigma_{rr}}\right)^{N} \epsilon^{mc}_{rr} \ ,$$

where ϵ^{mc}_{ii} ($\epsilon^{mc}_{ii}=\epsilon^{mc}_{\theta\theta}+\epsilon^{mc}_{rr}+\epsilon^{mc}_{zz}$) is the total volumetric strain due to microcracking and $\sigma^{cr}_{\theta\theta}$ is the critical value of the tangential stress required to initiate the first microcrack. For the Westerly granite this stress is $\sigma^{cr}_{\theta\theta} \cong 22{,}500 + 2.40\ \sigma_{rr}$. This stress can be determined from the triaxial compression test [where the intermediate and least principal stresses are equal ($\sigma_{22}=\sigma_{33}$)] by measuring the magnitude of the maximum principal stress (σ_{11}) required to initiate the first microcrack. This testing technique has been described in detail by Brace, et al., (1966) as well as the procedure required to measure this quantity. The approximation is made in this problem that the exponent N in equation 52 is one. To calculate this quantity, the values of the microcrack strains in the multiaxial test

($\sigma_{11} \neq \sigma_{22} \neq \sigma_{33}$) must be known. Such test data for the Westerly granite, or for that matter any brittle rock, does not exist at this time. However, the exponent N might be close to unity, such as in metals (Lubahn and Felgar, 1961).

The length in the axial direction does not change since the total change in axial strain due to driving the tunnel is zero:

$$\Delta\lambda_{zz} = \Delta\epsilon_{zz} + \epsilon_{zz}^{mc} = 0 \tag{53}$$

where $\Delta\lambda_{zz}$ and $\Delta\epsilon_{zz}$ denote the changes in the total and intrinsic elastic strains due to driving the tunnel.

Since there is cylindrical symmetry, the force equilibrium and strain compatibility (for small strains) conditions in differential form are (Lubahn and Felgar, 1961).

$$\begin{aligned} \frac{d(r\sigma_{rr})}{dr} &\cong \sigma_{\theta\theta} \\ \frac{d(r\lambda_{\theta\theta})}{dr} &= \lambda_{rr} \quad , \end{aligned} \tag{54}$$

where $\lambda_{\theta\theta}$ ($\lambda_{\theta\theta}=\epsilon_{\theta\theta}+\epsilon_{\theta\theta}^{mc} \cong \epsilon_{\theta\theta}$) and λ_{rr} ($\lambda_{rr}=\epsilon_{rr}+\epsilon_{rr}^{mc}$) are the total tangential and radial strains, respectively.

To calculate the stress distribution within the rock structure, the calculations are begun at large radial distances from the tunnel wall where the stress conditions are known. If a is the radius of the tunnel, then at radial distances (r) into the rock equal to r_c (3a or 4a, perhaps) the stress distribution is given accurately by elasticity theory, i.e.,

$$\sigma_{\theta\theta} = P\left[1 + \left(\frac{a}{r}\right)^2\right]$$

$$\sigma_{rr} = P\left[1 - \left(\frac{a}{r}\right)^2\right] \quad (r_c < r < \infty) \tag{55}$$

$$\sigma_{zz} = P \quad ,$$

where P is the hydrostatic pressure existing in the rock at a large radial distance from the opening[9]. We now work toward the tunnel in small intervals of radius until we come to the opening. At this point, the radial stress is zero. Equation 54 can be applied to each interval of radius by expressing these relations in finite difference form:

$$\frac{r_2\sigma_{rr(2)} - r_1\sigma_{rr(1)}}{r_2 - r_1} = \frac{1}{2}\left[\sigma_{\theta\theta(1)} + \sigma_{\theta\theta(2)}\right]$$

$$\frac{r_2\lambda_{\theta\theta(2)} - r_1\lambda_{\theta\theta(1)}}{r_2 - r_1} = \frac{1}{2}\left[\lambda_{rr(1)} + \lambda_{rr(2)}\right] \quad , \tag{56}$$

where numerical subscripts $_1$ and $_2$ on the stresses and total strains refer to their evaluation at r_1 and r_2 $(r_2 < r_1)$, respectively.

Conditions at all radial distances less than $r = r_c$ can be determined by iteration if it is recognized that a small change in radius will cause only a small change in the stress or strain values. Therefore equation 56 provides a good first approximation to σ_{rr} and $\lambda_{\theta\theta}$ just below r_c if $\sigma_{\theta\theta}$ and λ_{rr} are assumed to be uniform at their values at r_c over a short distance below this point. Taking note of the fact that $\lambda_{\theta\theta} \cong \varepsilon_{\theta\theta}$ solving equation 56 for the

[9] The radial distance (r_c) is taken to be much larger than the radial distance (r_e) (see figure 13d), a location where the radial stress (σ_{rr}) is large enough to prohibit the formation of the first microcrack.

subsurface conditions (subscript 2) in terms of the known conditions (subscript 1) gives

$$\sigma_{rr(2)} = \frac{r_1}{r_2}\,\sigma_{rr(1)} + \frac{\Delta r}{2r_2}\,[\sigma_{\theta\theta(1)} + \sigma_{\theta\theta(2)}]$$
$$\epsilon_{\theta\theta(2)} = \frac{r_1}{r_2}\,\epsilon_{\theta\theta(1)} + \frac{\Delta r}{2r_2}\,[\lambda_{rr(1)} + \lambda_{rr(2)}] \qquad (57)$$

where Δr ($\Delta r = r_2 - r_1$) is the incremental change in radius. If we assume that $\sigma_{\theta\theta}$ and λ_{rr} are uniform between r_2 and r_1, the first approximation to σ_{rr} and $\epsilon_{\theta\theta}$ can be found. We can now find the other stresses and strains at $r=r_2$ by combining equations 51 and 52. In particular, we wish to find the values of $\sigma_{\theta\theta}$ and λ_{rr} at $r=r_2$ so that these new values can be used again in equation 57 to obtain still better values of σ_{rr} and $\epsilon_{\theta\theta}$ at $r=r_2$. With these new values of $\sigma_{\theta\theta}$ and λ_{rr}, still more accurate values of the stresses and total strains are possible. This iteration process is continued until convergence of the stress and strain values to exact values is obtained. Thus in the first cycle of the iteration procedure, the values of $\sigma_{\theta\theta}$ and λ_{rr} at $r=r_1$ are used in equations 51, 52, and 57. In subsequent cycles, values from the previous cycle are used.

The same procedure as discussed above can be used for successive radius intervals $r=r_1$ to $r=r_1-\Delta r$, $r=r_1-2\Delta r$ to $r=r_1-n\Delta r$, et cetera, starting with the known conditions at the larger radius and calculating the unknown quantities at the smaller radius. In this way the entire family of stress distributions for one value of the pressure (P) can be found. The curves for other pressures can be obtained similarly by starting with other values of

$\sigma_{\theta\theta}$ and σ_{rr} at $r=r_c$. In principal, the stresses and strains could be determined by directly solving equations 51, 52, and 54. However, the procedure is not simple because the relation between the volumetric microcrack strain and the tangential stress is not a simple algebraic expression. Therefore, a numerical procedure to determine the stresses and strains is required.

Figure 13 (a,b,c) shows the effect of microcracking on the tangential, radial, and axial stress distributions for values of applied pressure ranging from 11,250 psi (at which microcracking begins at a=r) to 31,250 psi (which is larger than the collapse pressure). Also shown adjacent to each curve in figure 13a is the value of the volumetric microcrack strain component at the tunnel wall. A CDC 3800 digital computing machine was used to obtain these solutions[10]. Notice that once microcracking is initiated in the rock ($P \geq 11,250$ psi), the tangential stress begins to increase near the tunnel wall to values greater than would be predicted from elasticity theory, i.e., $\sigma_{\theta\theta}$ $(r=a) > 2P$. For the range of pressure values studied, the radial stress remained unaffected by microcracking, i.e., $\sigma_{rr} \cong P\left[1 - \left(\frac{a}{r}\right)^2\right]$ for all values of r. The boundary delineating the microcrack zone and the purely elastic zone is clearly indicated in figure 13b.

---

[10]For purposes of calculation, the radius of tunnel was 72 inches, the radius width interval (Δr) was 2 inches, and the radius r_c (that radius where no microcracking can occur) was taken to be 244 inches. A total of six iterations for each radius interval was found adequate to ensure convergence of the stresses and strains to their exact values.

The value of the collapse pressure (pressure required to give a value of the volumetric microcrack strain equal to 1.15×10^{-3}) is approximately 18,500 psi (obtained from figure 13a by crossplotting at r/a and reading off P at $\varepsilon_{ii}^{mc} = 1.15 \times 10^{-3}$). The depth corresponding to this pressure is 14,755 ft using a pressure gradient of 1.24 psi/ft. Therefore, the maximum safe depth at which an unsupported circular tunnel can be driven in this rock structure is 14,755 ft. This depth is somewhat different from the depth of 16,900 ft that would be found if one obtained the stress distribution by simple elasticity theory, instead of using the correct combination of elasticity theory and microcracking theory, but used the same failure criterion, namely that failure occurs at a critical value of the volumetric microcracking strain. In this case, equal values of critical volumetric microcracking strain in the compression test specimen and at the tunnel wall also means equal values of longitudinal stress in the compression specimen and tangential stress at the tunnel wall, because of the similarity of the state of stress and the fact that there is no effect of the intermediate principal stress.

Summary

The material properties used in this problem were those for Westerly granite. For this rock material, the tangential stresses at r = a required for microcrack initiation and rupture correspond to 22,500 psi and 42,000 psi, respectively.

It was shown that microcracking is initiated at the tunnel opening at an applied pressure of 11,250 psi. This pressure corresponds to a tangential stress value of 22,500 psi at the tunnel opening. Once microcracking is initiated in the structure, both the tangential and axial stresses tend to increase near the tunnel wall to values greater than the values predicted by elasticity theory. The applied pressure required to initiate rupture was shown to be approximately 18,500 psi. This pressure value results in a maximum design depth for the tunnel of 14,755 ft for a region where the pressure gradient is 1.24 psi/ft.

SUMMARY AND CONCLUSIONS

The results of a theoretical study of the stress-strain behavior of homogeneous brittle rocks up to and including total failure has been presented. To simulate the grain boundary cracks and microfractures commonly found in natural brittle rock structures, it was assumed that brittle rock can be mathematically modeled by an elastically isotropic continuum containing a large number of narrow ellipsoidal-like cracks collectively characterized by a statistical distribution function which specifies both the geometry and the orientation of the cracks to a coordinate system fixed with respect to the specimen. It was shown that this model of brittle rock admitted an analytical representation of both the closure of open cracks under compressive stress and the frictional sliding of closed cracks which are favorably oriented with respect to the applied stress system. Analytical expressions were presented for the stress-strain relationships of brittle materials displaying these characteristics.

Experimental data on the fracturing characteristics of brittle rock has shown that when the applied stresses are large enough, failure initiation or microcracking occurs within the rock structure. We considered two models of microcracking in this thesis. (1) Failure initiation from closed cracks ("cls" failure class) was assumed to occur when the orientation of the cracks satisfies the modified Griffith criterion which states that closed crack failure initiation occurs when the difference between the shear stress and the frictional shear stress acting along a crack surface exceeds a critical value. (2) Failure initiation from open cracks ("opt" failure class) was assumed to occur once the applied tensile stress acting normal to the crack surface exceeds a critical value.

Three relationships between the microcracking strains for either failure mode and the principal stresses were hypothesized to describe the behavior of brittle materials undergoing failure. The three relationships are: (1) The constant microcrack strain criterion. This rule states that the principal microcrack strain in the direction of the maximum principal stress axis is approximately zero for either failure mode. (2) The constant stress difference-microcrack strain difference ratio criterion. This rule states that there is a constant ratio between the difference of any two principal stresses and the difference of the two corresponding principal microcrack strains. (3) The mechanical equation of state for brittle materials. This rule states that the constant temperature behavior for either failure mode of brittle materials can be described by an equation of the form $S_o = H_1 (\epsilon_{1f}^{m,c})^n (\mathring{\epsilon}_{1f}^{m,c})^m$, where S_o is an equivalent stress, H_1, n, and m are material constants,

ϵ^{mc}_{ii} is the volumetric microcrack strain, and $\dot{\epsilon}^{mc}_{ii}$ is the volumetric microcrack strain rate. The quantities H_1, n, and m are constants which can be measured from the uniaxial stress-strain test; uniaxial compression test for the "cls" class, uniaxial tension test for the "opt" class. This relationship was applied to the uniaxial compression data of the Westerly granite. It was shown that the equation of state written as $S_o = \frac{\sigma_{11}-\sigma^{cr}_{11}}{\sigma^{cr}_{11}} \cong 544\ (\epsilon^{mc}_{ii})^{0.29}\ (\dot{\epsilon}^{mc}_{ii})^{0.26}$, where σ^{cr}_{11} is the applied uniaxial stress required to initiate microcracking, could accurately predict the observed stress-strain behavior of this rock.

The three rules were applied to solve a hypothetical engineering design problem in brittle rock. The problem was concerned with predicting the collapse pressure of a circular tunnel in a brittle rock which is subject to a uniform hydrostatic stress at large radial distances from the opening.

Let us note that the need for further experimental work on the mechanical behavior of brittle rock is apparent. While rules 1 and 3 governing the "cls" failure class appear to satisfactorily predict the observed dependence of the stresses, microcrack strains, and microcrack strain rates of one rock (the Westerly granite) deformed under uniaxial compression, rule 2 for the "cls" class and rules 1, 2, and 3 for the "opt" class cannot be checked at the present time due to the absence of experimental observations on both the stress-strain behavior of brittle rock under true triaxial stress conditions and the stress-strain behavior of brittle rock under applied tension stresses. Further experimental work should be concentrated at first on

determining the behavior of homogeneous monomineralic (single crystal phase) rock structures. A monomineralic rock structure avoids some of the problems involved in using polyphase structures, like granite, which can exhibit a wide range in values of the friction coefficients along crack surfaces. It has been shown that this additional variable considerably complicates the detailed study of the experimental results (see appendix K).

REFERENCES

1. Bieniawski, Z. T., Mechanism of Brittle Fracture of Rock, Parts I, II, and III, Int. J. Rock Mech. Min. Sci., v. 4, pp. 395-430, 1967.
2. Birch, F., The Velocity of Compressional Waves in Rocks to 10 Kilobars, Part I, J. J. Geoph. Res., v. 65, pp. 1083-1102, 1960.
3. Bishop, J. F. W. and R. Hill, A Theory of Plastic Distortion of a Polycrystalline Aggregate Under Combined Stresses, Phil. Mag. 42, p. 414, 1951.
4. Brace, W. F., Brittle Fracture of Rock, in State of Stress in the Earth's Crust, Elsevier Press, pp. 111-178, 1964.
5. Brace, W. F. and A. S. Orange, Electrical Resistivity Changes in Saturated Rocks During Fracture and Frictional Sliding, J. Geophys. Res., 73 (4), pp. 1433-1445, 1968.
6. Brady, B. T., A Statistical Theory of Brittle Fracture for Rock Materials, Part I, Brittle Fracture Under Homogeneous Axisymmetric States of Stress, Int. J. Rock Mech. Min. Sci. (in press), 1968a.
7. Brady, B. T., A Statistical Theory of Brittle Fracture for Rock Materials, Part II, Brittle Fracture Under Homogeneous Triaxial States of Stress, Int. J. Rock Mech. Min. Sci. (in press), 1968b.
8. Brady, B. T. and W. Blake, An Elastic Solution of the Laterally Constrained Circular Cylinder Under Uniaxial Loading, Proc. of Tenth Rock Mechanics Symp. (in press), Austin, Texas, 1968c.
9. Brady, B. T., On Solid Friction Attenuation Scheme for Dry Brittle Rock, Proc. of the Ninth Rock Mechanics Symp. (in press), 1968d.
10. Broutman, L. J. and R. H. Cornish, Effects of Polyaxial Stress States on the Failure Strength of Alumina Ceramics, J. Am. Ceram. Soc., v. 48, pp. 519-525, 1965.
11. Brown, J. W. and M. M. Singh, An Investigation of Microseismic Activity in Rock, Trans. AIME, v. 238, pp. 255-264, 1966.

12. Byerlee, J. D., Frictional Characteristics of Westerly Granite, Ph.d. thesis, Massachusetts Institute of Technology, 1966.
13. Cook, N. G. W., J. C. Jaeger, and G. A. Wiebols, Rock Property Tests in a Stiff Testing Machine, Proc. of the Tenth Rock Mechanics Symp. (in press), 1968.
14. Fisher, J. C. and J. H. Holloman, A Statistical Theory of Fracture, Trans. of the AIME, pp. 546-561, 1947.
15. Frenkel, J., II, and T. A. Kontorova, A Statistical Theory of the Brittle Strength of Real Crystals, J. Phys. U.S.S.R. 7, 108, 1943.
16. Griffith, A. A., The Phenomena of Rupture and Flow in Solids: Roy. Soc. London Philos. Trans., ser. A., v. 221, pp. 163-198, 1921.
17. Grigg, D. T., F. J. Turner, and H. C. Heard, Deformation of Rocks at 500° to 800° C., Geol. Soc. Amer. Mem., v. 79, pp. 39-104, 1960.
18. Handin, J. and R. V. Hager, Jr., Experimental Deformation of Sedimentary Rocks Under Confining Pressure: Tests at Room Temperature on Dry Sample, Bull. Am. Assoc. Petro. Geol., v. 41, pp. 1-50, 1957.
19. Handin, J., H. C. Heard, and J. N. Magouirk, Effects of the Intermediate Principal Stress on the Failure of Limestone, Dolomite, and Glass at Different Temperatures and Strain Rates, J. Geophys. Res., 72, pp. 611-640, 1967.
20. Hashin, A., The Moduli of an Elastic Solid, Containing Spherical Particles of Another Elastic Material, in Nonhomogeneity in Elasticity and Plasticity, edited by W. Olszak, Pergamon Press, New York, pp. 463-478, 1959.
21. Hast, N., The Measurement of Rock Pressure in Mines, Sveriges Geol. Underskn., Arsbok, 52, No. 3, 1958.
22. Heard, H. C. Transition From Brittle Fracture to Ductile Flow in Solenhofen Limestone as a Function of Temperature, Confining Pressure and Interstitial Fluid Pressure, Geol. Soc. Amer. Mem., v. 79, pp. 193-226, 1960.

23. Hill, R., The Elastic Behavior of a Crystalline Aggregate, Proc, Phys. Soc. London, A., 65, pp. 349-354, 1952.

24. Hubbert, M. K. and W. W. Rubey, Role of Fluid Pressure in Mechanics of Overthrust Faulting, Full. Geol. Soc. Am., v. 70, pp. 115-166, 1959.

25. Jaeger, J. C., Elasticity, Fracture and Flow, John Wiley and Sons, Inc., New York, 208 p., 1962.

26. Lubahn, J. D. and R. P. Felgar, Plasticity and Creep of Metals, John Wiley and Sons, Inc., New York, 608 p., 1961.

27. Matsushima, S., On the Flow and Fracture of Igneous Rocks: Disaster Research Inst. Bull., No. 36, pp. 1-9, 1960.

28. McClintock, F. A. and J. Walsh, Friction on Griffith Cracks in Rocks Under Pressure, Proc. Fourth Nat. Cong. Appl. Mech., pp. 1015-1021, 1962.

29. Mogi, K., Experimental Study of Deformation and Fracture of Marble (1st paper), On the Fluctuation of Compressive Strength of Marble and the Relation to the Rate of Stress Application, Bull. Earthquake Res. Inst. Tokyo Univ., 37, pp. 155-170, 1959.

30. Mogi, K., Some Precise Measurements of Fracture Strength of Rocks Under Uniform Compressive Stress, Rock Mech. Eng. Geol., 4, pp. 41-55, 1966.

31. Mogi, K., Effect of the Intermediate Principal Stress on Rock Failure, J. Geophys. Res. 72, pp. 5117-5131, 1967.

32. Nadai, A., Theory of Flow and Fracture of Solids, McGraw-Hill, New York, v. 1, 2nd ed., 572 pp., 1950.

33. Odė, H., Faulting as a Velocity Discontinuity in Plastic Deformation, Geol. Soc. Amer. Mem., v. 79, pp. 293-323, 1960.

34. Paulding, B. W., Jr., Crack Growth During Brittle Fracture in Compression, Ph.d. thesis, Massachusetts Institute of Technology, 1965.

35. Reuss, A., Berechnung der Fleissgrenze von Mischkristallen auf Grund der Plastizitats bedingung fur Einkrisalle, Z. Angew. Math. Mech., 9, 49, 58, 1929.

36. Scholz, C. H., Microfracturing and the Inelastic Deformation of Rock in Compression, J. Geophys. Res., v. 73, No. 4, pp. 1417-1432, 1968.

37. Scholz, C. H., Mechanism of Creep in Brittle Rock, J. Geophys. Res., v. 73, No. 10, pp. 3295-3302, 1968.

38. Simmons, G. and W. F. Brace, Comparison of Static and Dynamic Measurements of Compressibility of Rocks, J. Geophys. Res., 70 (22), pp. 5649-5656, 1965.

39. Stevenson, A. C., Complex Potential in Two-Dimensional Elasticity, Proc. Roy. Soc. London, A., 184, pp. 129-179, 1945.

40. Timoshenko, S. and J. N. Goodier, Theory of Elasticity, McGraw-Hill, Book 6, 506 pp., 1951.

41. Voight, W., Lehrbuch der Kristallphysik, B. G. Terebner, Leipzig, 1928.

42. Walsh, J. B., The Effect of Cracks on the Compressibility of Rock, J. Geophys. Res., v. 70, No. 2, pp. 381-389, 1965a.

APPENDIX A

EVALUATION OF $\oint\!\!\oint u_i \bar{v}_i dA_c$ (i = 1,3) FOR THE CASE OF AN ELLIPTICAL CRACK UNDER BIAXIAL STRESS

The displacement field of an inclined narrow elliptical flaw in a body under the condition of plane stress or plane strain can be calculated by a technique established by Stevenson (1945). If the intermediate principal stress (σ_{22}) is normal to the plane of the crack, the displacements u_1 and u_3 at the crack boundary due to the biaxial stresses σ_{11} and σ_{33} ($\sigma_{11} \geq \sigma_{33}$) can be evaluated by using Stevenson's complex variable method. The displacements u_1 and u_3 are related to stress functions $\Omega(z)$ and $\omega(z)$ by the equation

$$8G\,(u_1+u_3) = e^{-i\beta}\left[\,\theta_o \Omega(z) - z\bar{\Omega}'(\bar{z}) - \bar{\omega}'(\bar{z})\,\right] , \qquad \text{(A1)}$$

where G is the shear modulus of the solid material, bars indicate complex conjugate, primes signify derivatives with respect to the complex variable z, β is the inclination of the crack major axis to the axis of the maximum principal stress (σ_{11}) and

$$\begin{aligned} (1+\theta_o) &= 4(1-\nu) && \text{Plane Strain} \\ (1+\theta_o) &= 4/(1+\nu) && \text{Plane Stress} \end{aligned} \qquad \text{(A2)}$$

ν = Poisson's ratio .

The Cartesian coordinates ($z = x_1 + ix_3$) are related to the elliptical hyperbolic coordinates ($\zeta = \xi + i\eta$) (figure A1) by the transformation

$$z = c(\cosh\zeta) \quad , \qquad \text{(A3)}$$

where $\underline{c}$ is the major semi-axis of the crack ellipse. For an elliptical crack the stress functions $\Omega(z)$ and $\omega(z)$ are

$$\begin{aligned} \Omega(z) &= c(A\cosh\zeta + B\sinh\zeta) \\ \omega(z) &= c^2(C\zeta + D\cosh 2\zeta + E\sinh 2\zeta) \quad , \end{aligned} \tag{A4}$$

where A, B, C, D, E are complex constants which depend on the boundary conditions (Timenshenko, 1951). If α ($\alpha=\frac{b}{c}$, b and c are the minor and major axes half lengths, respectively) is the crack eccentricity and if $\alpha^2 \cong 0$, then the substitution of equation A4 into equation A1 gives

$$8G\ (u_1 - u_3) = e^{-i\beta}(M^* + iN^*) \quad , \tag{A5}$$

where

$$\begin{aligned} M^* &= (1+\theta_o)\, c\, (A_1\cos\eta - C_1\alpha\cos\eta - B_2\sin\eta) \\ N^* &= (1+\theta_o)\, c\, (A_1\alpha\sin\eta + B_1\sin\eta + B_2\alpha\cos\eta) \quad . \end{aligned} \tag{A6}$$

Equation A5 can be rewritten as

$$\begin{aligned} 8G\ u_1 &= M^*\cos\beta - N^*\sin\beta \\ 8G\ u_3 &= (M^*\sin\beta + N^*\cos\beta) \quad , \end{aligned} \tag{A7}$$

where the angle β is the inclination of the crack major axis to the axis of the maximum principal stress. For an open crack, the coefficients ($A=A_1+iA_2$) are (Timenshenko, 1951)

$$\begin{aligned} A_1 &= N(1+2\alpha)\cos 2\beta & C_2 &= 0 \\ A_2 &= 0 & D_1 &= -\frac{1}{2}N(1+2\alpha)\cos 2\beta \\ B_1 &= M - N(1+2\alpha)\cos 2\beta & D_2 &= -\frac{1}{2}N(1+2\alpha)2\alpha\sin 2\beta \\ B_2 &= -N(1+2\alpha)\sin 2\beta & E_1 &= \frac{1}{2}N(1+2\alpha)2\alpha\cos 2\beta \\ C_1 &= -(M - N\cos 2\beta) & E_2 &= \frac{1}{2}N(1+2\alpha)\sin 2\beta \quad , \end{aligned} \tag{A8}$$

and for the closed crack (assuming that Amonton's law of dry friction is valid) the coefficients are

$$\begin{aligned} A_1 &= M & C_2 &= 0 \\ A_2 &= 0 & D_1^2 &= \tfrac{1}{2}\cos 2\beta \\ B_1 &= 0 & D_2 &= \tfrac{1}{2}\mu(M-N\cos 2\beta) \\ B_2 &= N\sin 2\beta - \mu(M-N\cos 2\beta) & E_1 &= 0 \\ C_1 &= 0 & E_2 &= -\tfrac{1}{2}B_2 \end{aligned} \tag{A9}$$

where $M = (\sigma_{11}+\sigma_{33})$ and $N = (\sigma_{11}-\sigma_{33})$.

Following the procedure outlined by Walsh (1965b), the surface displacement integrals are[1A/]

$$\begin{aligned} \iint u_1 \bar{\nu}_1 dA_c &\cong \frac{2\pi c^3(1+\theta_o)}{8G}\,(2\sigma_{11}\sin^2\beta) \\ \iint u_3 \bar{\nu}_3 dA_c &\cong \frac{2\pi c^3(1+\theta_o)}{8G}\,(2\sigma_{33}\cos^2\beta) \end{aligned} \tag{A10}$$

for the open crack and

$$\iint u_1 \bar{\nu}_1 dA_c \cong \frac{\pi c^3(1+\theta_o)}{2G}\,\sin\beta\cos\beta\,\left[\,(\sigma_{11}-\sigma_{33})(\sin\beta\cos\beta-\mu\sin^2\beta) - \mu\sigma_{33}\right] \tag{A11}$$

$$\iint u_3 \bar{\nu}_3 dA_c \cong -\iint u_1 \bar{\nu}_1 dA_c$$

for the closed sliding crack. When the least principal stress (σ_{33}) is zero, equations A10 and A11 reduce to Walsh's (1965b) relationships.

[1A/] A_c = surface area of crack.
$\bar{\nu}_j$ = normal to the surface in the j^{th} direction.

APPENDIX B

EVALUATION OF $\oiint u_i \bar{\nu}_i dA_c$ (i=1,2,3) FOR THE CASE OF AN ELLIPTICAL CRACK UNDER TRIAXIAL STRESS

For the case of open cracks under biaxial loading, it is shown in Appendix A that the resulting strains can be derived by assuming that the volumetric open strain component ($d\epsilon_{ii}^{op}$) is proportional to the stress normal to the plane of the crack[1B]. If we assume that a similar condition holds for the three-dimensional case, the open crack strain increments in differential form are

$$(d\epsilon_{11}^{op})_n = \frac{1}{V}\left[d\oiint u_1\bar{\nu}_1 dA_c\right]_{op} \cong \frac{\pi A c^3}{2V}\sin^2\beta d\sigma_{11}$$

$$(d\epsilon_{22}^{op})_n = \frac{1}{V}\left[d\oiint u_2\bar{\nu}_2 dA_c\right]_{op} \cong \frac{\pi A c^3}{2V}\cos^2\beta\cos^2\varphi d\sigma_{22} \qquad \text{(B1)}$$

$$(d\epsilon_{33}^{op})_n = \frac{1}{V}\left[d\oiint u_3\bar{\nu}_3 dA_c\right]_{op} \cong \frac{\pi A c^3}{2V}\cos^2\beta\sin^2\varphi d\sigma_{33} \ ,$$

where A is a constant.

To estimate the strain due to frictional sliding on an arbitrarily oriented crack under triaxial loading, we have

$$(d\epsilon_{pr}^{cls})_n \cong l_{pn}l_{rq}(d\epsilon_{nq}^{cls})_n \ , \qquad \text{(B2)}$$

where $(d\epsilon_{nq}^{cls})_n$ is the shearing strain (acting in the direction of τ) resulting from sliding on the n^{th} crack surface[2B]. The magnitude of this strain is

$$(d\epsilon_{nq}^{cls})_n = \frac{\pi A c^3}{2V} d(\tau - \tau_f) \qquad \text{(B3)}$$

[1B] The superscript "op" refers to the open crack component.

[2B] The superscript "cls" refers to the closed sliding crack component.

by analogy with the two-dimensional case outlined in Appendix A. The direction cosines (l_{pn}, l_{rq}) and the stresses (τ, τ_f) are (Jaeger, 1962)

$$
\begin{aligned}
&l_{1n} \equiv l = \sin\beta \quad ; \qquad l_{2n} \equiv m = \cos\beta\cos\varphi \quad ; \qquad l_{3n} \equiv n = \cos\beta\sin\varphi \\
&l_{1q} = a\left[l\{(\sigma_{11}-\sigma_{33})\, n^2 - (\sigma_{22}-\sigma_{11})\, m^2\}\right] \\
&l_{2q} = a\left[m\{(\sigma_{22}-\sigma_{11})\, l^2 - (\sigma_{33}-\sigma_{22})\, n^2\}\right] \\
&l_{3q} = a\left[n\{(\sigma_{33}-\sigma_{22})\, m^2 - (\sigma_{11}-\sigma_{33})\, l^2\}\right] \qquad \text{(B4)} \\
&\tau_f = \mu\sigma_N = \mu(l^2\sigma_{11}+m^2\ \sigma_{22}+n^2\sigma_{33}) \\
&\tau = \sqrt{l^2\sigma_{11}^2+m^2\ \sigma_{22}^2+n^2\ \sigma_{33}) - \sigma_N^2}
\end{aligned}
$$

The unknown quantity $\underline{a}$ is evaluated from the relation $l_{1q}^2+l_{2q}^2+l_{3q}^2 = 1$. When $\varphi = 90°$, the two-dimensional equations result. For an axisymmetric stress state $(\sigma_{22} = \sigma_{33})$, equation B2 gives

$$
\begin{aligned}
(d\epsilon_{11}^{cls})_n &= \sin\beta\ \cos\beta\ (d\epsilon_{nq}^{cls})_n \\
(d\epsilon_{22}^{cls})_n &= -\ \sin\beta\ \cos\beta\ \cos^2\varphi\ (d\epsilon_{nq}^{cls})_n \qquad \text{(B5)} \\
(d\epsilon_{33}^{cls})_n &= -\ \sin\beta\ \cos\beta\ \sin^2\varphi\ (d\epsilon_{nq}^{cls})_n \quad ,
\end{aligned}
$$

for the closed sliding crack("cls") strain components along the coordinate axes. The strain $(d\epsilon_{nq}^{cls})_n$ is defined to be

$$
(d\epsilon_{nq}^{cls})_n = \frac{\pi A c^3}{2V}\left[(1-k)\ (\sin\beta\cos\beta - \mu\sin^2\beta) - \mu\, k\right] d\sigma_{11} \quad . \qquad \text{(B6)}
$$

APPENDIX C

STRESS REQUIRED TO CLOSE AN ECCENTRIC ELLIPTICAL CRACK

The normal displacement ($u_\perp$) of the crack boundary due to the principal stress components (σ_{11}, σ_{33}) is

$$u_\perp = u_1 \sin\beta + u_3 \cos\beta \quad . \tag{C1}$$

We shall consider that the crack has closed when $u_\perp = b$ at $\eta = \pi/2$ (refer to figure A1). From equations A6 and A7,

$$8G\, b = (1 + \theta_o)c(A_1\alpha + B_1) \quad , \tag{C2}$$

where the coefficients A_1 and $B_\perp$ are defined as

$$\begin{aligned} A_1 &= (\sigma_{11} - \sigma_{33})(1 + 2\alpha) \cos 2\beta \\ B_1 &= (\sigma_{11} + \sigma_{33}) - (\sigma_{11} - \sigma_{33})(1 + 2\alpha) \cos 2\beta \quad . \end{aligned} \tag{C3}$$

The critical stress required to close the crack is

$$\sigma_{11}^c = \frac{4\alpha G / (1+\theta_o)}{\sin^2\beta + k\cos^2\beta} \quad , \tag{C4}$$

where $k = \sigma_{33}/\sigma_{11}$. If we solve equation C4 for the angular coordinate β, then the angular limit of open cracks for values of $\sigma_{11} \geq \sigma_{11}^{cr}$ is

$$\begin{aligned} \beta_o &= \sin^{-1}\left[\frac{\frac{4bG}{c(1+\theta_o)\sigma_{11}} - k}{1-k} \right]^{\frac{1}{2}} \\ &= \sin^{-1}\left[\frac{\frac{B}{c\sigma_{11}} - k}{1-k} \right]^{\frac{1}{2}} \quad \sigma_{11} \geq \sigma_{11}^{cr}) \quad , \end{aligned} \tag{C5}$$

where the constant B is equal to $\dfrac{4bG}{1+\theta_o}$.

APPENDIX D

A STATISTICAL ESTIMATE OF THE OPEN AND CLOSED CRACK DENSITIES DURING A LOADING OR UNLOADING CYCLE

To develop general expressions for the crack densities, a knowledge of the angular limits for open and closed sliding cracks under triaxial loading is essential.

It is shown in Appendix C that crack closure occurs when the normal stress to the crack surface attains a critical value, i.e., closure when $\sigma_N \geq \sigma_c = {}^{B}/c$ where B is a constant. For values of σ_{11} ($\geq {}^{B}/c$), the angular limits of open cracks $[(0, \beta_o), (0, \varphi_o)]$ are calculated by solving the equation $\sigma_N = {}^{B}/c$ for the angular coordinate β. The results are

$$\beta_o = \sin^{-1}\left[\frac{\frac{B}{c\sigma_{11}} - (k_2\cos^2\varphi + k_3\sin^2\varphi)}{1 - (k_2\cos^2\varphi + k_3\sin^2\varphi)}\right]^{\frac{1}{2}}$$

$$\varphi_o = \cos^{-1}\left[\frac{\frac{B}{c\sigma_{22}} - k_4}{1 - k_4}\right]^{\frac{1}{2}} , \tag{D1}$$

where $k_2 = {}^{\sigma_{22}}/\sigma_{11}$, $k_3 = {}^{\sigma_{33}}/\sigma_{11}$ and $k_4 = {}^{\sigma_{33}}/\sigma_{22}$. Equation D1 reduces to C5 when $k_4 = 1$.

The open crack density is

$$\rho_{op} = 4\rho_e \rho_{op}^{I} \int_{c_{max}}^{c_{min}} \int_{\varphi_o}^{\pi/2} \int_{-\beta_o}^{\beta_o} P(c, \beta, \varphi)\, d\beta\, d\varphi\, dc \quad , \tag{D2}$$

$$P(c, \beta, \varphi) = P(c, \beta, \pi - \varphi) \quad ; \qquad \rho_e = {}^{N_e}/V \quad ,$$

where $\rho_{op}^{I} = {}^{N_{op}^{I}}/N_e$. The closed crack density is $\rho_{cL} \equiv \rho_e - \rho_{op}$.

The density of closed cracks undergoing frictional sliding is

$$\rho_{cLs} = 8\rho_{cL} \int_{c_{min}}^{c_{max}} \int_{\varphi_{min}}^{\varphi_{max}} \int_{\beta_{min}}^{\beta_{max}} P(\beta,\varphi)\,d\beta\,d\varphi$$

$$P(c,\beta,\varphi) = P(c,\beta,\pi-\varphi) \quad , \tag{D3}$$

where the angular limits can be determined by solving $\tau-\mu\sigma_N \geq 0$ (equation B4) for β. This calculation is quite lengthy and is not presented here.

In the special case where $P(c,\beta,\varphi) = P(c)P(\beta)P(\varphi)$, and where all cracks are of equal length, equations D2 and D3 reduce to

$$\rho_{op} = \rho_e \rho_{op}^{I} \sin\beta_o$$

$$\rho_{cLs} = (\rho_e - \rho_{op})(\sin\beta_{max} - \sin\beta_{min})$$

$$\beta_{max} = \frac{1}{2}\left[\tan^{-1}\frac{1}{\mu} + \cos^{-1}\frac{\mu(1+k)}{(1-k)\sqrt{1+\mu^2}}\right] \tag{D4}$$

$$\beta_{min} = \frac{1}{2}\left[\tan^{-1}\frac{1}{\mu} - \cos^{-1}\frac{\mu(1+k)}{(1-k)\sqrt{1+\mu^2}}\right] \quad ,$$

when the cracks are uniformly distributed throughout the structure, i.e., $P(\beta,\varphi) = P(\beta)P(\varphi) = \frac{\cos\beta}{4\pi}\,d\beta d\varphi$.

A problem of some importance is concerned with the behavior of a material containing a large number of closed cracks during an unloading cycle. Walsh (1965b) showed that during the initial stages of unloading the direction of the frictional shearing stress is reversed. Accordingly, work is done

against friction as the crack proceeds to return along its "initial" path. If we follow the procedure outlined by Walsh, the reduction in applied stress ($\Delta\sigma_{11}^{cr}$) ($\sigma_{22} = \sigma_{33}$) required to initiate reverse sliding is

$$\Delta\sigma_{11}^{cr} = \frac{2\mu\sigma_{11}^{(o)}(k+\tan^2\beta)}{(1-k)\tan\beta+\mu(k+\tan^2\beta)} \qquad (D5)$$

$$(\beta_{min} \leq \beta \leq \beta_{max}) \quad ,$$

where $\sigma_{11}^{(o)}$ is the value of the principal compressive stress when unloading begins. When k = 0, equation D5 reduces to Walsh's (1965b) value.

If we solve equation D5 for β, the angular limits of cracks undergoing reverse frictional sliding are

$$\beta_3^{max} = \tan^{-1}\left[\frac{(1-k)H+\sqrt{(1-k)^2H^2-4k(1-\mu H)^2}}{2(1-\mu H)}\right]$$
$$\beta_3^{min} = \tan^{-1}\left[\frac{(1-k)H-\sqrt{(1-k)^2H^2-4k(1-\mu H)^2}}{2(1-\mu H)}\right] \quad , \qquad (D6)$$

where $H = \Delta\sigma_{11}/2\mu\sigma_{11}^{(o)}$ and $\Delta\sigma_{11} = \sigma_{11}^{(o)} - \sigma_{11}$ is the stress drop. The reverse sliding crack density is ($\sigma_{22} = \sigma_{33}$)

$$\rho_{rs} = 2\rho_{cL}\int_{c_{max}}^{c_{min}}\int_{0}^{2\pi}\int_{\beta_3^{min}}^{\beta_3^{max}} P(c,\beta,\varphi)\,d\beta\,d\varphi\,dc \quad . \qquad (D7)$$

APPENDIX E

LOADING STRESS-STRAIN BEHAVIOR OF BRITTLE ROCK DURING REGIONS I AND II

We shall rely on the basic assumption that crack interaction effects can be neglected as a first-order approximation. Therefore, the total strain energy density of an elastic material containing N_e voids is (Hashin, 1959)

$$\sigma_{ij} d\epsilon^{*}_{ij} = \sigma_{ij} d\epsilon^{o}_{ij} + \frac{1}{V} \sum_{n=1}^{N_e} \left[\sigma_{ij} d \left(\oiint u_i \bar{\nu}_j dA_c \right)_n \right] , \qquad \text{(E1)}$$

where the superscripts "*" and "o" refer to the effective and purely elastic strains in the specimen respectively, u_i is the displacement of the void surface in the $\bar{\nu}_i$ direction, and $\bar{\nu}_j dA_c$ is the cross sectional area of the void normal to the $\bar{\nu}_j$ direction. The latter expressions in equation E1 are the additional strain energy density components resulting from the presence of the N_e flaws in a specimen of volume V . The effective strains are

$$\begin{aligned}
d\epsilon^{*}_{11} &= d\epsilon^{o}_{11} + \frac{1}{V} \sum_{n=1}^{N_e} d \left[\oiint u_1 \bar{\nu}_1 dA_c \right]_n \\
d\epsilon^{*}_{22} &= d\epsilon^{o}_{22} + \frac{1}{V} \sum_{n=1}^{N_e} d \left[\oiint u_2 \bar{\nu}_2 dA_c \right]_n \qquad \text{(E2)} \\
d\epsilon^{*}_{33} &= d\epsilon^{o}_{33} + \frac{1}{V} \sum_{n=1}^{N_e} d \left[\oiint u_3 \bar{\nu}_3 dA_c \right]_n .
\end{aligned}$$

If the voids can be mathematically modeled by cylindrical ellipsoids, the strain components and the effective elastic moduli can be calculated for the cases where some of the N_e flaws are open and where others are both closed and undergoing frictional sliding (Appendix A). Unfortunately, a major difficulty arises in calculating these integrals, namely, the determination of the boundary conditions to be applied to the crack regions (see Appendix A). For example, if the stress at the region boundary containing a crack is assumed to equal the externally applied stress, then the deformation of the region boundary is not uniform. In this case, strain continuity cannot be maintained at the boundary of two regions containing cracks of differing sizes and orientations. Similarly, if the strain at the boundary of a region is assumed uniform and equal to that of the body as a whole, the stress on the boundary is not uniform and stress equilibrium between adjacent regions is not fulfilled. However, Hill (1952) showed that the above approximations form lower and upper bounds on the effective moduli, respectively. Walsh (1965a) considered both types of boundary conditions in his analysis and established (for reasonable crack concentrations) that the difference between the two bounds is not significant. Equations E1 and E2 express the assumption that the stress distribution throughout the specimen is uniform and equal to the externally applied stresses.

As an example of the use of equation E2, assume for case of calculation that (1) the crack distribution function has the property that

$P(c,\beta,\varphi) = P(c)P(\beta)P(\varphi)$, (2) $P(c) = \delta(c-c_o)$ (i.e., all cracks are of equal length[1E]), (3) the stress system is axisymmetric ($\sigma_{22} = \sigma_{33}$). The average values of the strain components are then (appendices B and C)

$$d\langle\epsilon_{11}^*\rangle = \frac{1-2k\nu_o}{E_o}\,d\sigma_{11} + \frac{\pi A c_o^3 \rho_e}{2}\left[H_1(k,\sigma_{11}) + H_2(k,\sigma_{11})\right]d\sigma_{11}$$

$$d\langle\epsilon_{22}^*\rangle = \frac{k-\nu_o(1+k)}{E_o}\,d\sigma_{22} + \frac{\pi A c_o^3 \rho_e}{4}\left[H_3(k,\sigma_{11}) + H_4(k,\sigma_{11})\right]d\sigma_{11} \qquad \text{(E3)}$$

$$d\langle\epsilon_{33}^*\rangle = d\langle\epsilon_{22}^*\rangle \quad ,$$

where A is a constant, ρ_e ($\rho_e = \frac{N_e}{V}$) is the crack density, and $k = \frac{\sigma_{33}}{\sigma_{11}}$. The functions $H_1(k,\sigma_{11})$, $H_2(k,\sigma_{11})$, $H_3(k,\sigma_{11})$ and $H_4(k,\sigma_{11})$ are

$$H_1(k,\sigma_{11}) = \rho_{op}^I \int_o^{2\pi}\int_{-\beta_o}^{\beta_o} \sin^2\beta P(\beta,\varphi)\,d\beta d\varphi$$

$$H_2(k,\sigma_{11}) = 2\rho_{op}^I \int_o^{2\pi}\int_{L_1}^{\beta_{max}} F(\mu,k,\beta)P(\beta,\varphi)\,d\beta d\varphi + 2\rho_{cL}^I \int_o^{2\pi}\int_{\beta_{min}}^{\beta_{max}} F(\mu,k,\beta)P(\beta,\varphi)\,d\beta d\varphi$$

$$H_3(k,\sigma_{11}) = 2k\rho_{op}^I \int_o^{2\pi}\int_{-\beta_o}^{\beta_o} \cos^2\beta\cos^2\varphi P(\beta,\varphi)\,d\beta d\varphi; \;;$$

$$H_4(k,\sigma_{11}) = -4\rho_{op}^I \int_o^{2\pi}\int_{L_1}^{\beta_{max}} F(\mu,k,\beta)\cos^2\varphi P(\beta,\varphi)\,d\beta d\varphi - 4\rho_{cL}^I \int_o^{2\pi}\int_{\beta_{min}}^{\beta_{max}} F(\mu,k,\beta)\cos^2\varphi P(\beta,\varphi)\,d\beta d\varphi \qquad \text{(E4)}$$

$$F(k,\mu,\beta) = \sin\beta\cos\beta\left[(1-k)(\sin\beta\cos\beta - \mu\sin^2\beta) - \mu k\right]; \quad \beta_o = \sin^{-1}\left[\frac{\frac{B}{c_o\sigma_{11}} - k}{1-k}\right]^{\frac{1}{2}} \text{(B=constant)}$$

$$\beta_{max} = \tfrac{1}{2}\left[\tan^{-1}\frac{1}{\mu} + \cos^{-1}\frac{\mu(1+k)}{\sqrt{1+\mu^2}(1-k)}\right]$$

$$\beta_{min} = \tfrac{1}{2}\left[\tan^{-1}\frac{1}{\mu} - \cos^{-1}\frac{\mu(1+k)}{\sqrt{1+\mu^2}(1-k)}\right] \quad ,$$

[1E] $\delta(c-c_o)$ is the Dirac delta function with the property that $\delta(c-c_o) = 0$ for $c \neq c_o$ and $\delta(c-c_o) = 1$ for $c = c_o$.

where $\rho_{op}^{I} = N_{op}^{I}/N_e$. The angle β_o represents the angular limit of open cracks (appendix C). The angles (β_{max}, β_{min}) are derived by solving the equation ($\tau-\mu\sigma_N \geq 0$) governing frictional sliding for β. In equation E4, the lower limit L_1 for H_2 and H_4 is β_o for $\beta_o > \beta_{min}$ and β_{min} when $\beta_o < \beta_{min}$. The quantities ρ_{op}^{I} and ρ_{cL}^{I} represent the open and closed crack "densities" under no external load.

Notice that we are assuming that A and B in equations E3 and E4 are constants and that they can be evaluated from test data. In this manner, we are postulating that the theory can be geared to fit the experimental results. The resulting analysis is therefore an analytical-empirical theory. The constants of the analysis must be evaluated for each rock type.

When the cracks are randomly distributed throughout the rock structure and are of equal length, the uniaxial Young's modulus and Poisson's ratio during the initial stages of regions I (β_o=90°) and II (β_o=0°) are

$$\begin{aligned}
\frac{1}{E_i} &= \frac{1}{E} + A_1\rho_e\left(\tfrac{1}{3}\rho_{op}^{I} + B_2\rho_{cL}^{I}\right) \\
\frac{1}{E_f} &= \frac{1}{E} + A_1\rho_e\left(B_2\right) \\
\frac{\nu_i}{E_i} &= \frac{\nu}{E} + \tfrac{1}{2}A_1\rho_e\left(B_2\rho_{cL}^{I}\right) \\
\frac{\nu_f}{E_f} &= \frac{\nu}{E} + \tfrac{1}{2}A_1\rho_e\left(B_2\right) \quad ,
\end{aligned} \tag{E5}$$

where $B_2 = \int_{\beta_{min}}^{\beta_{max}} F(\mu, o, \beta)\cos\beta d\beta$, and $A_1 = \frac{1}{2}\pi A c_o^3$. The "subscripts "i" and "f" refer to the initial stages of regions I and II, respectively.

Equation E5 gives a relationship for the unknowns $A_1 \rho_e$ and ρ_{cL}^{I}. They are

$$\rho_{cL}^{I} = \left(\frac{\nu_i}{E_i} - \frac{\nu}{E}\right) \Big/ \left(\frac{\nu_f}{E_f} - \frac{\nu}{E}\right) .$$

$$A_1 \rho_e = 3 \left[\left(\frac{1}{E_f} - \frac{1}{E}\right) - 2\left(\frac{\nu_i}{E_i} - \frac{\nu}{E}\right)\right] \left[\frac{\nu_f}{E_f} - \frac{\nu}{E}\right] \Big/ \left(\frac{\nu_f}{E_f} - \frac{\nu_i}{E_i}\right) . \tag{E6}$$

Therefore when the initial, final, and intrinsic Young's moduli and Poisson's ratios are known, the complete stress-strain relations under any loading strain can be determined provided the constant $\underline{B}$ (equation E4) is known. An estimate of this quantity can be obtained by determining the stress and total strain at an intermediate point between regions I and II on the uniaxial stress-strain curve and substituting these values into equation E3 and solving for B.

Equation E5 can be rearranged to give the initial and final (regions I and II, respectively) Poisson's ratios. They are

$$\nu_i = \nu \left(\frac{E_i}{E}\right) + \rho_{cL}^{I} E_i \left(\frac{\nu_f}{E_f} - \frac{\nu}{E}\right)$$

$$\nu_f = \nu + \frac{1}{2}\left(1-2\nu\right)\left(1 - \frac{E_f}{E}\right) . \tag{E7}$$

When $\rho_{cL}^{I} = 0$, equation E7 reduces to Walsh's (1965c) relation between the initial and final values of Poisson's ratio.

APPENDIX F

UNLOADING STRESS-STRAIN BEHAVIOR OF BRITTLE ROCK DURING REGIONS I AND II

During the initial stages of unloading, the direction of the frictional shear stress is reversed (Walsh, 1965b,c). Accordingly, work must be done against friction as the cracks proceed to return along the initial paths. Therefore, during an unloading cycle, there is an angular range of closed cracks which are suitably oriented for frictional sliding in the reverse sense. Following a procedure used by Walsh for analysizing the reverse frictional sliding of cracks, the angular limits of closed cracks undergoing reverse frictional sliding are (Appendix D).

$$(\beta_3)_{\substack{max\\min}} = \tan^{-1}\left[\frac{(1-k)H \pm \sqrt{(1-k)^2H^2-4k(1-\mu H)^2}}{2(1-\mu H)}\right], \qquad (F1)$$

where $H = \frac{\Delta\sigma_{11}}{2\mu\sigma_{11}^{(o)}}$ and $k = \sigma_{33}/\sigma_{11}$. The stress $\sigma_{11}^{(o)}$ is the stress level at which unloading begins, and $\Delta\sigma_{11} = \sigma_{11}^{(o)} - \sigma_{11}$ is the stress drop $(\sigma_{11} \leq \sigma_{11}^{(o)})$.

When the stresses are axisymmetric ($\sigma_{22}=\sigma_{33}$) and the cracks are of equal length and uniformly distributed over the angular coordinate φ, the unloading stress-strain relations can be written

$$\langle \overset{*}{\epsilon}_{11} \rangle_{uL} = \langle \epsilon_{11}^{o} \rangle_{uL} + \frac{\pi}{2} Ac_o^3 \rho_e \int_{\sigma_{11}^{(o)}}^{\sigma_{11}} \left[H_1(k,\sigma_{11}) + H_2^{uL}(k,\sigma_{11})\right] d\sigma_{11}$$

$$\langle \overset{*}{\epsilon}_{22} \rangle_{uL} = \langle \epsilon_{22}^{o} \rangle_{uL} + \frac{\pi}{4} Ac_o^3 \rho_e \int_{\sigma_{11}^{(o)}}^{\sigma_{11}} \left[H_3(k,\sigma_{11}) + H_4^{uL}(k,\sigma_{11})\right] d\sigma_{11} \qquad (F2)$$

$$\langle \overset{*}{\epsilon}_{33} \rangle_{uL} = \langle \overset{*}{\epsilon}_{22} \rangle_{uL} ,$$

where

$$H_2^{ul}(k,\sigma_{11}) = 2\rho_{op}^{I}\int_0^{2\pi}\int_{L_1}^{\beta_3^{max}} F(\mu,k,\beta)P(\beta,\varphi)d\beta d\varphi + 2\rho_{cL}^{I}\int_0^{2\pi}\int_{\beta_3^{min}}^{\beta_3^{max}} F(\mu,k,\beta)P(\beta,\varphi)d\beta d\varphi$$

$$H_4^{ul}(k,\sigma_{11}) = -4\rho_{op}^{I}\int_0^{2\pi}\int_{L_1}^{\beta_3^{max}} F(\mu,k,\beta)\cos^2\varphi P(\beta,\varphi)d\beta d\varphi - 4\rho_{cL}^{I}\int_0^{2\pi}\int_{\beta_3^{min}}^{\beta_3^{max}} F(\mu,k,\beta)\cos^2\varphi P(\beta,\varphi)d\beta d\varphi \qquad \text{(F3)}$$

$$L_1 = \beta_o \quad , \qquad \beta_o \geq \beta_3^{min}$$

$$= \beta_3^{min} \quad , \qquad \beta_o < \beta_3^{min} \quad .$$

Figure F1 illustrates a typical loading and unloading stress-strain curve specified by equations E3 and #8. Notice that when the specimen has been completely stress relieved $\left(\Delta\sigma_{11} = \sigma_{11}^{(o)}\right)$, some residual strain remains, i.e.,

$$\delta\langle\epsilon_1^P{}_1\rangle = \pi A c_o^3 \rho_e \int_{\sigma_{11}^{(o)}}^{o}\int_0^{2\pi}\int_{\beta_3^{max}}^{\beta_{max}} F(\mu,k,\beta)P(\beta,\varphi)d\beta d\varphi d\sigma_{11} \geq 0$$

$$\delta\langle\epsilon_2^P{}_2\rangle = \delta\langle\epsilon_3^P{}_3\rangle = -\frac{1}{2}\delta\langle\epsilon_1^P{}_1\rangle \quad . \qquad \text{(F4)}$$

Therefore, not all the cracks which undergo frictional sliding during a loading cycle return to their original positions at the end of an unloading cycle. This may account for some of the residual axial and lateral strain experimentally observed by Brace (1964)(refer to figure 6 in Walsh, 1965b).

The extension of the above equations to the general case of arbitrary $P(c,\beta,\varphi)$ and true triaxial loading ($\sigma_{11}\geq\sigma_{22}\geq\sigma_{33}$) is straightforward (see Appendices B and D). It can be shown that for true stress triaxiality, the stress-strain relationships and accordingly, the effective elastic moduli, are affected by the value of the intermediate principal stress.

APPENDIX G

A STATISTICAL ESTIMATE OF THE MICROCRACK DENSITY

Permanent changes are occurring within the microscopic fabric of brittle rock during regions III and IV. Brace et al. (1966) have demonstrated that brittle rock is nonelastic at high stress, even at high confining pressure. This effect, noticeable at stresses on the order of half the compressive strength, is characterized by dilatancy, where dilatancy refers to an increase in volumetric strain relative to the increase, that would be expected if the material were linearly elastic. The dilatancy was traced to the formation of small cracks (microcracks) within the rock.

If a satisfactory theory describing these experimental results is to be achieved, an analytical procedure must be developed which enables both an estimate of the microcrack density for values of the applied stress above the critical level to initiate a microcrack and the magnitude of the strains due to microcracking within the specimen.

The following assumptions are necessary to estimate the microcrack density during regions III and IV. (1) The crack interaction effects can be neglected. (2) Failure initiation of closed cracks ("cls" mode) occurs only if the orientation of the cracks satisfies the modified Griffith condition which governs the failure initiation of closed cracks suitably oriented for frictional sliding, i.e., $\tau-\mu\sigma_N \geq \tau_c$ (Brady, 1968a).

(3) Failure initiation of open cracks ("opt" mode) occurs when the applied tensile stress(es) acting normal to the crack surfaces exceeds σ_c (one or more of the principal stresses must be tensile for this failure mode) [1G/]

In three dimensions, the variation of the normal and shear stress with orientation of a plane surface can be written in the form (Jaeger, 1962)

$$\sigma_N = \frac{1}{4}\,(a_1 + a_2\cos 2\beta)$$

$$\tau^2 = \frac{1}{4}\,(b_1 + b_2\cos 2\beta) - \sigma_N^2 \quad , \tag{G1}$$

where

$$\begin{aligned} a_1 &= 2\sigma_{11}+(\sigma_{22}+\sigma_{33})+(\sigma_{22}-\sigma_{33})\cos 2\varphi \\ a_2 &= 2\sigma_{11}+(\sigma_{22}+\sigma_{33})+(\sigma_{22}-\sigma_{33})\cos 2\varphi \\ b_1 &= 2\sigma_{11}^2+(\sigma_{22}^2+\sigma_{33}^2)+(\sigma_{22}^2-\sigma_{33}^2)\cos 2\varphi \\ b_2 &= 2\sigma_{11}^2+(\sigma_{22}^2+\sigma_{33}^2)+(\sigma_{22}^2-\sigma_{33}^2)\cos 2\varphi \quad , \end{aligned} \tag{G2}$$

where $\sigma_{11} \geq \sigma_{22} \geq \sigma_{33}$ and β and φ are the angular specifications of the plane surface with respect to a fixed coordinate system (figure G1).

McClintock and Walsh (1962) have shown that when a closed Griffith crack is subjected to a biaxial stress field the criterion for failure initiation is simply

$$\tau^{(n)} - \tau_f^{(n)} \geq \tau_c \tag{G3}$$

where $\tau^{(n)}$ and $\tau_f^{(n)}$ are the shear and frictional shear stress ($\cong \mu\sigma_N^{(n)}$) respectively on the n^{th} crack surface. If we postulate that this rule is valid for the three-dimensional case, then by solving equation G3 for β, we

[1G/] The stress σ_c represents the magnitude of the applied tensile stress (acting normal to a primary crack) required to initiate growth of microcrack (see figure 6).

find that for values of $\sigma_{11} \geq \sigma_{11}^{cr}$ (σ_{11}^{cr} = stress required for microcrack initiation) [2G]

$$\beta_2^{cls} = \frac{1}{2}\cos^{-1}\left[\frac{-A_2-\sqrt{A_2^2-4A_1A_3}}{2A_1}\right]$$
$$\beta_1^{cls} = \frac{1}{2}\cos^{-1}\left[\frac{-A_2+\sqrt{A_2^2-4A_1A_3}}{2A_1}\right], \tag{G4}$$

where

$$A_1 = (1+\mu^2)a_2^2$$
$$A_2 = 2(1+\mu^2)a_1a_2 + 8\mu\tau_c a_2 - 4b_2 \tag{G5}$$
$$A_3 = (a_1^2-4b_1)+(\mu a_1+4\tau_c)^2 \quad .$$

To determine the angular limits on φ, equation G3 must be maximized with respect to β. This gives the orientation of the critically oriented crack as a function of φ to be

$$\beta_c(\varphi) = \frac{1}{2}\cos^{-1}\frac{-\alpha_2+\sqrt{\alpha_2^2-4\alpha_1\alpha_2}}{2\alpha_1}, \tag{G6}$$

where

$$\alpha_1 = a_2^4(1+\mu^2)$$
$$\alpha_2 = 2(1+\mu^2)a_2^2(a_1a_2-2b_2) \tag{G7}$$
$$\alpha_3 = (2b_2-a_1a_2)^2 - \mu^2a_2^2(a_1^2-4b_1) \quad .$$

[2G] The critical stress system required to <u>initiate</u> failure of the critically oriented primary crack is obtained by maximizing equation G3 with respect to β and letting $\varphi=90°$. The result is

$$\sigma_{11}^{cr} = \frac{2\tau_c + \sigma_{33}(\sqrt{1+\mu^2}+\mu)}{(\sqrt{1+\mu^2}-\mu)} \quad .$$

The angular limits on φ are $(\varphi_1^{cLs}, \frac{\pi}{2})$. The angle φ_1^{cLs} is determined by equating β_2^{cLs} to $\beta_c(\varphi)$. For angles of $\varphi \leq \varphi_1^{cLs}$, failure initiation is prohibited while for $\varphi_1^{cLs} < \varphi \leq \frac{\pi}{2}$, failure initiation is theoretically possible. The critically oriented "cls" crack occurs at $\varphi_c = 90°$ and $\beta_c = \frac{1}{2} \tan^{-1} \frac{1}{\mu}$ and the critical stress required to initiate failure of this crack is

$$\sigma_{11}^{cr} = \frac{2\tau_c + \sigma_{33}\left(\sqrt{1+\mu^2}+\mu\right)}{\sqrt{1+\mu^2} - \mu} \quad . \tag{G8}$$

When $\sigma_{22} = \sigma_{33}$, there is no φ dependence and equation G4 becomes

$$\beta_2^{cLs} = \frac{1}{2}\left[\tan^{-1}\frac{1}{\mu} + \cos^{-1}\frac{2\tau_c + \mu(\sigma_{11}+\sigma_{33})}{\sqrt{1+\mu^2}\,(\sigma_{11}-\sigma_{33})} \right]$$

$$\beta_1^{cLs} = \frac{1}{2}\left[\tan^{-1}\frac{1}{\mu} - \cos^{-1}\frac{2\tau_c + \mu(\sigma_{11}+\sigma_{33})}{\sqrt{1+\mu^2}\,(\sigma_{11}-\sigma_{33})} \right] \quad . \tag{G9}$$

Thus for values of $\sigma_{11} \geq \sigma_{11}^{cr}$ and for cracks satisfying the conditions $\beta_1^{cLs} \leq \beta \leq \beta_2^{cLs}$ and $\varphi_1^{cLs} \leq \varphi \leq \frac{\pi}{2}$, microcrack initiation is theoretically possible.

If $P(c,\beta,\varphi)$ describes the distribution of cracks in the specimen, the density of cracks suitably oriented for microcrack initiation is

$$\rho_{m\,c}^{cls} = \rho_e \int_{c_{max}}^{c_1^{cls}} \int_{\varphi_1^{cls}}^{\frac{\pi}{2}} \int_{\beta_1^{cls}}^{\beta_2^{cls}} P)c,\beta,\varphi)d\beta d\varphi dc \quad , \tag{G10}$$

where $\rho_e = {}^{N_e}/_{V}$ is the density of cracks within a specimen of volume V [3G]. The quantities c_{max} and c_1^{cls} are the maximum crack size and the length of closed crack just undergoing failure initiation [4G].

To estimate the tension failure initiation of open cracks, we shall assume that microcrack initiation occurs whenever $\sigma_n \leq -\sigma_c$. Solving this equation for β gives the angular limits within which the "opt" failure occurs, namely

$$\beta_3^{opt} = \frac{1}{2}\cos^{-1}\left[\frac{4\sigma_c + (2\sigma_{11} + \sigma_{aa})}{(2\sigma_{11} - \sigma_{aa})}\right]$$

$$\varphi_3^{opt} = \frac{1}{2}\cos^{-1}\left[\frac{-4\sigma_c - 2(\sigma_{22} + \sigma_{33})}{2(\sigma_{22}-\sigma_{33})}\right] \quad , \tag{G11}$$

where $\sigma_{aa} = (\sigma_{22} + \sigma_{33}) + (\sigma_{22} - \sigma_{33})\cos 2\varphi$. When $\sigma_{22} = \sigma_{33}$, the φ dependence vanishes and β_3^{opt} reduces to the value $\beta_3^{opt} = \frac{1}{2}\cos^{-1}\left[\frac{2\sigma_c+(\sigma_{11}+\sigma_{33})}{(\sigma_{11}-\sigma_{33})}\right]$.

[3G] $\int_{c_{max}}^{c_{min}} \int_{0}^{\pi/2} \int_{0}^{\pi/2} P(c,\beta,\varphi)d\beta d\varphi dc = 1$. ($c_{min}$ = minimum crack in length in the specimen.

[4G] If $\tau_c \cong \sqrt{\frac{B_1}{c_{max}}}$ (B_1 = constant), then the length of crack just undergoing failure initiation can be estimated from

$$c_1^{cls} \cong \frac{16B_1}{\left[\sigma_{11}\left(\sqrt{1+\mu^2}-\mu\right) - \sigma_{33}\left(\sqrt{1+\mu^2}+\mu\right)\right]^2} \quad ,$$

where $\sigma_{11} \geq \sigma_{11}^{cr}$. When $\sigma_{11} = \sigma_{11}^{cr}$, $c_1^{cls} \equiv c_{max}$.

The "opt" microcrack density is

$$\rho_{m\,c}^{opt} = 2\rho_e \int_{c_{max}}^{c_1^{opt}} \int_{\varphi_3^{opt}}^{\pi/2} \int_{0}^{\beta_3^{opt}} P(c,\beta,\varphi)\,d\beta\,d\varphi\,dc \quad , \tag{G12}$$

where c_{max} and c_1^{opt} are the lengths of open cracks which have and are currently undergoing failure initiation respectively. The upper limit in equation G12 is $c_1^{opt} \cong \left(\frac{\sigma_c}{\sigma_{33}}\right)^2 c_{max}$, where $\sigma_{33} \leq \sigma_{33}^{cr} \cong -\sqrt{\frac{B_1}{c_{max}}}$.

APPENDIX H

AN EMPIRICAL ESTIMATE OF THE MICROCRACKING STRAINS IN BRITTLE ROCK DURING REGIONS III AND IV

The complexity of the problem of brittle rock behavior during regions III and IV defies an exact analytical determination of the microcracking strains. It is therefore essential to develop an empirical approach to this problem which yields results consistent with experimental observations. With this in mind, it is logical to postulate that the empirical expressions for the microcracking strains should be chosen so as to satisfy three essential conditions. (1) The microcracking strains are proportional to the density of microcracks[1H] within the specimen. (2) Since the microcrack growth process is not an instantaneous process, the volumetric microcrack strain vs. stress relations should be of a form such that the volume of the specimen tends to increase as the applied stress is increased above the critical stress. (3) Near incipient failure, the microcrack strain expressions should

---

[1H] We shall assume that ρ_m^{cls} and ρ_m^{opt} are proportional to the actual number of microcracks for either failure mode.

express the result that microcracks are in the process of joining, i.e., at total failure, where the specimen ruptures into two or more parts, the lateral strains and hence the volumetric strains tend to become quite large.

If crack interaction effects are neglected, the incremental stress-strain relations, modified to include microcracking, can be written

$$
\begin{aligned}
d\epsilon_{11} &\cong d\epsilon_{11}^{*} + \frac{1}{V}\sum_{n=1}^{M_c} d\left[\oiint u_1 \nu_1 dA_c\right]_c^{(n)} \\
d\epsilon_{22} &\cong d\epsilon_{22}^{*} + \frac{1}{V}\sum_{n=1}^{M_c} d\left[\oiint u_2 \nu_2 dA_c\right]_c^{(n)} \qquad \text{(H1)} \\
d\epsilon_{33} &\cong d\epsilon_{33}^{*} + \frac{1}{V}\sum_{n=1}^{M_c} d\left[\oiint u_3 \nu_3 dA_c\right]_c^{(n)} ,
\end{aligned}
$$

where M_c is the total number of microcracks.

To obtain an estimate of the microcrack strains, we can use Paulding's (1965) result that for the "cls" cracking mode the planes of the microcracks tend to be inclined at relatively low angles to the maximum principal stress direction. He observed that for failure in compression there is little or no permanent axial strain and that the volume change is almost entirely due to a permanent increase in the cross-sectional area of the specimen.

By postulating that the microcracking process can be approximated by a system in which voids whose major planes are inclined at a low angle to the maximum principal stress direction are opening spontaneously as the applied

stress increased above a certain critical level, Brady (1968a,b) presented empirical expressions for the microcrack strains. For the "cls" failure mode, these strains are

$$\left[d\epsilon_{11}^{(n)}\right]_{m\,c}^{cls} \cong \frac{1}{V} d\left[\oiint u_1^{(n)} \nu_1^{(n)} dA_c^{(n)}\right]_{m\,c}^{cls} \cong 0$$

$$\left[d\epsilon_{22}^{(n)}\right]_{m\,c}^{cls} \cong \frac{1}{V} d\left[\oiint u_2^{(n)} \nu_2^{(n)} dA_c^{(n)}\right]_{m\,c}^{cls} \cong - B_1^{cls}\, g(\alpha)\cos^2\gamma \frac{d\sigma_{11}}{(\sigma_{11}^f - \sigma_{11})^m} \quad \text{(H2)}$$

$$\left[d\epsilon_{33}^{(n)}\right]_{m\,s}^{cls} \cong \left[d\epsilon_{22}^{(n)}\right]_{m\,c}^{cls} \cong - B_1^{cls}\, g(\alpha)\sin^2\gamma \frac{d\sigma_{11}}{(\sigma_{11}^f - \sigma_{11})^m} \,,$$

where α is the inclination of the plane of the microcrack to the x_1 axis, γ is the angle between the microcrack normal projected onto the x_2, x_3, $g(\alpha)$ is an unknown function, and B_1^{cls} and m are unknown constants. For the "opt" failure mode ($\sigma_{33} \leq - T_o$), the strains are

$$\left[d\epsilon_{11}^{(n)}\right]_{m\,c}^{opt} \cong 0$$

$$\left[d\epsilon_{22}^{(n)}\right]_{m\,c}^{opt} \cong B_1^{opt}\, f(\alpha)\cos^2\gamma \frac{d\sigma_{33}}{(\sigma_{33}^f - \sigma_{33})^p} \quad \text{(H3)}$$

$$\left[d\epsilon_{33}^{(n)}\right]_{m\,c}^{opt} \cong B_1^{opt}\, f(\alpha)\sin^2\gamma \frac{d\sigma_{33}}{(\sigma_{33}^f - \sigma_{33})^p}$$

where $f(\alpha)$, B_2^{opt}, and p are unknowns and $(\sigma_{11}^f, \sigma_{33}^f)$ are the stresses at total failure for the 'cls" and "opt" mode respectively. The unknown constants are evaluated from the experimental data.

If we sum the individual microcrack strains and average[2H] the final expressions with respect to α and γ, the microcrack strains become

---

[2H] For a system containing a large number of microcracks and for effects large in comparison to the microcrack, the summation relationship can be approximated by an integral relationship.

$$
\begin{aligned}
d < \epsilon_{11}^{m\,c} >_{cls} &\cong 0 \\
d < \epsilon_{22}^{m\,c} >_{cls} &\cong - A_{12}\ \rho_{m\,c}^{cls}\ \frac{d\sigma_{11}}{(\sigma_{11}^{f}-\sigma_{11})^{m}} \\
d < \epsilon_{33}^{m\,c} >_{cls} &\cong - A_{13}\ \rho_{m\,c}^{cls}\ \frac{d\sigma_{11}}{(\sigma_{11}^{f}-\sigma_{11})^{m}}
\end{aligned}
\tag{H4}
$$

for the "cls" mode and

$$
\begin{aligned}
d < \epsilon_{11}^{m\,c} >_{opt} &\cong 0 \\
d < \epsilon_{22}^{m\,c} >_{opt} &\cong A_{22}\ \rho_{m\,c}^{opt}\ \frac{d\sigma_{33}}{(\sigma_{33}^{f}-\sigma_{33})^{p}} \\
d < \epsilon_{33}^{m\,c} >_{opt} &\cong A_{23}\ \rho_{m\,c}^{opt}\ \frac{d\sigma_{33}}{(\sigma_{33}^{f}-\sigma_{33})^{p}}
\end{aligned}
\tag{H5}
$$

for the "opt" mode. The A_{ij} are

$$
\begin{aligned}
A_{12} &= B_1^{cls} \int_{\gamma_1^{cls}}^{\gamma_2^{cls}} \int_{\alpha_1^{cls}}^{\alpha_2^{cls}} g(\alpha)\cos^2\gamma\ P_{cls}(\alpha,\gamma)\,d\alpha\,d\gamma \\
A_{13} &= B_1^{cls} \int_{\gamma_1^{cls}}^{\gamma_2^{cls}} \int_{\alpha_1^{cls}}^{\alpha_2^{cls}} g(\alpha)\sin^2\gamma\ P_{cls}(\alpha,\gamma)\,d\alpha\,d\gamma \\
A_{22} &= B_1^{opt} \int_{\gamma_1^{opt}}^{\gamma_2^{opt}} \int_{\alpha_1^{opt}}^{\alpha_2^{opt}} f(\alpha)\cos^2\gamma\ P_{opt}(\alpha,\gamma)\,d\alpha\,d\gamma \\
A_{23} &= B_1^{opt} \int_{\gamma_1^{opt}}^{\gamma_2^{opt}} \int_{\alpha_1^{opt}}^{\alpha_2^{opt}} f(\alpha)\sin^2\gamma\ P_{opt}(\alpha,\gamma)\,d\alpha\,d\gamma\ ,
\end{aligned}
\tag{H6}
$$

where the $(\gamma_1^{cls},\gamma_2^{cls})$, $(\alpha_1^{cls},\alpha_2^{cls})$, $(\gamma_1^{opt},\gamma_2^{opt})$ and $(\alpha_1^{opt},\alpha_2^{opt})$ are minimum and maximum angular orientations of the "cls" and "opt" microcracks.

The $P_{cls}(\alpha, \gamma)$ and $P_{opt}(\alpha, \gamma)$ are their respective normalized distribution functions. Figure H1 illustrates diagramatically the possible "cls" and "opt" microcrack distributions when $\sigma_{22} = \sigma_{33}$.

Because of the complexity of determining the A_{ij} coefficients in equation H6, an additional approximation in estimating the influence of σ_{22} on the microcrack strain is required. One possible mathematical format of the microcrack strains for the case of true stress triaxiality is

$$
\begin{aligned}
d < \epsilon_{11}^{mc} >_{cls} &\cong 0 \\
d < \epsilon_{22}^{mc} >_{cls} &\cong -\frac{1}{2} A_1 \left(\frac{\sigma_{11}-\sigma_{22}}{\sigma_{11}-\sigma_{33}}\right)^N \rho_{mc}^{cls} \frac{d\sigma_{11}}{(\sigma_{11}^f-\sigma_{11})^m} \\
d < \epsilon_{33}^{mc} >_{cls} &\cong -\frac{1}{2} A_1 \rho_{mc}^{cls} \frac{d\sigma_{11}}{(\sigma_{11}^f-\sigma_{11})^m}
\end{aligned}
\tag{H7}
$$

for the "cls" mode and

$$
\begin{aligned}
d < \epsilon_{11}^{mc} >_{opt} &\cong 0 \\
d < \epsilon_{22}^{mc} >_{opt} &\cong \frac{1}{2} A_2 \left(\frac{\sigma_{11}-\sigma_{22}}{\sigma_{11}-\sigma_{33}}\right)^N \rho_{mc}^{opt} \frac{d\sigma_{33}}{(\sigma_{33}^f-\sigma_{11})^p} \\
d < \epsilon_{33}^{mc} >_{opt} &\cong \frac{1}{2} A_2 \rho_{mc}^{opt} \frac{d\sigma_{33}}{(\sigma_{33}^f-\sigma_{11})^p} \quad ,
\end{aligned}
\tag{H8}
$$

for the "opt" mode. The functions A_1 and A_2 are given by $A_{12} = \frac{1}{2} A_1 \left(\frac{\sigma_{11}-\sigma_{22}}{\sigma_{11}-\sigma_{33}}\right)^N$, $A_{22} = \frac{1}{2} A_2 \left(\frac{\sigma_{11}-\sigma_{22}}{\sigma_{11}-\sigma_{33}}\right)^N$, $A_{13} = \frac{1}{2} A_1$, and $A_{23} = \frac{1}{2} A_2$. The quantity "N" is an unknown and must be determined by experiment.

The total average volumetric microcrack strain can then be expressed as

$$-d < \epsilon_{11}^{t} >_{m\,c} \cong \frac{1}{2} A_1 \rho_{m\,c}^{cls} \left[\left(\frac{\sigma_{11}-\sigma_{22}}{\sigma_{11}-\sigma_{33}} \right)^{N} + 1 \right] \frac{d\sigma_{11}}{(\sigma_{11}^{f}-\sigma_{11})^{m}} \qquad (H9)$$

for values of $\sigma_{33} \geq -\sigma_c$ and

$$-d<\epsilon_{11}^{t}>_{m\,c} \cong \frac{1}{2} A_1 \rho_{m\,c}^{cls} \left[\left(\frac{\sigma_{11}-\sigma_{22}}{\sigma_{11}-\sigma_{33}} \right)^{N} + 1 \right] \frac{d\sigma_{11}}{(\sigma_{11}^{f}-\sigma_{11})^{m}} + \frac{1}{2} A_2 \rho_{m\,c}^{opt} \left[\left(\frac{\sigma_{11}-\sigma_{22}}{\sigma_{11}-\sigma_{33}} \right)^{N} + 1 \right] \frac{d\sigma_{33}}{(\sigma_{33}^{f}-\sigma_{33})^{p}} \qquad (H10)$$

for $\sigma_{33} < -\sigma_c$ and $\sigma_{11} \geq \sigma_{11}^{cr}$, and

$$-d <\epsilon_{11}^{t}>_{m\,c} \cong \frac{1}{2} A_2 \rho_{m\,c}^{opt} \left[\left(\frac{\sigma_{11}-\sigma_{22}}{\sigma_{11}-\sigma_{33}} \right)^{N} + 1 \right] \frac{d\sigma_{33}}{(\sigma_{33}^{f}-\sigma_{33})^{p}} \qquad (H11)$$

for $\sigma_{11} < \sigma_{11}^{cr}$.

The total average strains for the case where σ_{11} is compressional ($\geq \sigma_{11}^{cr}$) and $\sigma_{22} = \sigma_{33}$ ($\leq -\sigma_c$) is tensional are

$$<\epsilon_{11}^{t}> \cong <\epsilon_{11}^{*}> \qquad (H12)$$

$$<\epsilon_{22}^{t}> = <\epsilon_{33}^{t}> = <\epsilon_{33}^{*}> + \frac{1}{2} \int_{-T_o}^{\sigma_{33}} A_2 \rho_{m\,c}^{opt} \frac{d\sigma_{33}}{(\sigma_{33}^{f}-\sigma_{33})^{p}} - \frac{1}{2} \int_{\sigma_{11}^{cr}}^{\sigma_{11}} A_1 \rho_{m\,c}^{cls} \frac{d\sigma_{11}}{(\sigma_{11}^{f}-\sigma_{11})^{m}} \quad ,$$

where the microcrack densities are specified by equation H1. Figure H2 illustrates the stress-strain behavior predicted by equation H12.

It is essential to determine if the quantities A_1 and A_2 are affected by the addition of confining pressure. Paulding's results suggest (at least for the "cls" mode) that the angles the microcracks make with σ_{11} are both small and little affected by the addition of confining pressure.

Brace and Orange (1968) have shown that for the Westerly granite the changes in volume due to microcracking are insensitive to the effective pressure. Their results suggest that total failure of the Westerly granite occurs at a critical crack density and that this critical density is pressure independent. This information suggests that A_1 and A_2 are little affected by the state of stress. Consequently, we shall postulate that the final expressions for the microcrack strain components contain unknown "constants" (A_1 and A_2) which must be evaluated from experimental data.

As an example of equations H9 through H12, consider the total average strains resulting from (1) a pure uniaxial compression and (2) a pure uniaxial tension. In the case of uniaxial compression,

$$\begin{aligned} d\langle\epsilon_{11}^t\rangle_c &\cong d\langle\epsilon_{11}^*\rangle \\ d\langle\epsilon_{33}^t\rangle_c = d\langle\epsilon_{22}^t\rangle_c &\cong d\langle\epsilon_{33}^*\rangle - \frac{1}{2} A_1 \rho_m^{cls}{}_c \frac{d\sigma_{11}}{(\sigma_{11}^f - \sigma_{11})^m} \quad , \end{aligned} \tag{H13}$$

while for uniaxial tension

$$\begin{aligned} d\langle\epsilon_{11}^t\rangle_t &\cong d\langle\epsilon_{11}^*\rangle + \frac{1}{2} A_2 \rho_m^{opt}{}_c \frac{d\sigma_{11}}{(\sigma_{11}^f - \sigma_{11})^p} \\ d\langle\epsilon_{33}^t\rangle_t = d\langle\epsilon_{22}^t\rangle_t &\cong d\langle\epsilon_{33}^*\rangle \quad , \end{aligned} \tag{H14}$$

where the "*" strain components were derived in Part I. From equation H13 and H14, the apparent[3H] "elastic" moduli are

$$\begin{aligned} E_f^* &\cong E_f \\ \nu_f^* &\cong \nu_f + E_f A_1 \frac{\rho_m^{cls}{}_c}{(\sigma_{11}^f - \sigma_{11})^m} \end{aligned} \tag{H15}$$

[3H] By apparent moduli is meant that the moduli are measured with respect to a fixed coordinate system--in this instance (x_1, x_2, x_3).

for compression and

$$E_1^* \cong \frac{E_1}{1+\frac{1}{2}A_2 E_1 \frac{\rho_{R\,c}^{opt}}{(\sigma_{11}^f-\sigma_{11})^p}}$$

$$\nu_1^* \cong \frac{\nu_1}{1+\frac{1}{2}A_2 E_1 \frac{\rho_{R\,c}^{opt}}{(\sigma_{11}^f-\sigma_{11})^p}} \qquad \text{(H16)}$$

for pure tension. The E_1, E_f, ν_1 and ν_f were derived earlier.

The "bulk" modulus ($<\epsilon_{11}^t>$ vs. σ_{11}) in compression and tension is

$$K_f^* \cong \frac{K_o}{1-A_1 K_o \frac{\rho_{R\,c}^{cl\,s}}{(\sigma_{11}^f-\sigma_{11})^m}}$$

$$K_1^* \cong \frac{K_1}{1+\frac{1}{2}A_2 K_1 \frac{\rho_{R\,c}^{opt}}{(\sigma_{11}^f-\sigma_{11})^m}} \quad . \qquad \text{(H17)}$$

APPENDIX I

BRITTLE FRACTURE UNDER HOMOGENEOUS AXISYMMETRIC STATES OF STRESS

A fundamental problem in developing a criterion of brittle fracture is that the criterion must be general enough to predict the failure characteristics under all states of stress. A criterion of this nature, should one in fact exist, must imply that there is something in common with each failure mode. From our earlier comments, it is apparent that neither the magnitudes of the stresses nor the strains at total failure saisfy the above requirement. However, the total volumetric strains at failure for each failure mode do have in common the fact that they express the result that microcracking (i.e., local volume increases) is occurring within the structure. Paulding's (1965) results indicate that in uniaxial and confined compression tests on the Westerly granite, the magnitudes of the volumetric microcrack strains appear to group about a value of 100×10^{-4} near structural instability with no apparent increase or decrease as the confining pressure is increased. This result suggests a critical volumetric microcrack strain criterion may be operative.

We have shown that the total volumetric strain due to microcracking can be expressed as

$$\left| \epsilon_{11}^{mc} \right| \cong \int_{\sigma_{11}^{cr}}^{\sigma_{11}^{f}} A_1 \rho_{mc}^{cls} \frac{d\sigma_{11}}{(\sigma_{11}^{f}-\sigma_{11})^{m}} + \int_{\sigma_{33}^{cr}}^{\sigma_{33}^{f}} A_2 \rho_{mc}^{opt} \frac{d\sigma_{33}}{(\sigma_{33}^{f}-\sigma_{33})^{p}} , \qquad (I1)$$

where the restrictions on the existence of the densities were discussed in appendix H. The stress $\sigma_1^f{}_1$ is the magnitude of the applied stress at total failure. The total volumetric work due to microcracking is

$$W_v^{m\,c} \cong V \int_0^{\epsilon_{11}^{m\,c}} \sigma_{11} \left| d\epsilon_{11}^{m\,c} \right| \quad , \tag{I2}$$

where V is the total volume of the specimen. We shall assume that total failure occurs when the total volumetric work expended in creating microcracks attains a critical value, i.e., total failure occurs when

$$W_v^{m\,c} \equiv \max \quad . \tag{I3}$$

This criterion is equivalent to stating that total failure occurs when the total volumetric strain due to microcracking attains a critical value, or alternatively, total failure occurs when the total microcrack density achieves a maximum value, i.e.,

$$C_1 \ (\rho_{m\,c}^{cls})_{max} + C_2 \ (\rho_{m\,c}^{opt})_{max} = C_3 \quad , \tag{I4}$$

where C_1, C_2, C_3 are unknown "constants" and the $(\rho_{m\,c}^{cls})_{max}$ and $(\rho_{m\,c}^{opt})_{max}$ are the values of the microcrack densities at incipient total failure.

Either form of the proposed failure criterion expresses the assumtion that total failure occurs when there are a sufficient number of microcracks available so that the probability of their joining up to form a macroscopic fracture surface is quite large (≈ 1).

As an example of the use of equation I4, assume for simplicity that $P(c) = \delta(c-c_o)$ (i.e., all flaws have a constant length). Equation I4 becomes

$$C_1 (\rho_{\text{max}}^{cls})_{\text{max}} + C_2 (\rho_{\text{max}}^{opt})_{\text{max}} = C_3 \quad . \tag{I5}$$

If we further assume that $P(\beta,\varphi)$ is uniformly distributed and independent of φ, equation I5 can be written as

$$C_1 \rho_e (\sin\beta_2^{cls} - \sin\beta_1^{cls}) + C_2 \rho_e \sin\beta_3^{opt} = C_3 \quad . \tag{I6}$$

When $\sigma_{33} \geqslant -\sigma_c$, failure results from the ρ_{max}^{cls} component, i.e.,

$$\sigma_{11}^f = \frac{2\tau_c + \sigma_{33}\,(\sqrt{1+\mu^2}\,\cos M_c^{cls} + \mu)}{(\sqrt{1+\mu^2}\cos M_c^{cls} - \mu)} \quad . \tag{I7}$$

where $M_c^{cls} = 2\sin^{-1}\left[\dfrac{C_3}{2C_1\rho_e \cos(\frac{1}{2}\tan^{-1}\frac{1}{\mu})}\right]$. Denoting the uniaxial compressive strength by c_o gives

$$\cos M_c^{cls} = \frac{2\tau_c + \mu c_o}{\sqrt{1+\mu^2}\; c_o} \quad . \tag{I8}$$

When $\sigma_{11} < \sigma_{11}^{cr}$, failure occurs from the ρ_{max}^{opt} component, i.e.,

$$-\sigma_{33}^{(f)} = \frac{2\sigma_c + \sigma_{11}\,(1-\cos 2M_c^{opt})}{1+\cos 2M_c^{opt}} \quad , \tag{I9}$$

where $M_c^{opt} = \sin^{-1}\dfrac{C_3}{C_2\rho_e}$. Denoting the biaxial tensile strength by t_o^* gives

$$1 + \cos 2M_c^{opt} = \frac{2\sigma_c}{t_o^*} \quad . \tag{I10}$$

Similarily, the uniaxial tensile strength (t_o) of the aggregate can be expressed as

$$t_o = \frac{\sigma_c}{(1-\sin M_c^{opt})^2} \quad . \tag{I11}$$

Comparison of equations I10 and I11 shows

$$\frac{t_o}{t_o^*} = \frac{1+\sin M_c^{opt}}{1-\sin M_c^{opt}} > 1 \quad , \tag{I12}$$

or simply, the uniaxial tensile strength of the aggregate is always larger than the biaxial tensile strength. Obviously, since $P(c) = \delta(c-c_o)$, the triaxial tensile strength is equal to $-\sigma_c$.

Therefore, when $P(c) = \delta(c-c_o)$, this analysis predicts that the stress space fracture surface of the aggregate can be subdivided into three zones, namely,

Zone I: Failure results from the microcracking of open flaws "opt". The least principal stress satisfies the inequality $\sigma_{33} \leqslant -\sigma_c$.

Zone II: Failure occurs by microcracking of both open and "cls" flaws. This region must terminate when the β_2^{cls} flaw begins to open, i.e., when $\beta_o = \beta_2^{cls}$, where

$$\beta_o = \sin^{-1}\sqrt{\frac{\frac{B}{c_o\sigma_{11}} - k}{1-k}}$$

Zone III: Failure takes place only by microcracking of the "cls" flaws. The least principal stress, σ_{33}, satisfies the condition $\sigma_{33} + \sigma_c \geq 0$.

Figure I1 illustrates the fracture surface based upon this analysis.

There are seven major conclusions which follow from the above critical microcrack density criterion. (1) There is a smooth transition between pure

compressional failure (all principal stresses are compressions), extensional (one or two principal stresses are tensile) failure, and true tensional failure (all principal stresses are tensile). (2) The stress-space fracture surface is smooth because there is a smooth transition between the above three types of failure. (3) The stress-space fracture surface possesses a corner which occurs when all three principal stresses are equal and tensile. (4) The stress-space failure envelope is convex. (5) The biaxial tensile strength is always less than or equal to the uniaxial tension strength. (6) The biaxial compressional strength is equal to the uniaxial compressional strength. (7) There is a slight tendency for the tensional strength to increase with confining pressure (see figure I1). With the exceptions of conclusions 3, 5, and 7, these observations have been substantiated experimentally by Brace (1964). There is insufficient experimental data to test conclusions 3, 5, and 7.

APPENDIX J

BRITTLE FRACTURE UNDER HOMOGENEOUS TRIAXIAL STATES OF STRESS

Failure criteria for rock materials are currently based upon the assumption that at constant temperature and strain rate, the failure characteristics of rock are dependent only upon the stress state ($\sigma_{11} \geq \sigma_{22} \geq \sigma_{33}$) within the material. Under these conditions, failure under confined pressure (two of the principal stresses equal) has been extensively studied (Brace, 1964; Handin, 1957; Mogi, 1966). However in recent years, it has become recognized (Brace, 1964; Mogi, 1967) that the intermediate principal stress may be of importance in governing the fracturing characteristics of rock exhibiting either brittle or ductile behavior.

For common metals exhibiting ductile behavior, it is well-known (Nadai, 1950) that the octahedral shear stress criterion fits the experimental data better than the critical shear stress (Tesca) criterion (figure J1). Figure J1 indicates that the intermediate principal stress has an influence (although not very significant) on the ductile behavior of metals. It should be noted that the biaxial ($\sigma_{11} = \sigma_{22}$) and uniaxial ($\sigma_{11}$) ductile strength are equal and that there is no difference between the extension ($\sigma_{11}=\sigma_{22}>\sigma_{33}$) and the compression ($\sigma_{11}>\sigma_{22}=\sigma_{33}$) Mohr envelope for the octahedral shear stress criterion.

The basic question as to the effect of σ_{22} on the fracturing characteristics of brittle materials has yet to be completely resolved although

recent experimenters (Handin, 1957; Mogi, 1967) report finding a discrepancy between the Mohr envelopes for extension and compression. Brace (1964), using a special test specimen design, found no detectable differences between the two envelopes.

By assuming a relationship between the various failure modes in brittle materials, it was stated in appendix I that one of the more fundamental problems in developing a useful criterion of brittle failure is that the criterion must be general enough so that it becomes possible to predict the failure characteristics of brittle materials under any and all states of stress. We shall again postulate that total failure occurs when the work done in creating microcracks attains a critical value, or alternatively, total failure occurs when the volumetric microcrack strain achieves a maximum value. We shall further postulate that this condition is completely independent of whether the applied stress system is axisymmetric or triaxial. Therefore, total failure takes place when

$$\left| \epsilon_{ii}^{mc} \right| = \left| \epsilon_{ii}^{mc} \right|_{max} \quad . \tag{J1}$$

This criterion is equivalent to assuming that total failure occurs whenever the total microcrack density attains a critical value, i.e., total failure occurs when

$$C_1 \left(\rho_{mc}^{cls}\right)_{max} + C_2 \left(\rho_{mc}^{opt}\right)_{max} = C_3 \quad , \tag{J2}$$

where

$$(\rho_{m\,c}^{cls})_{max} = 8 \int_{c_{max}}^{c_1^{cls}} \int_{\varphi_1^{cls}}^{\pi/2} \int_{\beta_1^{cls}}^{\beta_2^{cls}} P(c,\beta,\varphi)\,d\beta\,d\varphi\,dc$$

$$(\rho_{m\,c}^{opt})_{max} = 8 \int_{c_{max}}^{c_1^{opt}} \int_{\varphi_3^{opt}}^{\pi/2} \int_{0}^{\beta_3^{opt}} P(c,\beta,\varphi)\,d\beta\,d\varphi\,dc \quad . \tag{J3}$$

The limits of intergration are evaluated at failure (appendix D) and

$$c_1^{cls} = 4\left(\frac{T_c}{\sigma_{11}^f}\right)^2 \left[\left(\sqrt{1+\mu^2}-\mu\right) - k\left(\sqrt{1+\mu^2}+\mu\right)\right]^{-2} c_{max}$$

$$c_1^{opt} = \left(\frac{\sigma_c}{\sigma_{11}^f}\right)^2 c_{max} \quad . \tag{J4}$$

Figure J2(a) shows the influence of the intermediate principal stress on the biaxial compression fracturing characteristics of a hypothetical brittle rock. The least principal stress (σ_{33}) is equal to zero. For ease of calculation, all cracks in the rock are taken to be of equal length. The uniaxial compression strength (c_o) is 34,500 psi. The value of the stress required to initiate growth of the first microcrack under uniaxial compression (C_o) is 17,250 psi. The coefficient of friction along the crack surface is 0.70. We have assumed that the cracks are uniformly distributed throughout the rock structure. There are three conclusions to be drawn from figures J2(a) and J2(b). They are: (1) the uniaxial ($\sigma_{11}=c_o, \sigma_{22}=\sigma_{33}=0$) and biaxial ($\sigma_{11}=\sigma_{22}=c_o, \sigma_{33}=0$) compressive strengths are equal; (2) there is no effect of the intermediate principal stress for compressive values of σ_{33} in either the extension ($\sigma_{11}=\sigma_{22}$) or the compression ($\sigma_{22}=\sigma_{33}$) test (figure J2[b]); (3) the maximum effect of σ_{22} on the failure strength only amounts to approximately a 20 percent increase in strength over the uniaxial

compressive strength. We also considered a similar problem but with a friction coefficient equal to zero. In this case we found that the maximum strength increase (still approximately 20 percent) occurred at a value of σ_{22} equal to one-half of the uniaxial compressive strength. This is a location which would be expected if a distortional energy failure criterion (or octahedral shear stress criterion) were operative. The first and second conclusions are in agreement with Brace's (1964) experimental results.

Figure J2(b) shows the influence of σ_{22} on the extension and compression failure characteristics of the same hypothetical brittle rock. The uniaxial tensile strength (t_o) is assumed to be 1500 psi. The value of the critical stress (σ_c) required to initiate failure of the "opt" class is 1125 psi. If this data is substituted into equation J3 we find that there is an effect of the intermediate principal stress when the least principal stress (σ_{33}) is tensile and that the maximum effect occurs under biaxial tension when $\sigma_{22}=\sigma_{33}=-t_o^*$, where t_o^* denotes the biaxial tensile strength of the rock. The biaxial tensile strength (t_o) for this rock is approximately 1150 psi. This amounts to a reduction from the uniaxial tensile strength of only 23 percent. The triaxial tensile strength is 1125 psi since all the cracks are assumed to be of equal length. As the maximum principal stress (σ_{11}) increases in compression, the percent deviation between the extension and compression envelopes decreases as shown in figure J2(b).

APPENDIX K

EFFECT OF INHOMOGENEITY ON THE FRACTURE CHARACTERISTICS OF BRITTLE ROCK

The pressure dependence of rock strength in the "brittle" domain (figure K1) has been graphically categorized into three zones by Mogi (1966). These zones are: (1) B_i. The strength vs. pressure curve is nonlinear and concave downward. The breaking strength increases while the rate of the increase decreases with the addition of confining pressure. (2) B_o. The strength increases linearily with pressure. (3) B_t. The slope of the strength vs. pressure curve is gradually decreasing. This zone represents the transition between purely brittle and brittle-ductile behavior.

While these zones are typical of brittle rocks, some rock types such as quartzite consist primarily of B_o (figure K1) and lack the B_i zone. Other rock types such as granite tend to change continuously from B_i to B_t. In carbonate rocks, the strength vs. pressure curves vary continuously from B_o to B_t. However, for small values of confining pressure, carbonate rocks do display a linear strength-pressure relation (Mogi, 1966) (figure K2).

There is a tendency in some brittle rocks for the angle of the macroscopic fracture surface (the plane of which is measured with respect to the maximum principal stress) to increase as the confining pressure is increased. While there is no wealth of experimental information on this subject, the available data suggest that this behavior is more pronounced

in materials containing a number of different mineral phases, i.e., there appears to be less of an angular increase in quartzite (Brace, 1964) and carbonates (Mogi, 1966) than in granites (Brace, 1964; Mogi, 1966)(figures K1, K2) . These observations suggest that material inhomogeneity may to some degree affect the failure characteristics of brittle rock. In analyzing the possible effects of inhomogeneity on the fracturing of brittle rock, we shall make the following assumptions: (1) The specimen is optically isotropic in the sense that the grains of each phase are randomly distributed throughout the material; (2) the volume is sufficiently large so that the specimen will macroscopically behave as an elastically isotropic unit; (3) the inter-and transgranular cracks can be modeled by ellipsoidal-type cracks collectively characterized by a distribution function $P(c,\beta,\varphi)$. The inhomogeneity will be mathematically modeled by assuming a distribution of friction coefficients (μ_i, i=1,$\cdots$,M) and "tensile strengths" (T_{o_i}, i=1,$\cdots$,M) for the M possible types of contact surfaces (figure K3); (4) there are sufficient numbers of each type crack $[N_{e_i}(\mu_i, T_{o_i})]$ so that a continuum approach to the gross mechanical behavior is possible.

For the inhomogeneous case, equation 72 can be rewritten in the form

$$A_2 \left(\rho_m^{cl_s} c\right)_{max}^{T} + A_3 \left(\rho_m^{opt} c\right)_{max}^{T} = A_4 \quad , \tag{K1}$$

where

$$\left(\rho_{\text{max}}^{cls}\right)^{T} = 8\rho_e \sum_{i=1}^{M} \Psi_i \int_{c_{\text{max}}}^{c_1^{cls}} \int_{\varphi_1^{cls}}^{\pi/2} \int_{\beta_1^{cls}}^{\beta_2^{cls}} P(c,\beta,\varphi)\,d\beta\,d\varphi\,dc$$

$$\left(\rho_{\text{max}}^{opt}\right)^{T} = 8\rho_e \sum_{i=1}^{M} \Psi_i \int_{c_{\text{max}}}^{c_1^{opt}} \int_{\varphi_3^{opt}}^{\pi/2} \int_{0}^{\beta_3^{opt}} P(c,\beta,\varphi)\,d\beta\,d\varphi\,dc \qquad \text{(K2)}$$

$$\sum_{i=1}^{M} \Psi_i = 1 \quad ,$$

with $\Psi_i = N_{ei}/N_e$ (N_e = total number of primary cracks).

In the instance where $\sigma_{22} = \sigma_{33}$, and the P cracks are randomly distributed and are of equal length, equation K1 for the "cls" mode can be written as

$$\rho_e\, C_1 \sum_{i=1}^{M} \Psi_i \,(\sin\beta_{2i}^{cls} - \sin\beta_{1i}^{cls}) = C_3 \qquad \text{(K3)}$$

where

$$\beta_{2i}^{cls} = \tfrac{1}{2}\left[\tan^{-1}\frac{1}{\mu_i} + \cos^{-1}\frac{2\tau_{oi}+\mu_i(\sigma_{11}+\sigma_{33})}{\sqrt{1+\mu_i^2}\,(\sigma_{11}-\sigma_{33})}\right]$$

$$\beta_{1i}^{cls} = \tfrac{1}{2}\left[\tan^{-1}\frac{1}{\mu_i} - \cos^{-1}\frac{2\tau_{oi}+\mu_i(\sigma_{11}+\sigma_{33})}{\sqrt{1+\mu_i^2}\,(\sigma_{11}-\sigma_{33})}\right] \qquad \text{(K4)}$$

$$\tau_{ci} = \sqrt{\frac{B_i}{c_o}} \quad . \qquad [P(c) = \delta\,(c-c_o)]$$

Figure K4 illustrates the stress-space compression field failure envelope according to equation K3. The failure envelope is nonlinear and concave downward. The rate of decrease of the envelope decreases as the confining pressure increases. The physical reasoning for this decrease is that with the addition of confining pressure, primary cracks with high friction coefficients tend not to satisfy the modified Griffith failure initiation theory.

Therefore, the failure of additional primary cracks possessing lower friction coefficients are necessary for the development of a macroscopic fracture surface.

While there is little question that these equations represent a considerable simplification of the actual problem, two points are evident; namely, (1) the addition of confining pressure tends to inhibit sliding of high friction coefficient primary cracks and (2) the formation of a macroscopic fracture surface requires the formation of additional microcracks from the lower μ primary cracks. For a material exhibiting these properties, the failure envelope will be nonlinear in the compressive stress region and the degree of nonlinearity will tend to diminish as the confining pressure increases.

Due to the complexity of the above equations, an empirical approach is a necessity. The above model for nonhomogeneous materials indicates that the apparent friction coefficient is dependent on pressure and as the pressure increases, the apparent friction coefficient tends to decrease. Therefore, as a first approximation, it is logical to use the equations developed for the homogeneous case with the friction coefficient varying with pressure, say $\mu=ae^{-b\sigma_{33}}+c$, where a, b, and c are constants which must be evaluated from experimental data. This reduction in the effective friction coefficient has been discussed by several authors (Mogi, 1966; Byerlee, 1966). Finally, notice that this model suggests that the overall fracture angle increases as the confining pressure increases, i.e., the critical angle, $\frac{1}{2}\tan^{-1}\frac{1}{\mu_i}$ of sliding tends to increase as the confining pressure increases (see figure K2).

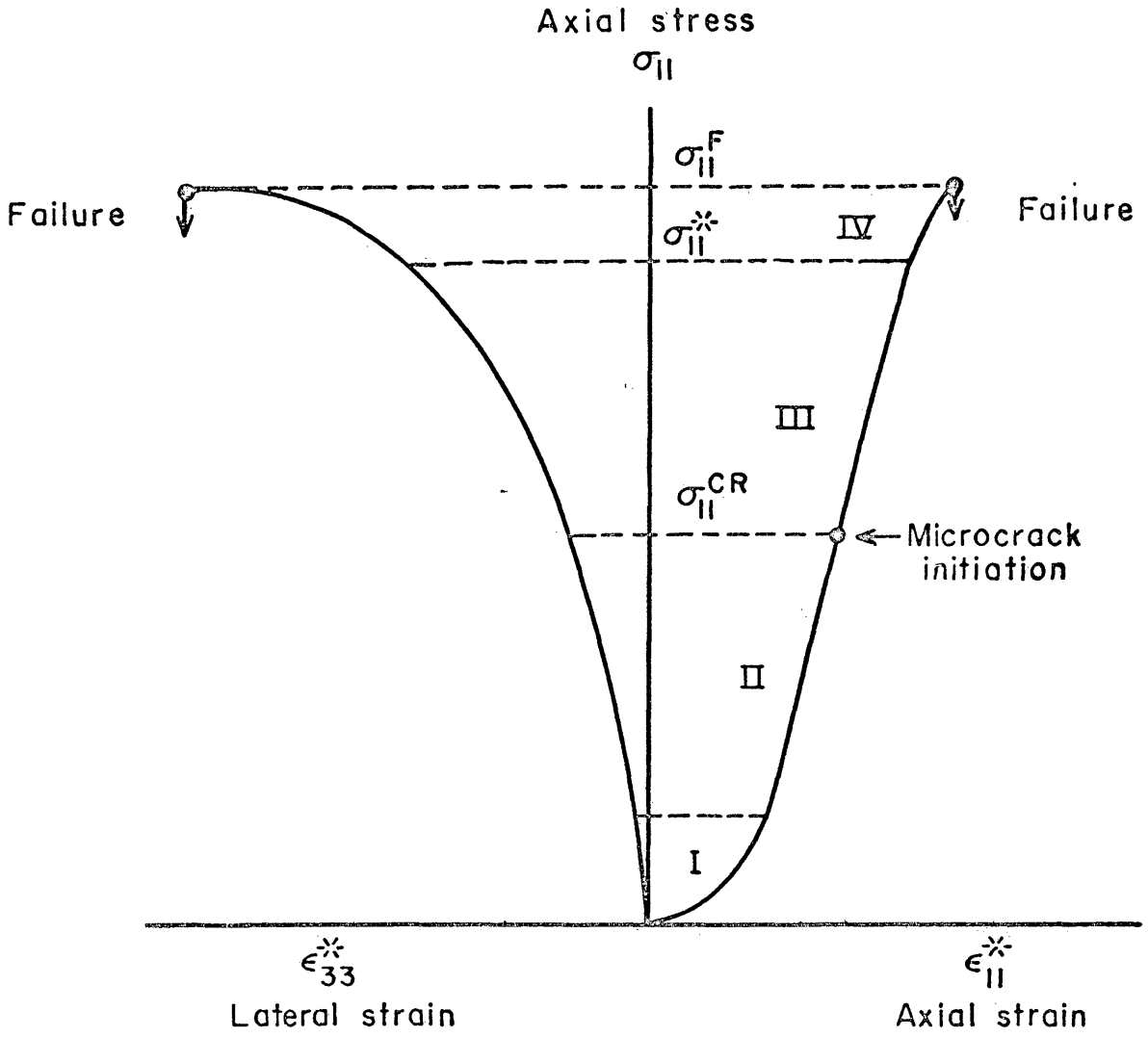

FIGURE 1.- Typical Axial and Lateral Stress Strain Behavior of Brittle Rock Under Uniaxial Loading. (Conventional testing machine)

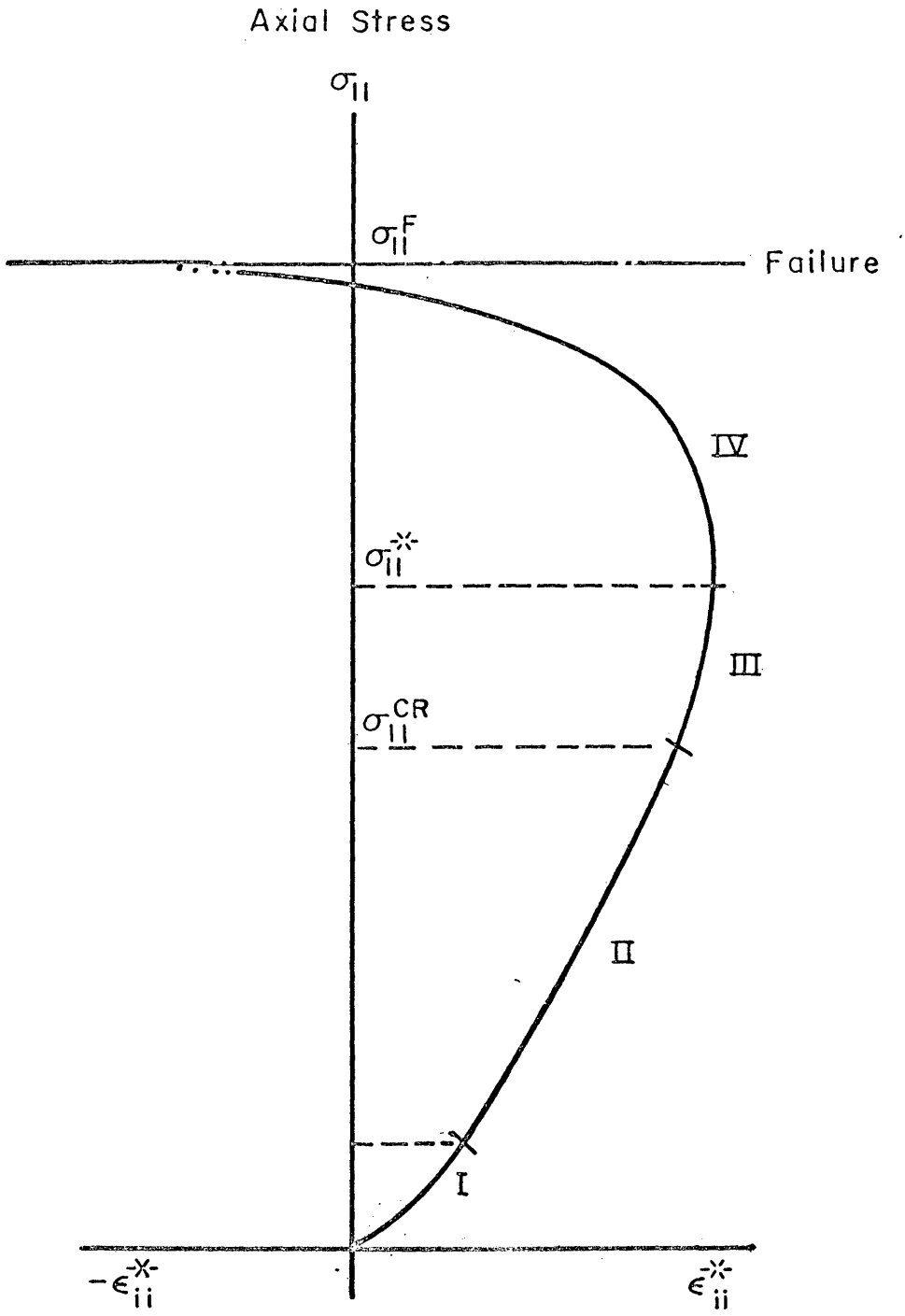

FIGURE 2.-Typical Volumetric Strain Plot for Brittle Rock. (Conventional testing machine)

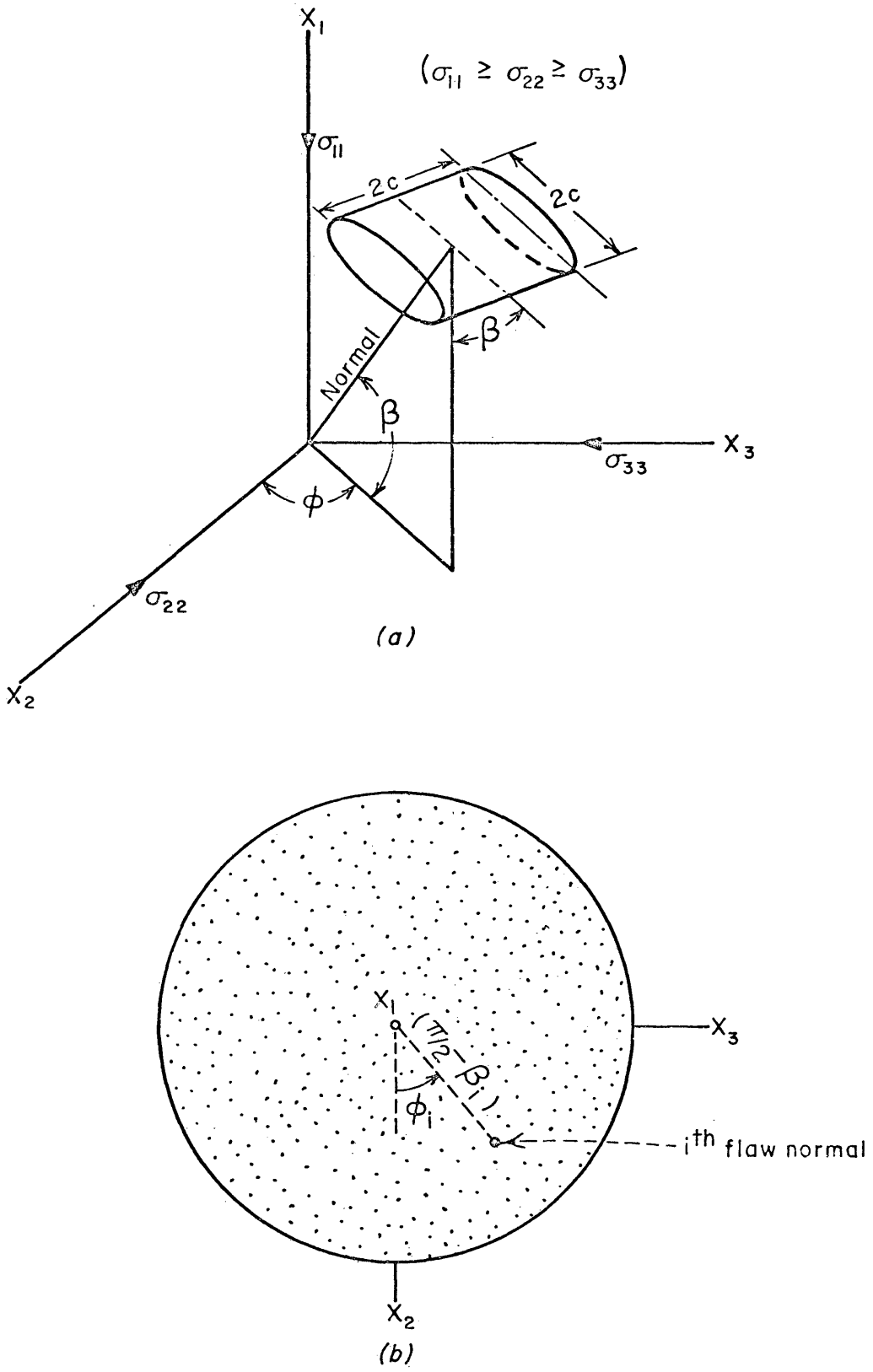

FIGURE 3.—Illustration of a Random Flaw Distribution Characterized by the Distribution Function $P(c, \beta, \phi)$

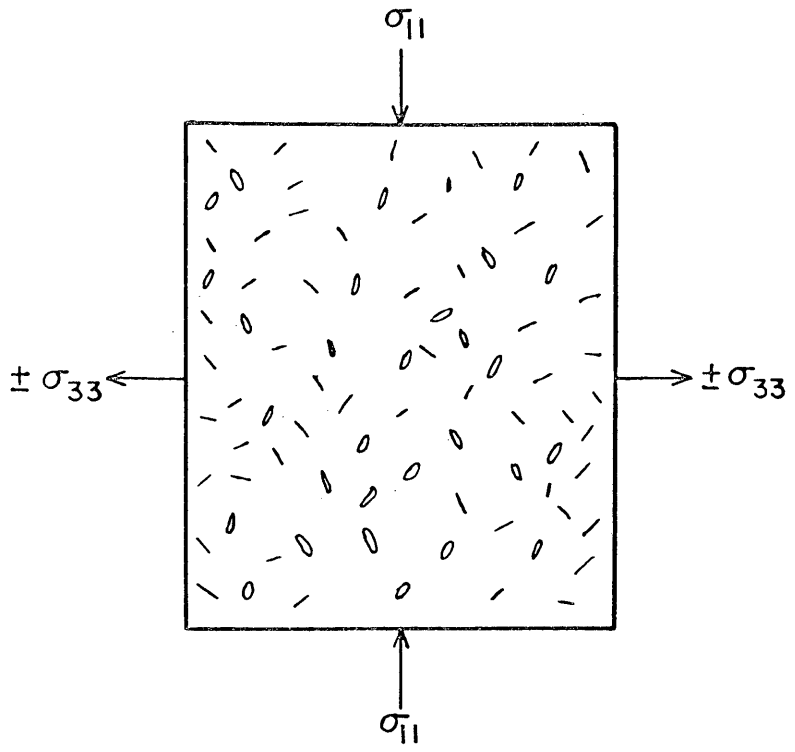

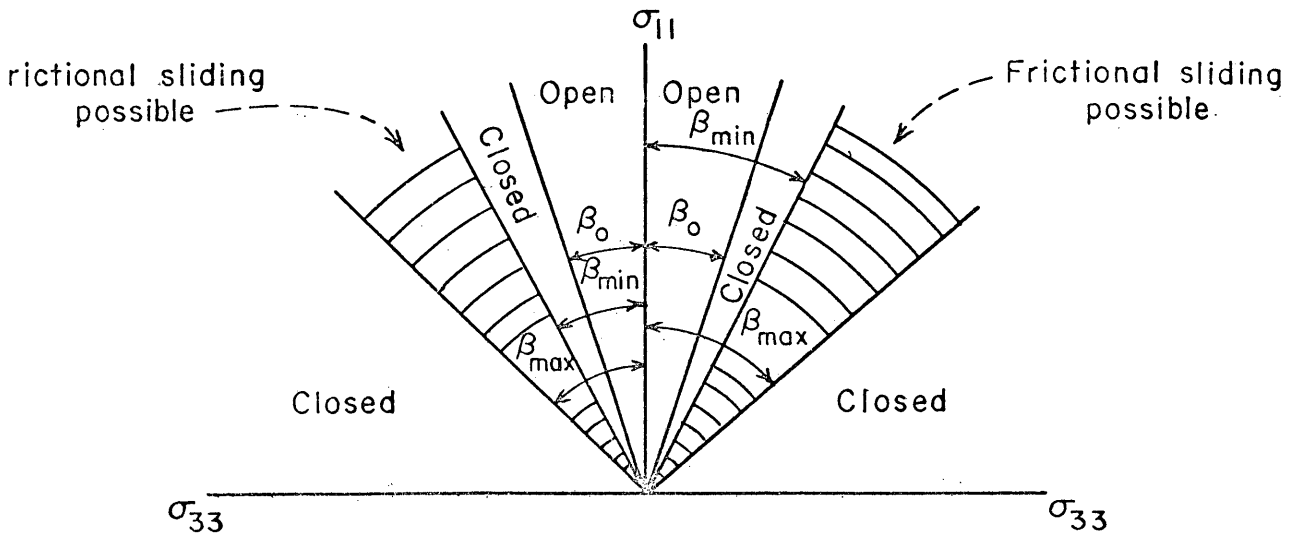

IGURE 4.-Specification of Angular Relations Between Closed and Open Flaws in a Specimen with N_e Flaws.

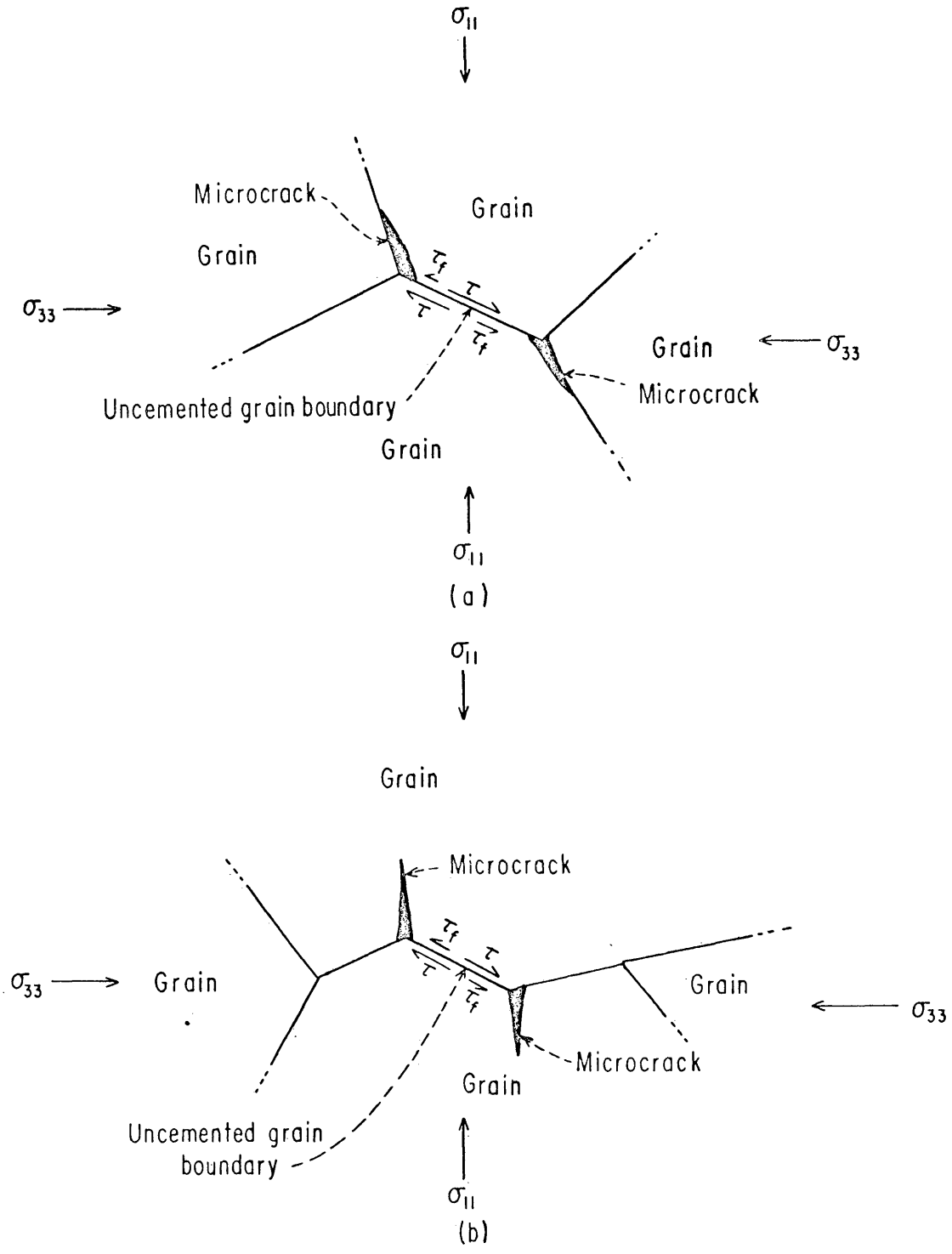

FIGURE 5.-Two Types of Microcracking in a Granular Brittle Rock Subjected to Compressive Loading.
a.-Intergranular Microcracking Model ("cls" class), $(\tau - \tau_f \geq \tau_{c1})$
b.-Intergranular Microcracking Model ("cls" class), $(\tau - \tau_f \geq \tau_{c2})$

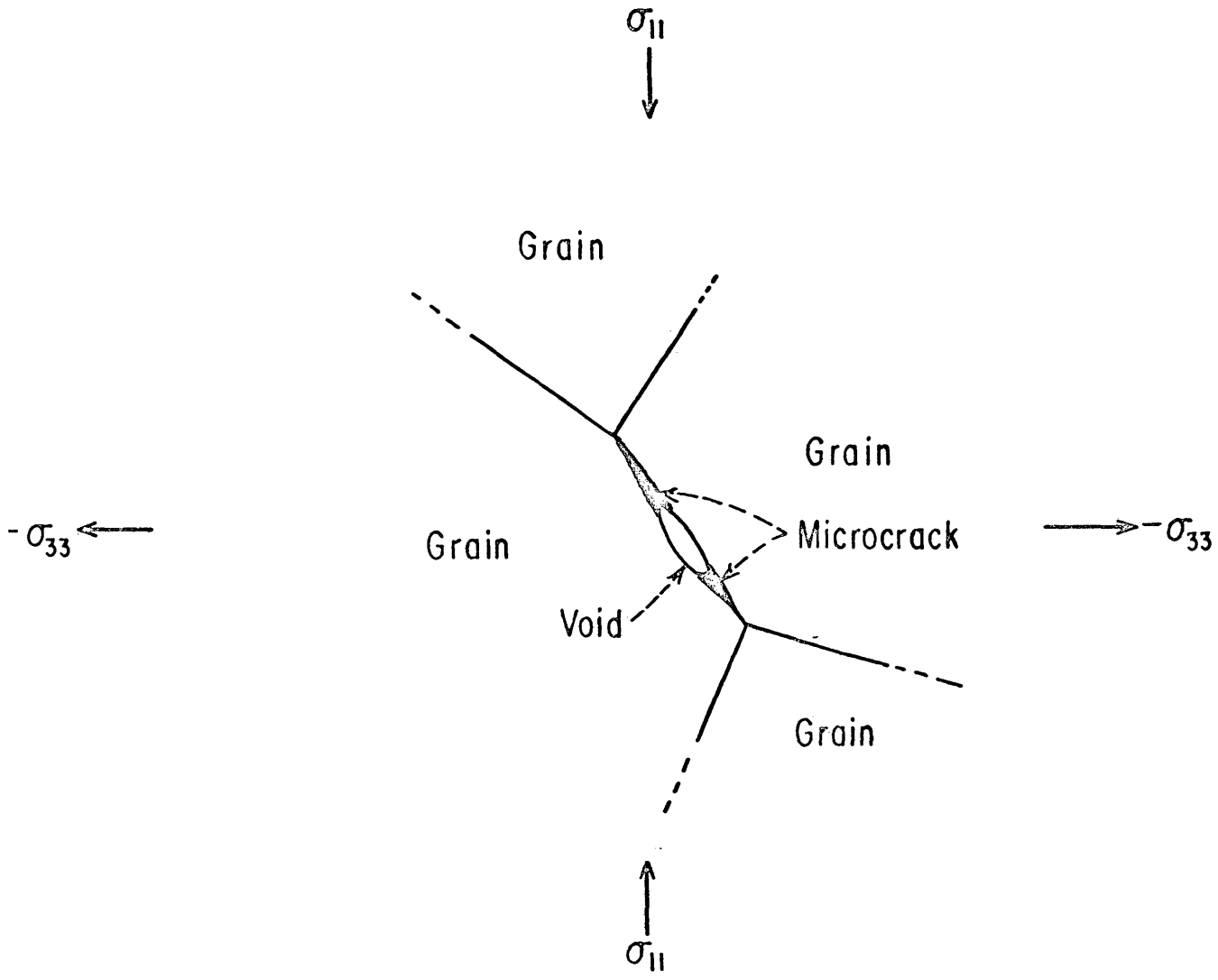

FIGURE 6.- Intergranular Microcracking in a Granular Brittle Rock Subjected to Tensile Loading ($\sigma_N \leq -\sigma_c$).

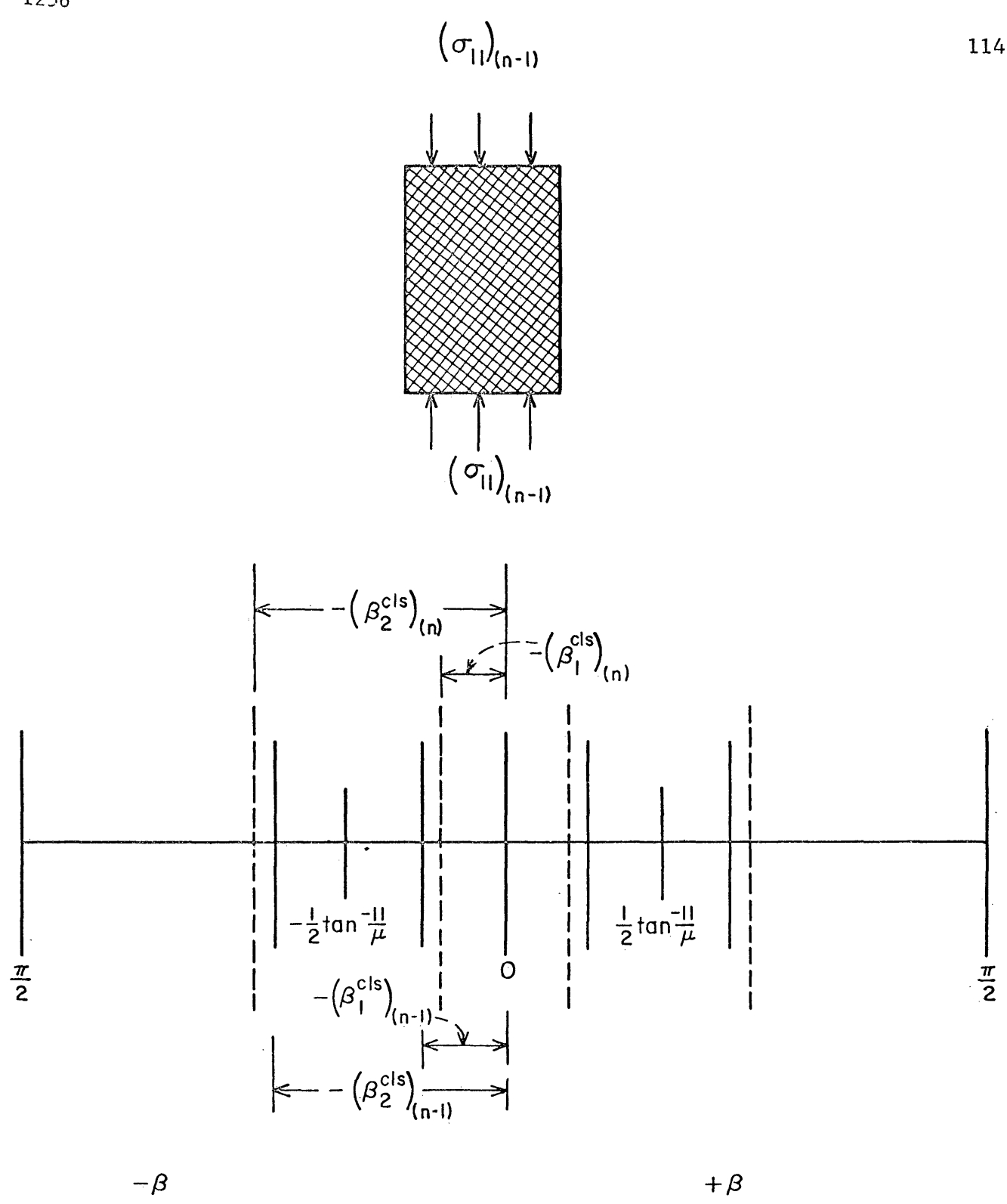

FIGURE 7.- Nomenclature Used to Specify the Angular Range of Closed Cracks Undergoing Failure as the Applied Axial Stress Increases in Compression From $(\sigma_{11})_{(n-1)}$ to $(\sigma_{11})_{(n)}$

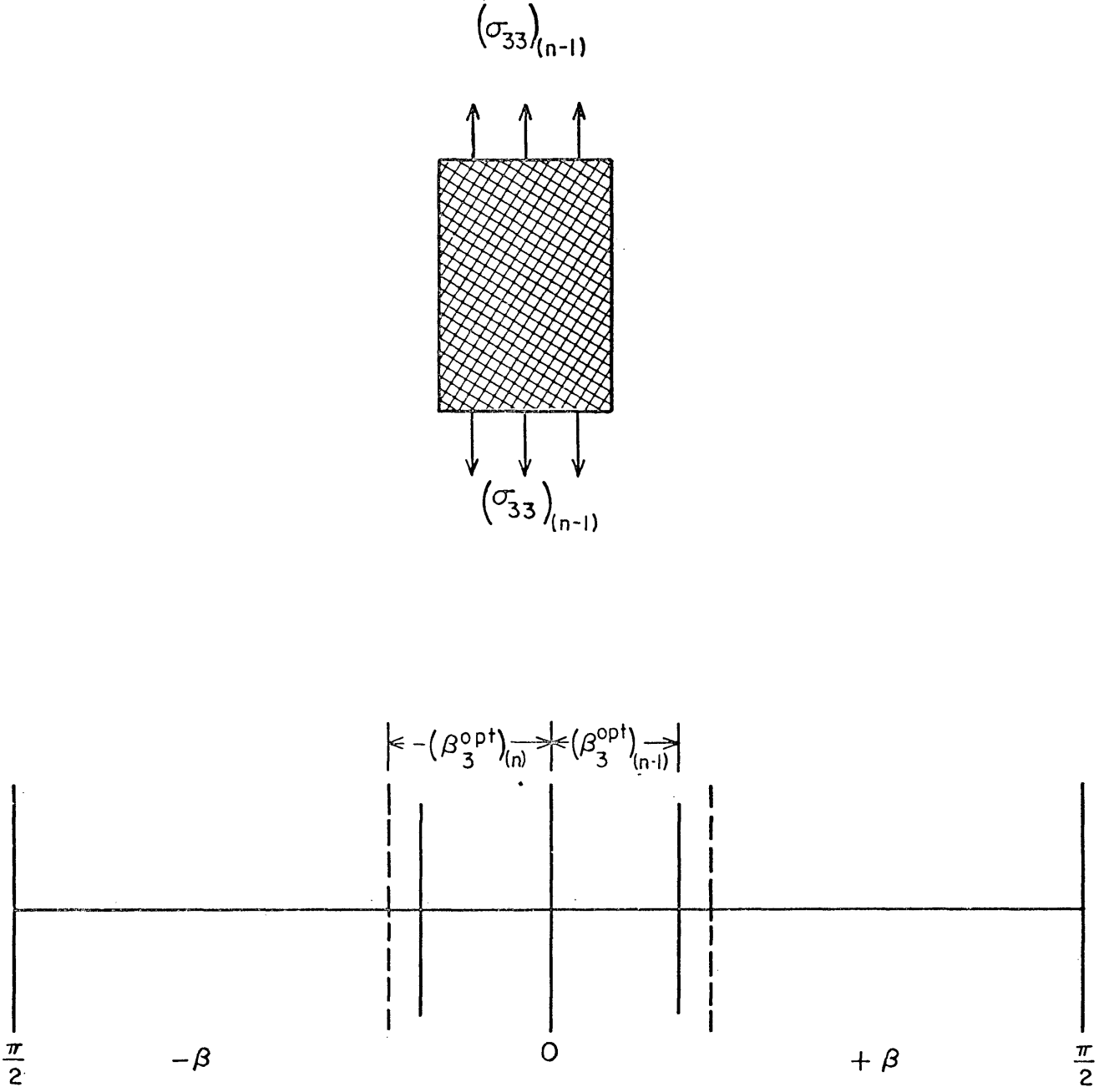

FIGURE 8.- Nomenclature Used to Specify the Angular Range of Closed Cracks Undergoing Failure as the Applied Axial Stress Increases in Compression From $(\sigma_{33})_{(n-1)}$ to $(\sigma_{33})_{(n)}$

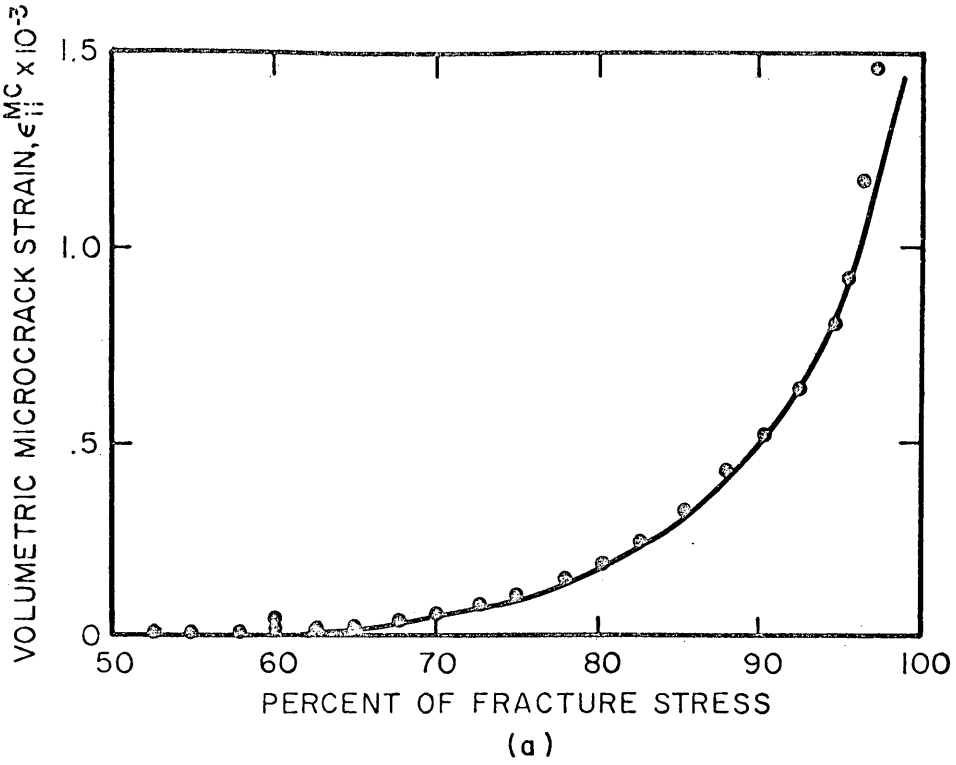

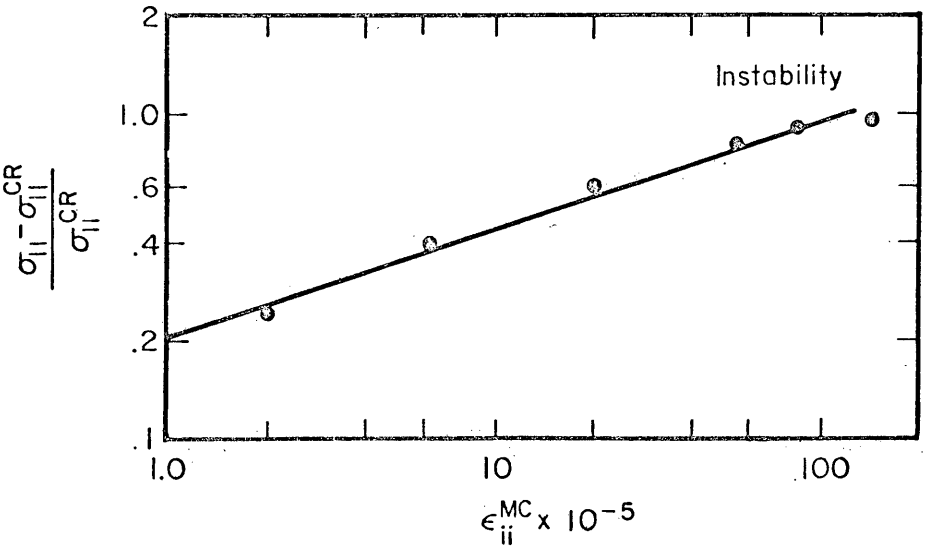

FIGURE 9.-(a) Variation of Volumetric Microcrack Strain of the Westerly Granite with Percent of Fracture Stress.
(b) Variation of Volumetric Microcrack Strain and $\left(\frac{\sigma_{ii} - \sigma_{ii}^{CR}}{\sigma_{ii}^{CR}}\right)$ For the Westerly Granite

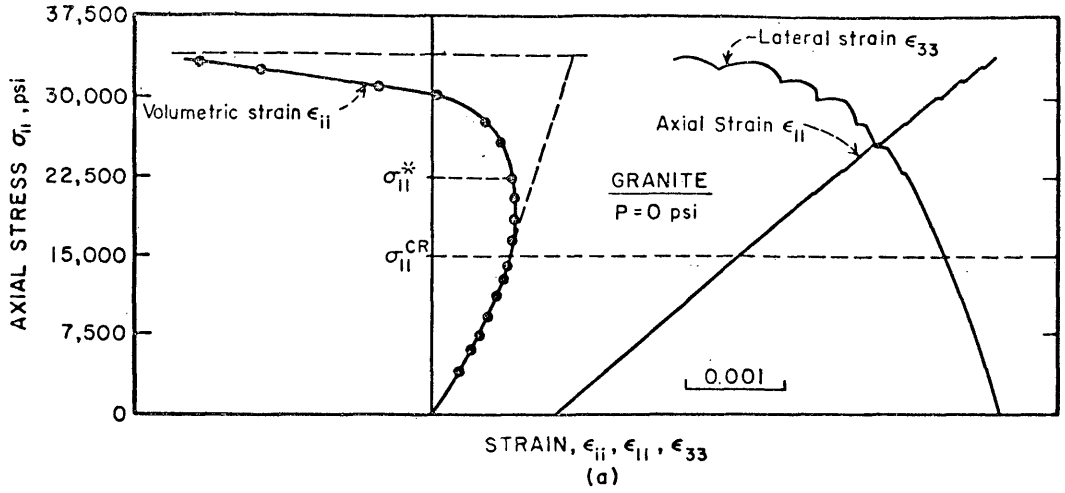

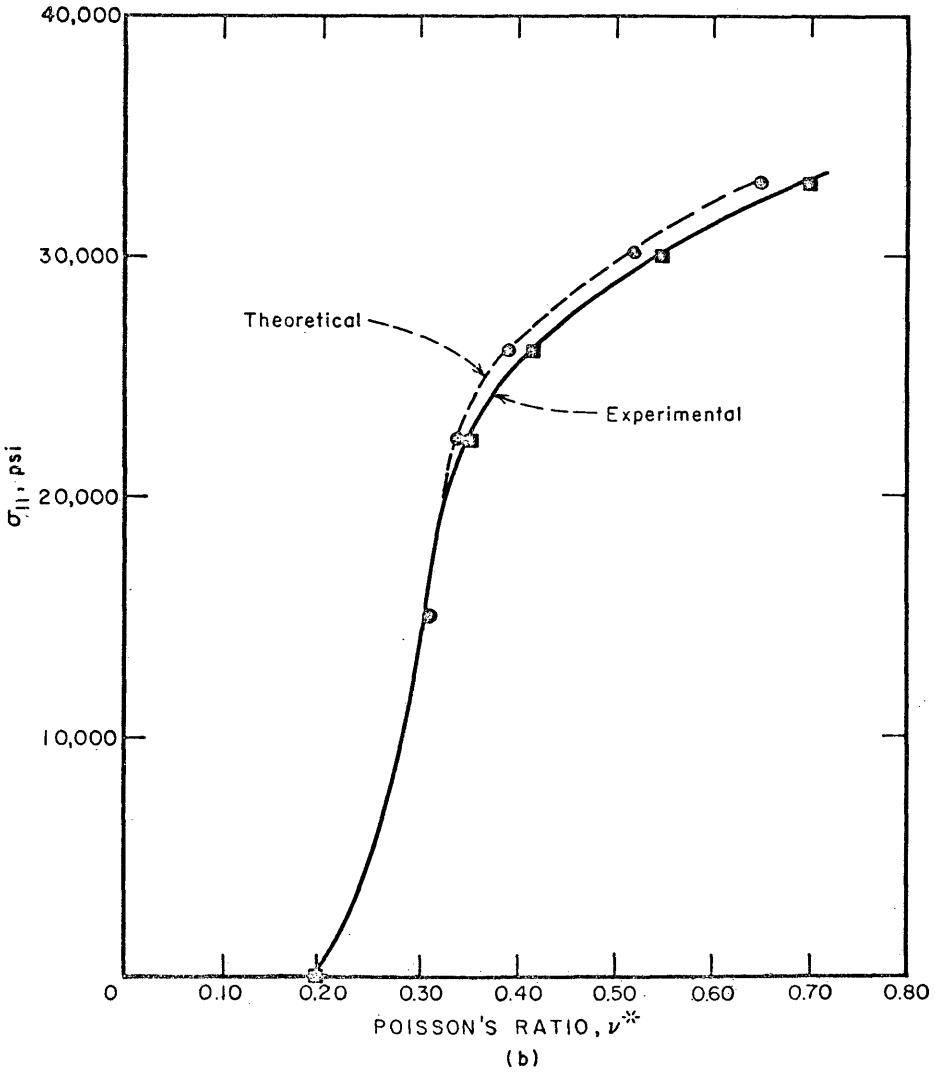

FIGURE 10.- Stress-Strain Behavior of the Westerly Granite (after Brace et al., 1966)

(a) Left-Hand Curve Shows Axial Stress Versus Volumetric Strain. Right-Hand Curve Shows Axial Stress Versus Axial and Lateral Strain.

(b) Theoretical and Experimental Predicted Variation of Poisson's Ratio with Axial Stress.

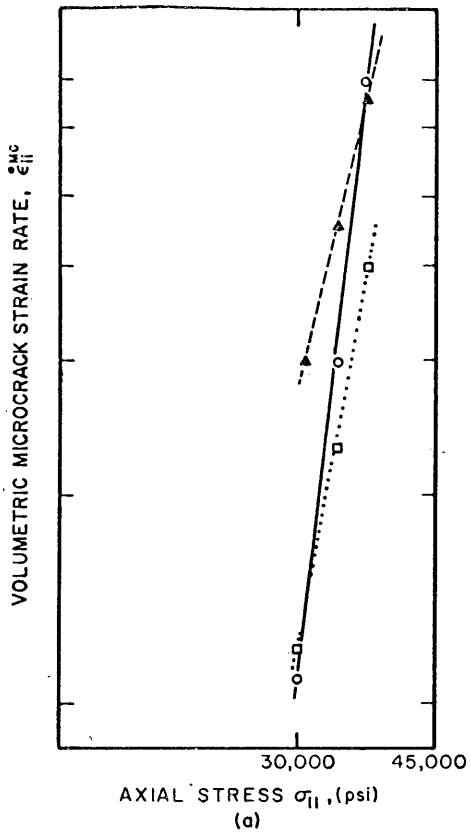

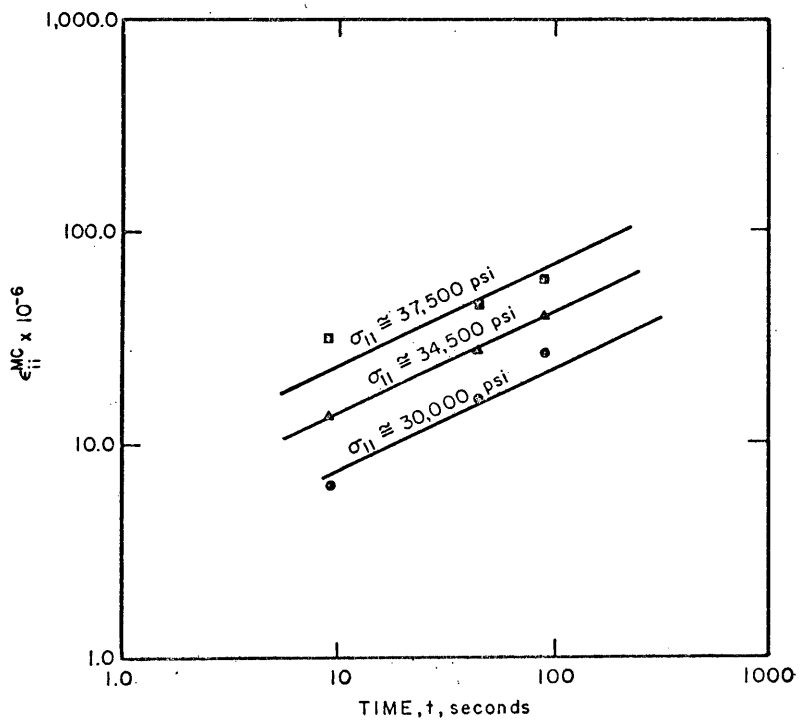

FIGURE 11.-(a) The Observed Stress Dependence of Creep for Westerly Granite Under Uniaxial Compression. The Scales are as Follows: (open circle) Δ at 9 sec, 0.5 X 10^{-6} sec^{-1}; (square) at 45 sec, 0.25 X 10^{-6} sec^{-1}; (solid triangle) at 90 sec, 0.1 X 10^{-6} sec^{-1} (after Scholz, 1968).

(b) Constant Stress Creep Data for the Westerly Granite.

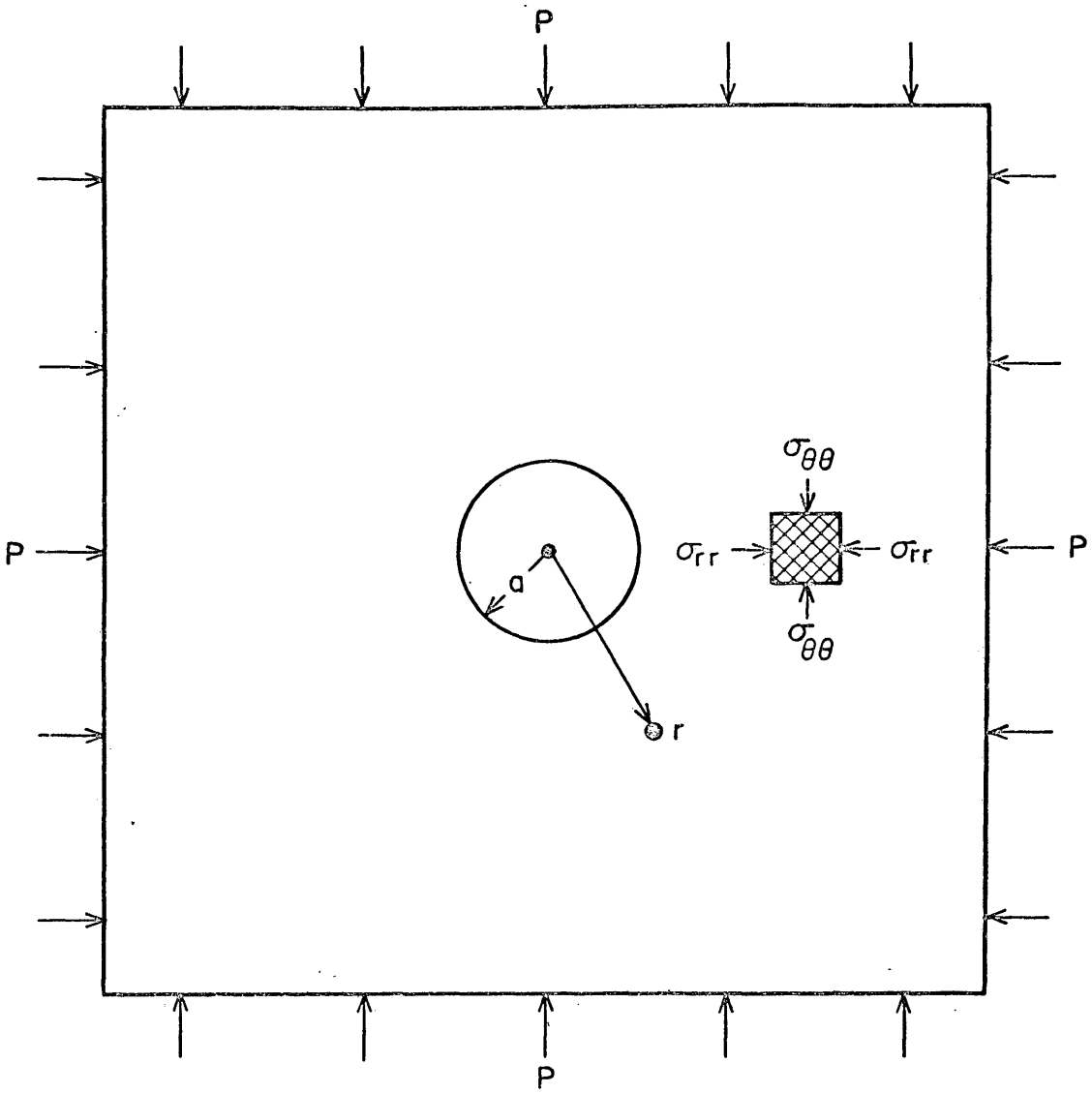

FIGURE 12.-Circular Tunnel in a Hydrostatic Stress Field, Associate Nomenclature, and Definition of Symbols.

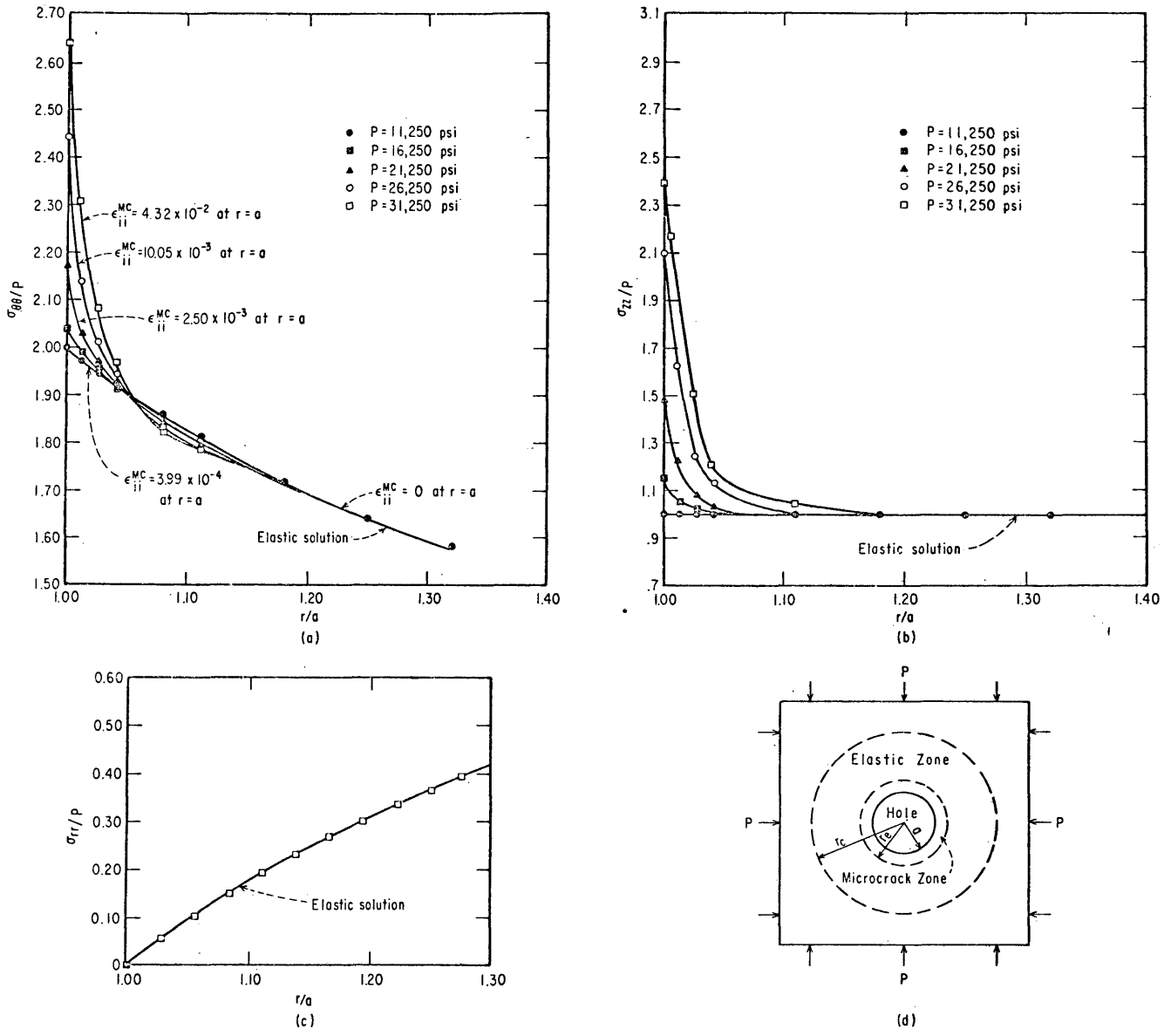

FIGURE 13.- Effect of Microcracking on the Stress Distribution Near a Cylindrical Tunnel in a Brittle Rock

$\left(A_1^{cls} = 6.82, n = 0.29\right)$

$\left(\sigma_{\theta\theta}^{CR} \cong 22.500 + 2.40\sigma_{rr}\right)$

(Elastic solution refers to the stress values predicted by equation 55)

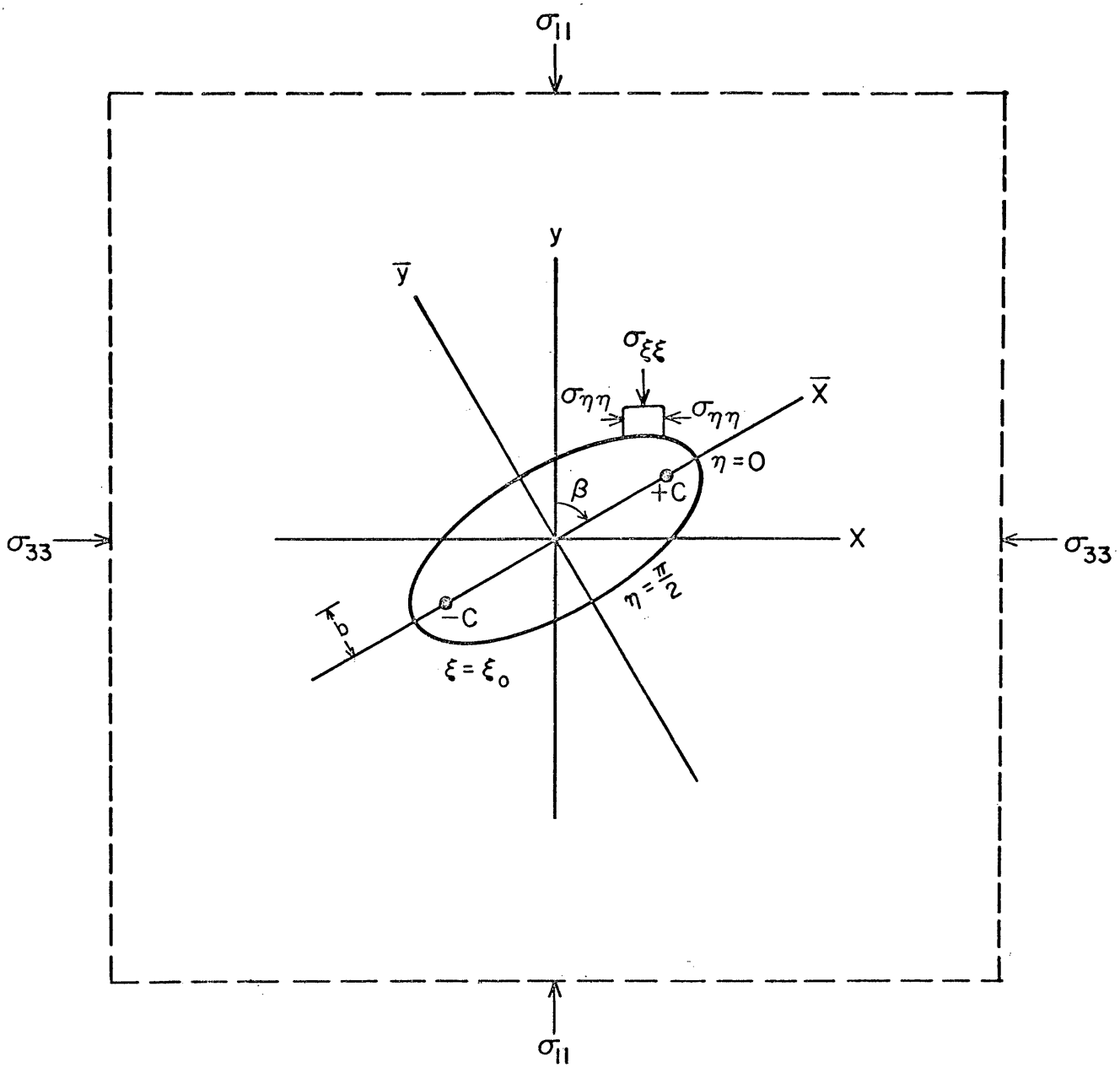

FIGURE A1.- Coordinate Systems Used For Elliptical Crack (after Odé, 1960)

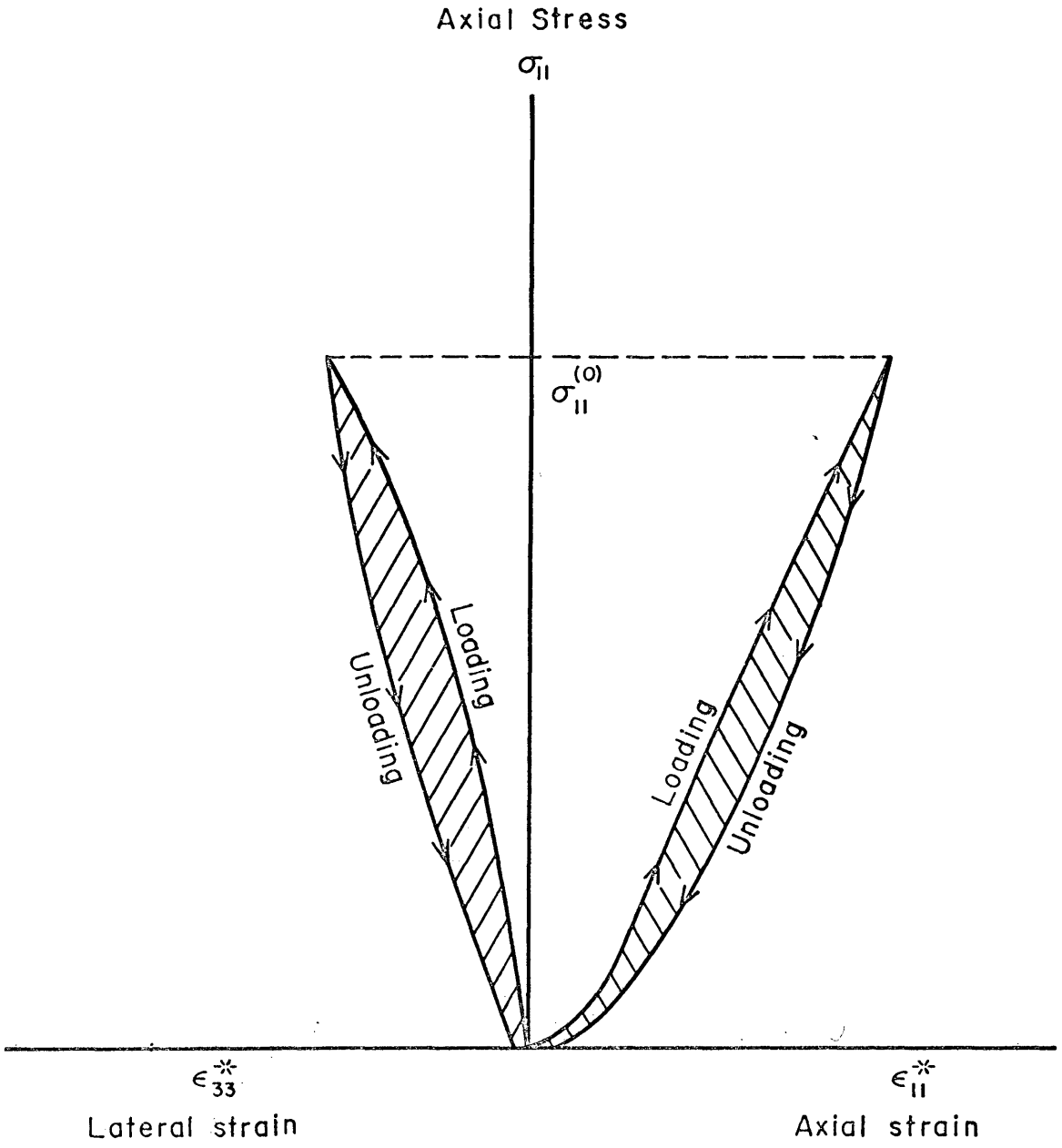

FIGURE F1.—Typical Loading and Unloading Stress–Strain Curve

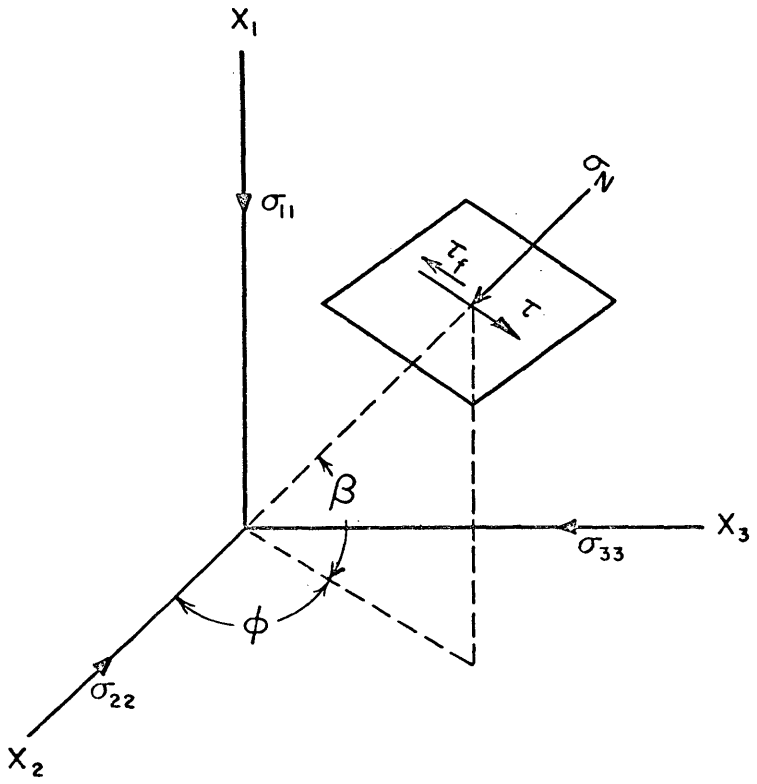

FIGURE G1.- Angular Specification of a Closed Griffith Crack.

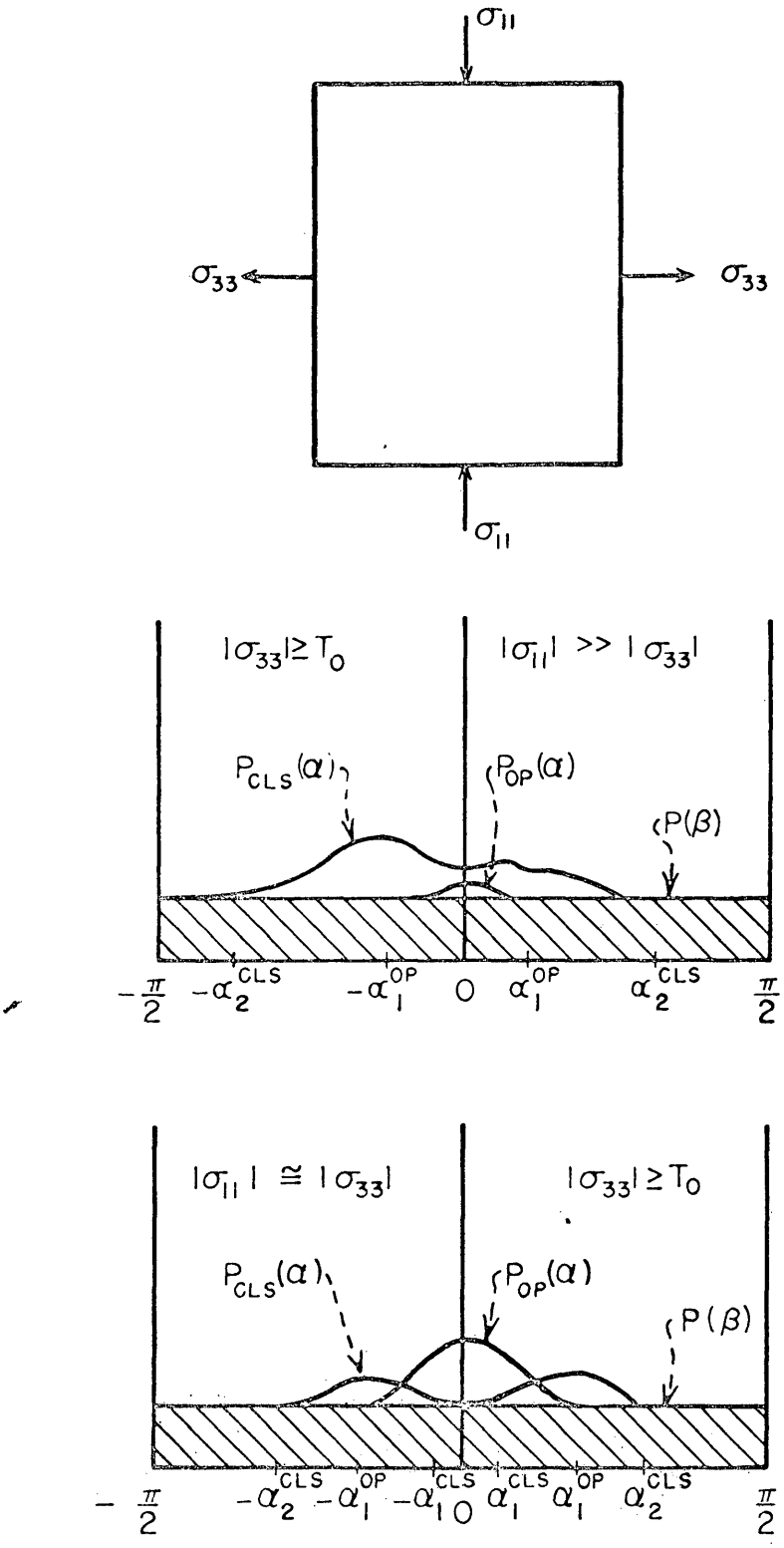

FIGURE H1.– Diagrammatic Illustration of the "CLS" and "OPT" Microcrack Distributions ($\sigma_{22} = \sigma_{33}$) $P(\alpha,\gamma) = P(\alpha)\,P(\gamma)$ [$P(\gamma)$ is uniformly distributed]

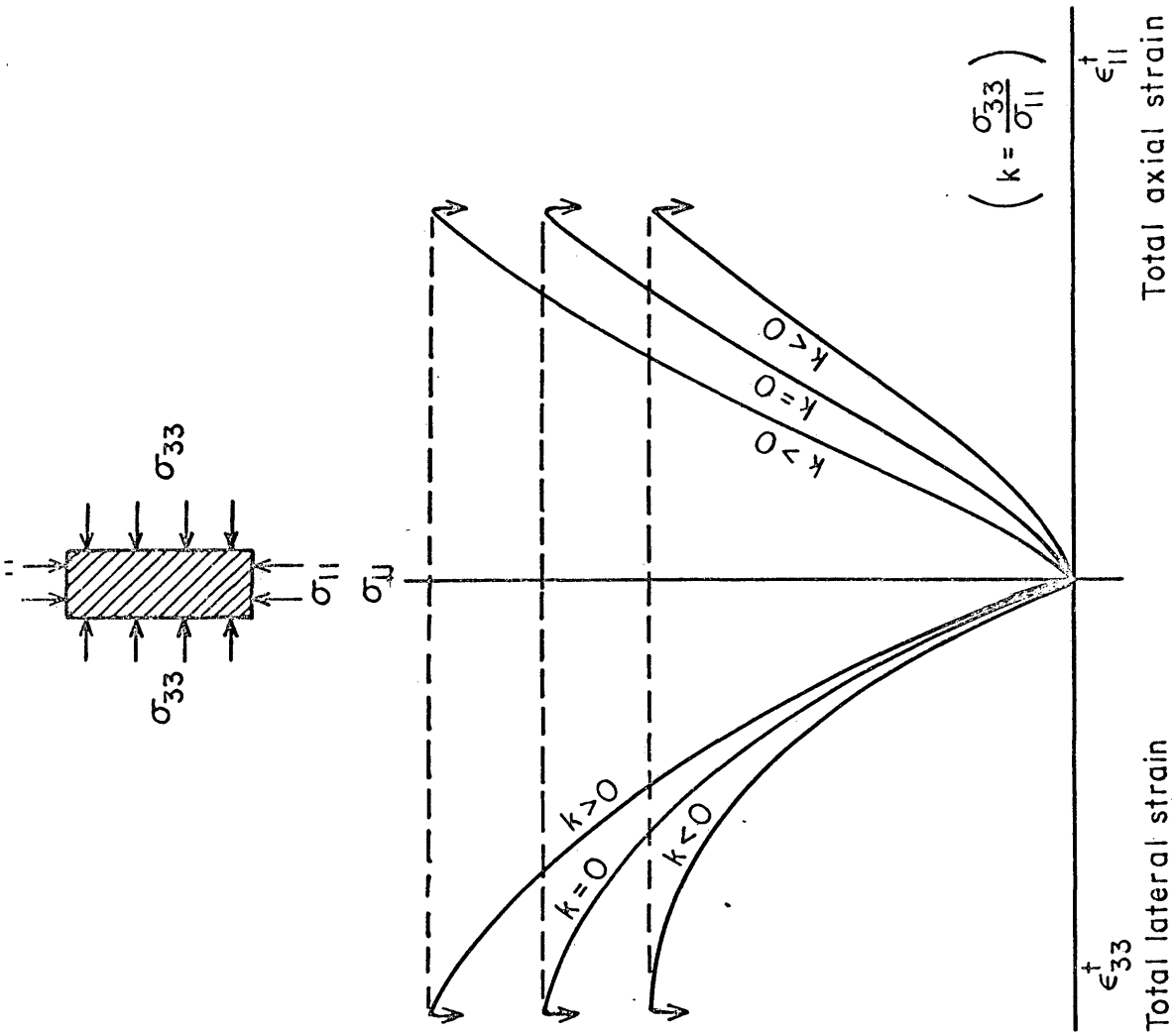

FIGURE H2.—Typical Stress-Strain Behavior of Brittle Rock Based upon the Microcrack Model.

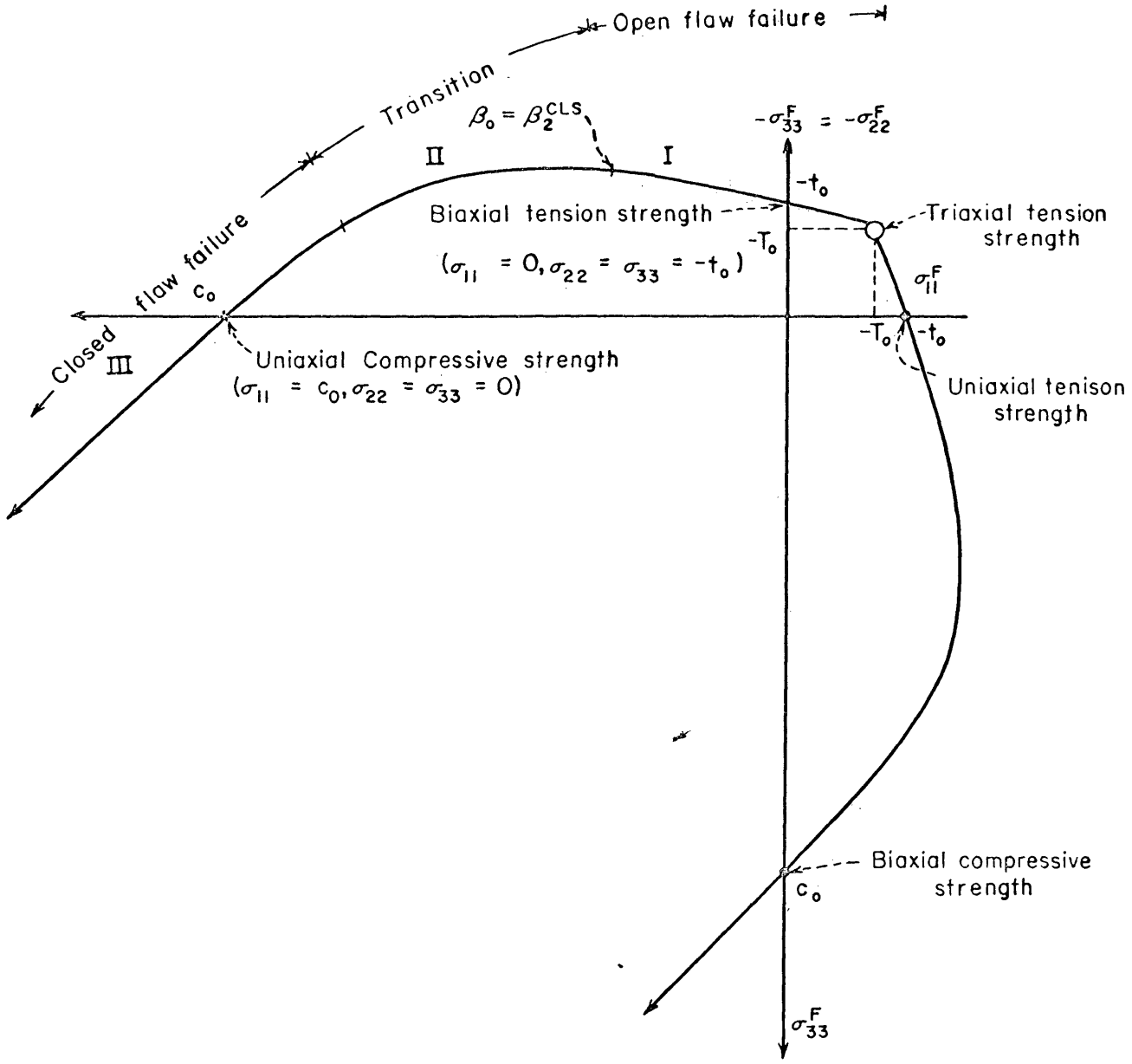

FIGURE 11.- Stress-Space Failure Envelope Based upon a Critical Volumetric Microcrack Strain Criterion (section shown is the intersection of the plane $\sigma_{22} = \sigma_{33}$ with the three-dimensional surface).

$$\Phi = \frac{\sigma_{22} - \frac{1}{2}(\sigma_{11} + \sigma_{33})}{\frac{1}{2}(\sigma_{11} - \sigma_{33})}$$

σ_0 = Yield stress

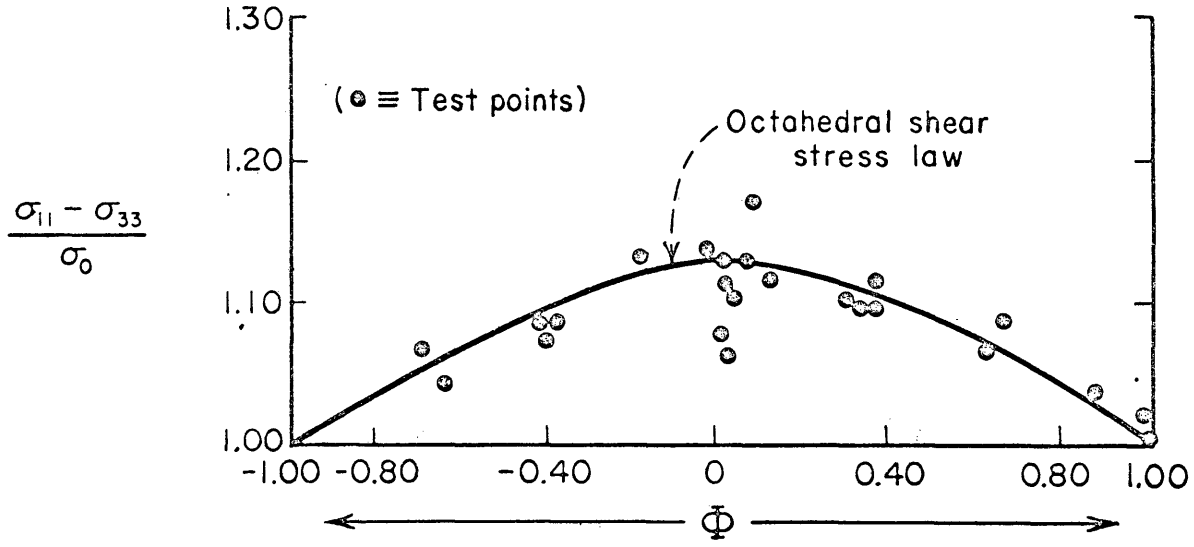

FIGURE J1.- Variation of the Greatest Principal Stress Difference with the Intermediate Principal Stress (after Nadai, 1950)

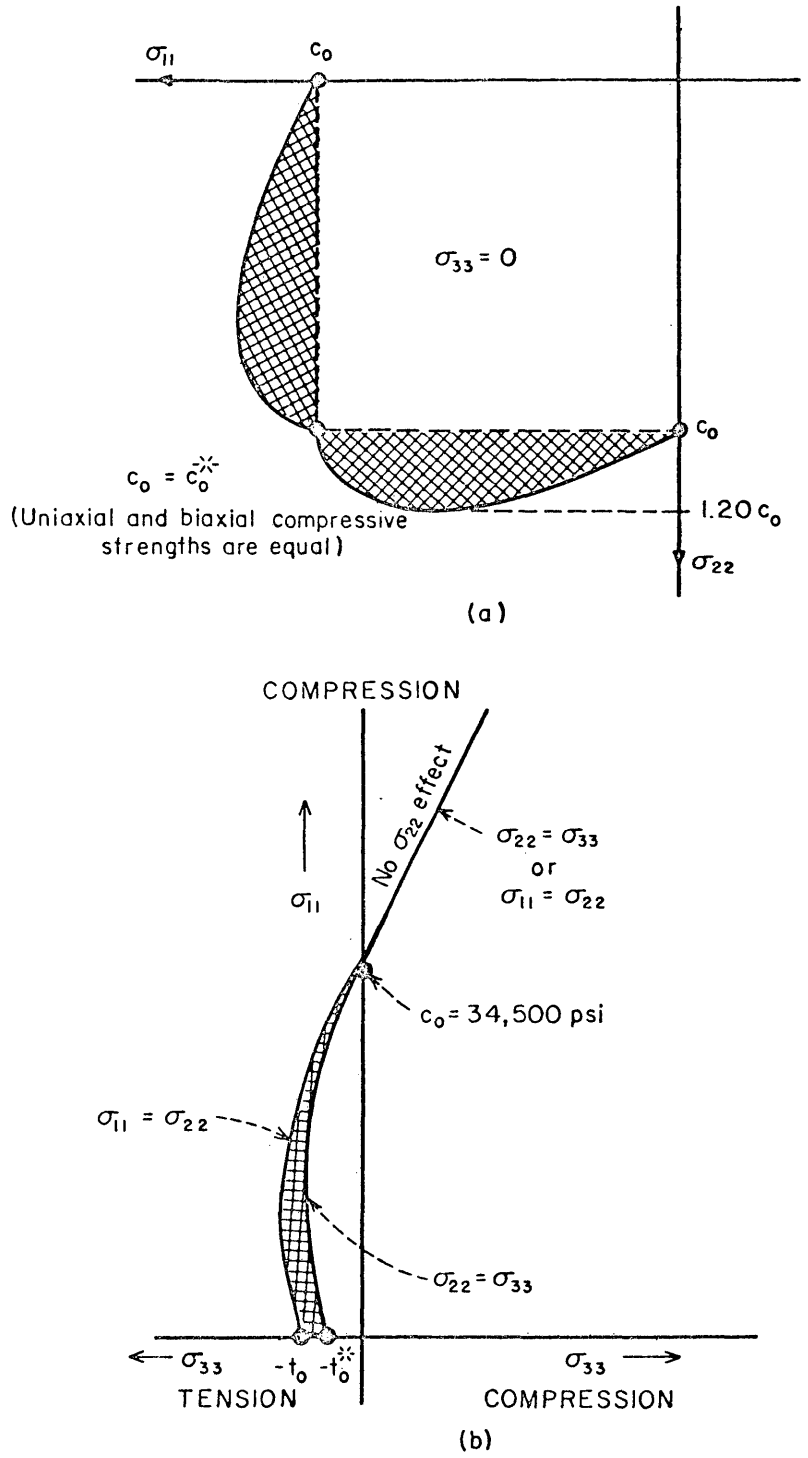

FIGURE J2.–Effect of the Intermediate Principal Stress on the Fracture of Brittle Rock.

a.- Influence of σ_{22} on the Biaxial Failure Characteristics ($\sigma_{11}^{CR} \cong \frac{1}{2} c_o$, $c_o = 34{,}500$ psi, $\mu = 0.70$)

b.- Influence of σ_{22} on the Extension ($\sigma_{11} = \sigma_{22}$) and Compression ($\sigma_{22} = \sigma_{33}$) Failure Characteristics of Brittle Rock ($\sigma_c = -1{,}125$ psi, $t_o = -1{,}500$ psi, $t_o^* \cong -1{,}150$ psi)

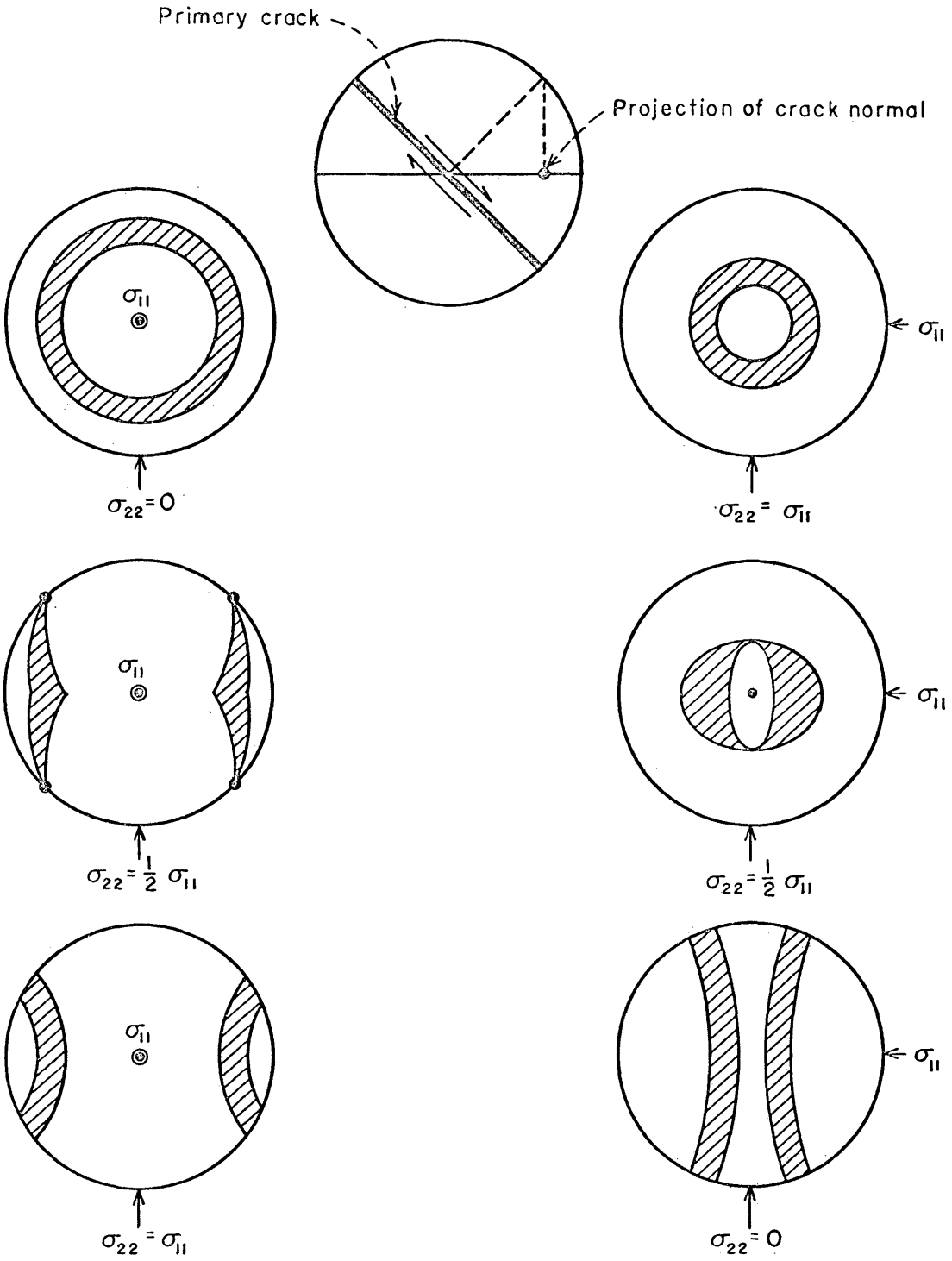

FIGURE J3.—Effect of σ_{22} Upon the Angular Spread and Distribution of Uniformly Distributed Primary Cracks Suitably Oriented for Failure (CLS Model) (Shaded area ≡ equal area projection of the normals to the primary cracks which are suitably oriented for failure). ($\sigma_{11}^{CR} \cong \frac{1}{2} c_0$, $c_0 = 2.50$ kb, $\mu = 0.70$)

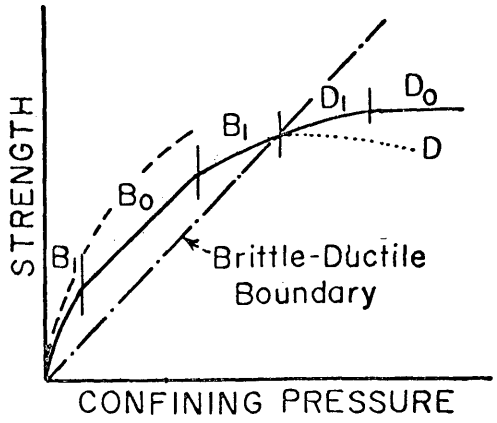

(*a*)

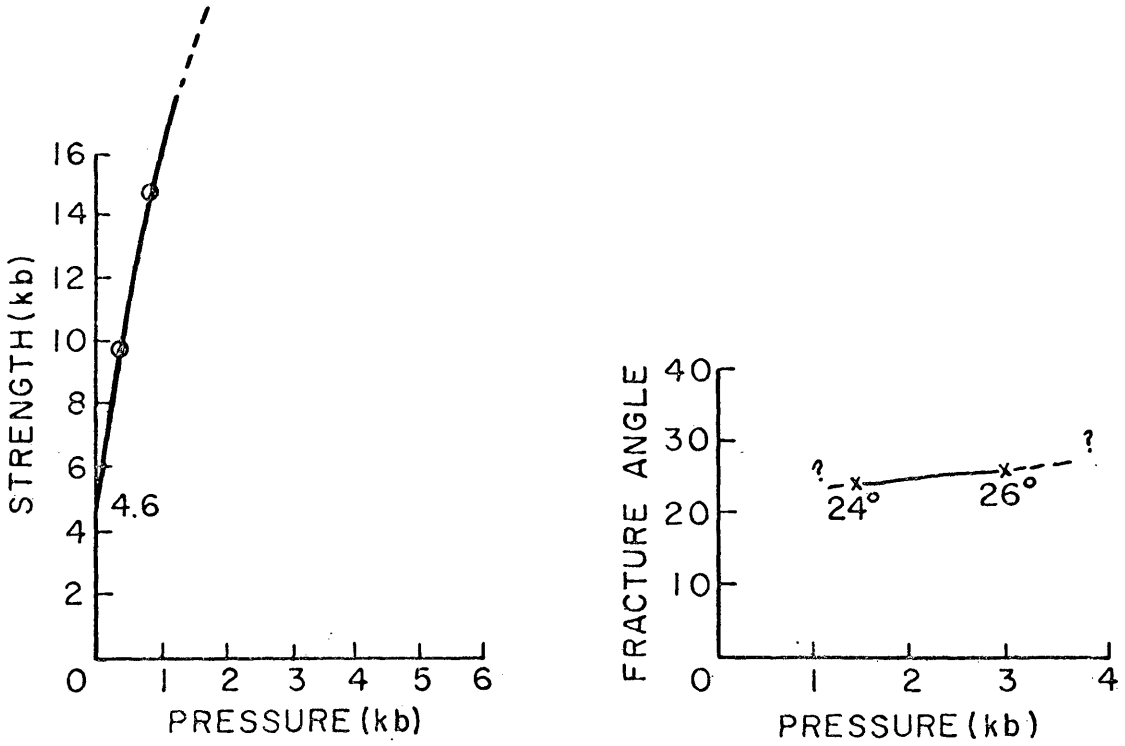

(*b*)

FIGURE K1(*a*).—A Typical Strength-Pressure Curve of Dry Rocks at Room Temperatures (after Mogi, 1966)

(*b*).—Strength vs Pressure and Fracture Angle vs Pressure for the Cheshire Quartzite (after Brace, 1964)

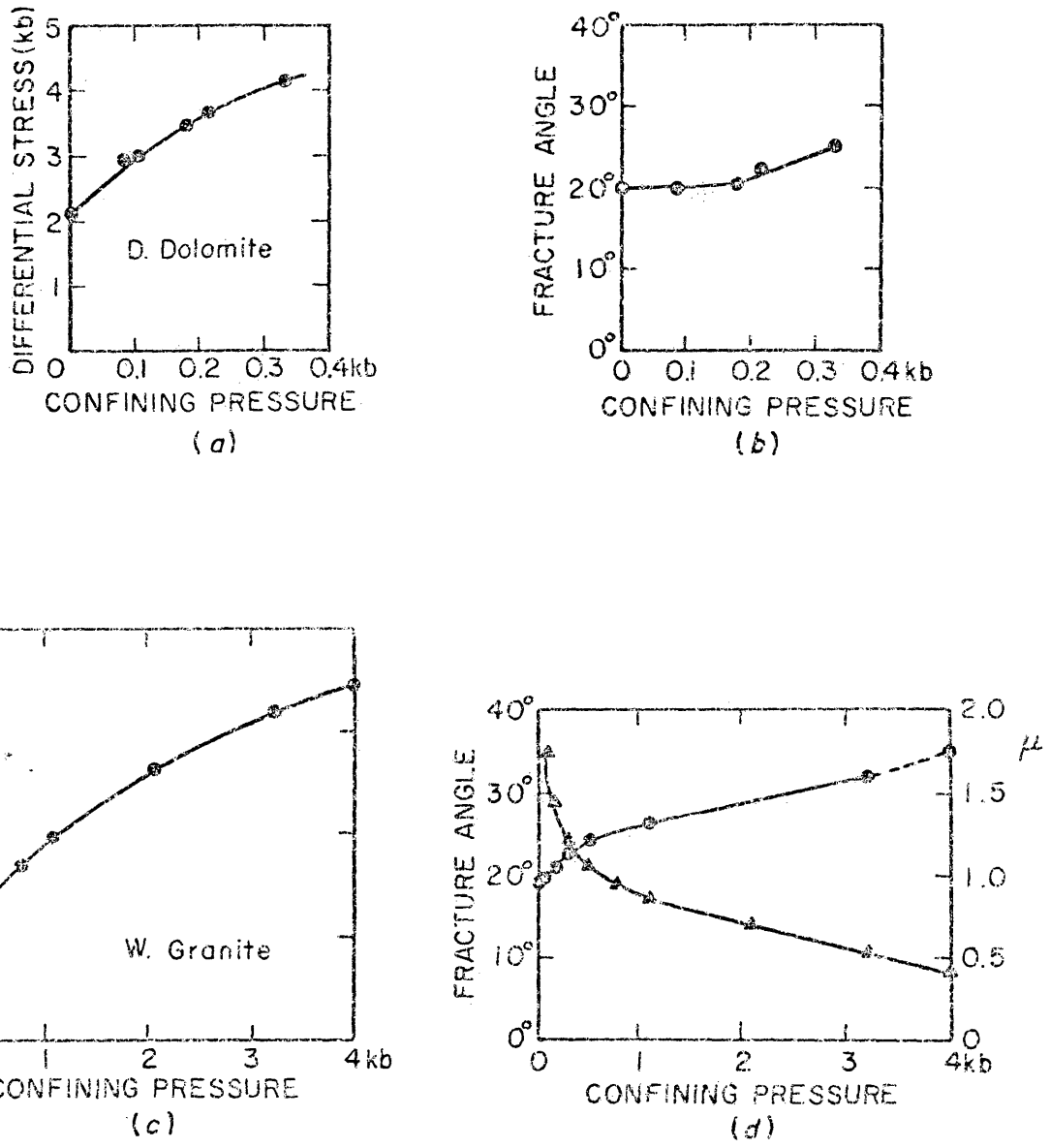

FIGURE K2.—Fracture Characteristics of a Granite and a Dolomite (after Mogi, 1966)

(*a*).—Relation between Compressive Strength and Confining Pressure in Dunham Dolomite

(*b*).—Relation between Fracture Angle and Confining Pressure in Dunham Dolomite

(*c*).—Relation between Compressive Strength and Confining Pressure in Westerly Granite

(*d*).—Relation between Fracture Angle and Confining Pressure in Westerly Granite, [internal friction coefficient (μ) calculated from the Mohr envelop.]

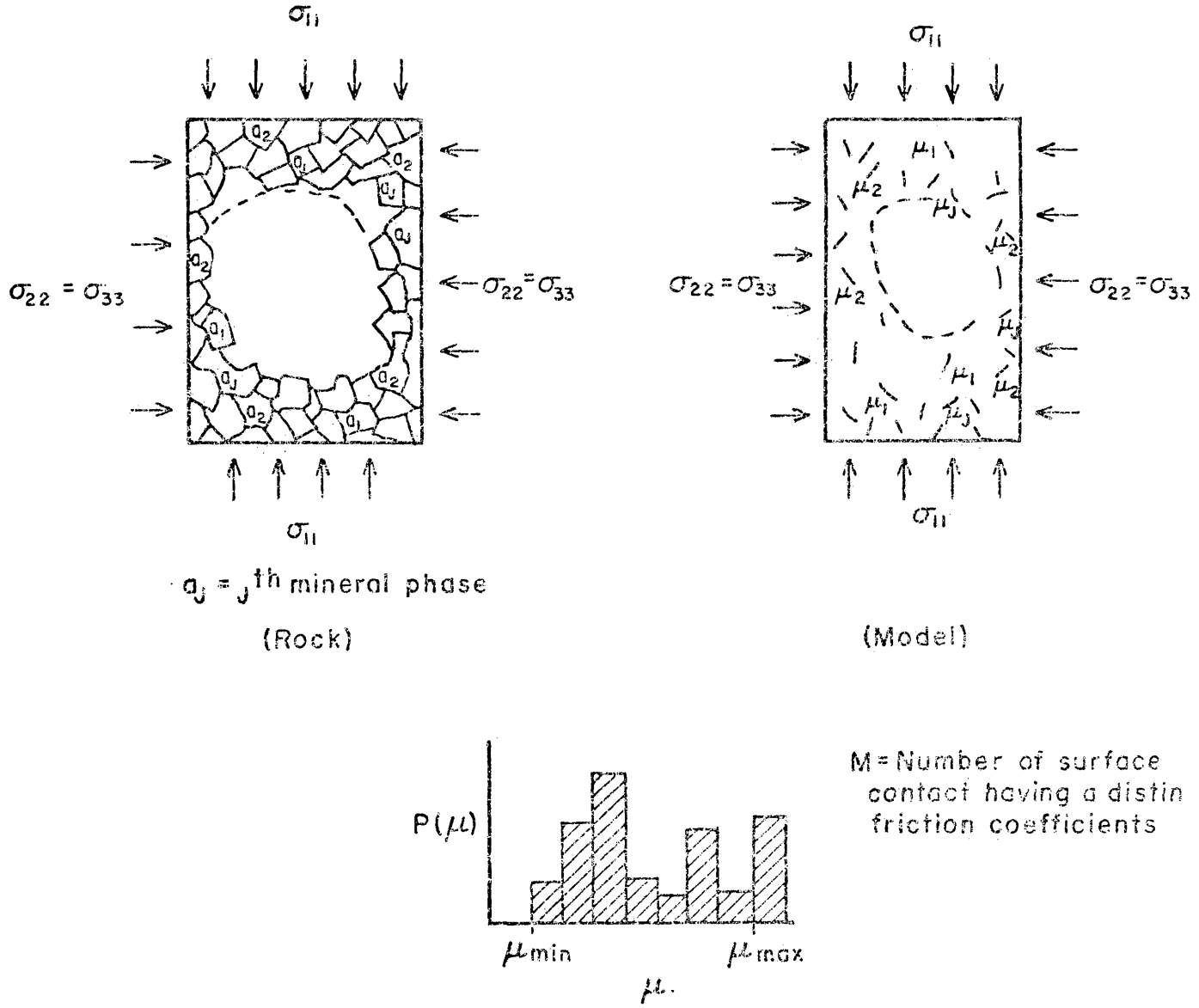

FIGURE K3.- Mathematical Model Simulating Material Heterogeneity.

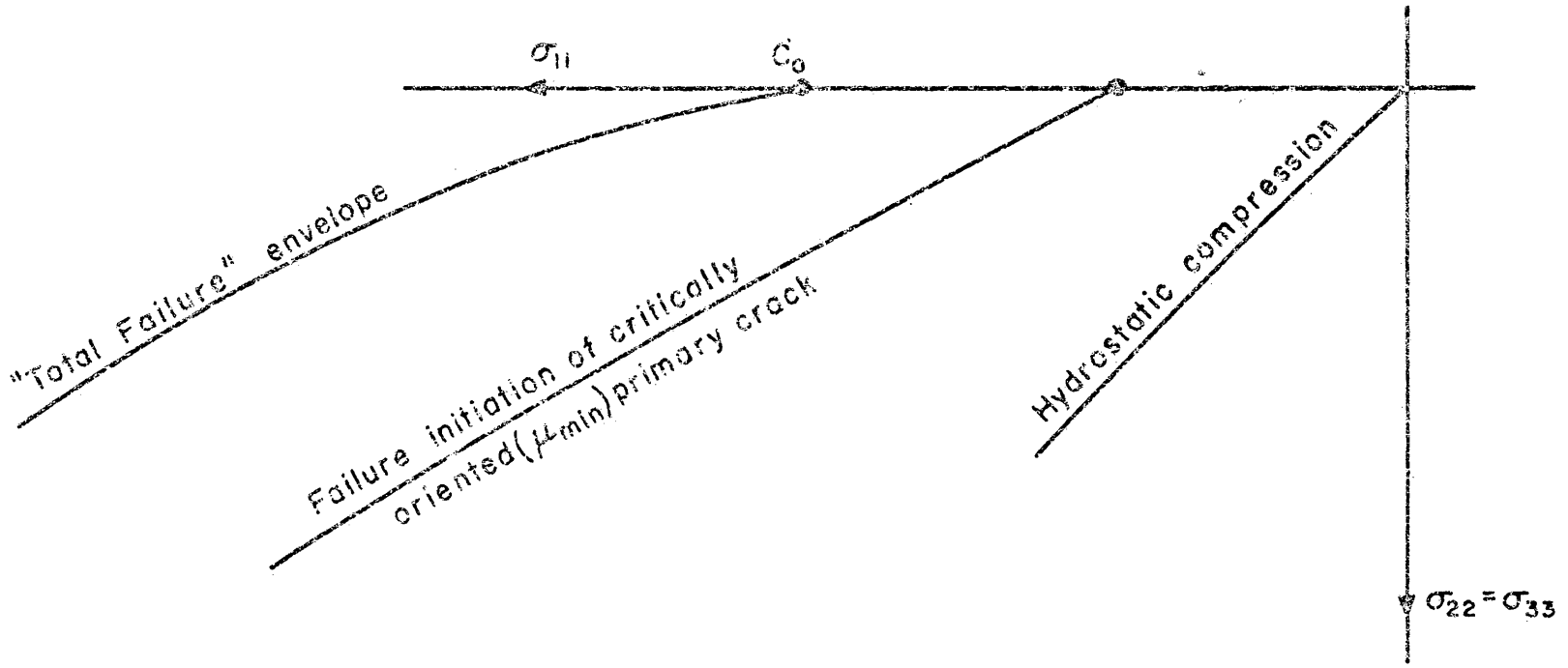

FIGURE K4.–A Compression Field Failure Envelope of a Brittle Material Characterized by a Distribution of Friction Coefficients.